NUMERICAL AND NONLINEAR DYNAMICAL SYSTEMS ANALYSIS FOR FLUID MECHANICS AND HEAT TRANSFER PROBLEMS

BY: NAHOM ALEMSEGED WORKU

GSR/2289/11

A THESIS SUBMITTED TO THE PROGRAM OF COMPUTATIONAL SCIENCE

ADDIS ABABA UNIVERISTY

IN PARTIAL FULFILMENT OF THE REQUIREMENT FOR THE DEGREE OF

MASTER OF COMPUTATIONAL SCIENCE

ADVISOR: PROF. OKEY OSELOKA ONYEJEKEWE

JULY 2020

Declaration

I, Nahom Alemseged Worku, hereby declare that, this thesis represents my own work and has not been submitted previously for examination towards any degree or diploma qualification at any other University.

Signed

Date

NUMERICAL AND NONLINEAR DYNAMICAL SYSTEMS ANALYSIS FOR FLUID MECHANICS AND HEAT TRANSFER PROBLEMS

NAHOM ALEMSEGED WORKU

JULY 2020

ADVISOR

_____ _____

Prof. Okey Oseloka Onyejekwe Date

Approved by:

Name	Signature
Dr. Solomon Gizaw (Director)	---
---	---
---	---
---	---

Acknowledgement

I would like to thank my God for his guidance and enormous help. He has been a father to me throughout my way.

I am indebted to Prof. Okey Oseloka Onyejekwe for his guidance and supervision throughout the course of the program.

My deepest gratitude goes to my loving and wonderful wife, Yordanos Kassa, for her greatest appreciation throughout this journey.

I am indebted to my parents Alemseged Worku and Debrework Zewdie for their direct support and guidance. I would like to extend my gratitude to my in laws Ato. Kassa Desseye, W/o Belaynesh Teklu and Lidiya Kassa for their enormous support and understanding.

I would also like to extend my gratitude to my brothers Ezra and Elroie Alemseged for their help and support.

I would finally like to thank my friends, colleagues, classmates and everyone involved in the process. Thank you all. Without you, this wouldn't have been possible.

Abstract

In this thesis, different Heat transfer and boundary layer flow problems coupled with heat transfer, thermodynamics and electromagnetism has been studied.

Problems concerning heat transfer in fins and thermal explosion end up in a second order nonlinear ODEs, which are then solved using Numerical method, specifically the Shooting Secant method. Dynamical systems analysis is also studied for these problems.

Boundary layer flow coupled with heat transfer, thermodynamics and electromagnetism, and Nano fluid flow is also studied in this thesis. They end up in highly nonlinear coupled ODEs, which are then solved using Numerical method (Shooting Secant).

Background of the specific problem introduced in the chapter, together with the Mathematical formulations of ythe problem and Descriptions of the results are then provided. The description based on the physics of the problems are discussed in detail for each chapters.

Keywords: Navier-Stokes equation, Conduction, Convection, Radiation, Boundary layer flow, Nano fluids, Magneto-hydrodynamics, Shooting Secant method, dynamical systems analysis, Coupled Higher order differential equations.

Table of Contents

List of Figures

List of Tables

Chapter One

Introduction

1.1. Background and Basic Terms

1.1.1. Heat Transfer

Heat transfer is the study of energy flow due to temperature difference. There are three types of heat transfer namely, Conduction, convection and Radiation. But all heat transfer types are driven by temperature difference.

1.1.1.A. Conduction

Conduction can be defined as a heat transfer type in all liquids, solids and gasses whereby energy transfer is occurred by molecular vibration of particles. Heat is transferred from a particle to its neighboring particle. Molecules vibrate about their equilibrium positions. Higher energy can be manifested by energetic vibrations. A hotter body has a high molecular vibration and the colder one has a slow and sluggish vibration. When a hot and a cold body meet, the molecular vibration of the hotter body excites the colder ones, in an attempt to maintain thermal equilibrium, the vibration of hotter body becomes less.

1.1.1.B. Convection

Convection occurs when a fluid (liquid, gasses or air) transports heat from one section to the other. The temperature of the fluid plays an important role in transferring heat throughout the solid body. It is basically Conduction but fluid medium is required.

1.1.1.C. Radiation

Radiation is a form of heat transfer occurring through electromagnetic waves. It occurs in all phases of materials i.e. Solids, fluids and gasses. But the difference with conduction is that radiation requires no medium and can travel through vacuum.

1.1.2 Thermodynamics

1.1.2.A. First Law of thermodynamics

The first law of thermodynamics states the basic law of Conservation of energy. It states that energy can neither be created nor destroyed, but can be transferred from one form to the other. The relation is given as follows.

$$\mathbf{\Delta E = Q - W} \qquad \text{Eq (1.1)}$$

Equation 1.1 states that the rate of change of all types of Energy in a system, Q is the rate of energy addition in a form of heat and W is the form of energy leaving the system in the form of Work done. The total change of energy term is regarded as the sum of the change in Kinetic Energy $(\Delta K.E)$, the change of the Potential Energy $(\Delta P.E)$, and the change in internal energy Δi. Therefore,

$$\mathbf{\Delta K.E + \Delta P.E + \Delta i = Q - W} \qquad \text{Eq(1.2)}$$

But in relation to fluids as shall be discussed later, Potential Energy is considered as a body force and is considered as a source term and the others are considered as surface forces.

The first law of thermodynamics is more general and doesn't go into detail as to what type of energy is used. The detail of energy types and the reversibility is considered in the second law of thermodynamics.

1.1.2.B. Second Law of Thermodynamics

The first law of thermodynamics gives incomplete picture in the conversion process of one form of energy into the other.

The second law states that all real processes are irreversible

Energy is ideally efficient and most efficient when it is used to do work. There is always irreversibility (an energy that is irreversible to do work is called entropy)

1.1.2.C. Entropy

As stated above, entropy is the measure of irreversibility in a real process, as per the second law of thermodynamics. As the entropy increases, the irreversible energy also increases thereby decreasing the quality of energy (exergy). Entropy generation in thermal systems destroys available work and thus reduces its efficiency.

Equation for entropy generation per volume is given as

$$S_G = \frac{k}{T_\infty^{\,2}}\left[\nabla T^2\right] + \frac{\mu}{T_\infty}\phi \ , \qquad \text{Eq(1.3)}$$

Where k=thermal Conductivity,

T_∞=ambient temperature,

μ= viscosity and Φ is the dissipation of heat due to viscosity.

The first term, According to Bejan[7], arise from heat conduction(1st term of eq(1.3) and the second term arises from viscosity (flow).

1.1.3. Buoyancy

Buoyancy, also called an up thrust force, can be defined as a force of a fluid applied on a body that develops when an object is submerged in a fluid.

Buoyancy is a very important concept applied in the area of ship design, design of submarines.

1.1.4. Viscosity

Viscosity is the measure of resistance to flow under shear stress. It is basically the thickness of flow. If a shear stress is applied to a stationary fluid, the fluid moves and the particle immediate vicinity to the solid boundary will move at the same speed with the solid boundary, as in the case of Couette and Poisuelle's flow.

The shear flow equation of Newtonian fluid flow is given as

$$\tau = \upsilon \frac{du}{dy} \qquad \text{Eq(1.4)}$$

Where υ is the Dynamic Viscosity

Viscosity is strongly related to the shear stress in fluids. This is better described in section 2.0.

1.1.5. Dimensionless Numbers

Thermal Diffusivity

The thermal diffusivity is intuitively defined as a measure of how fast a body changes temperature. It is defined as a ratio of thermal conductivity (heat dissipation) to the rate of storage of heat (specific heat capacity).

The relation of thermal diffusivity is given as

$$\alpha = \frac{k}{\rho Cp} \qquad \text{Eq(1.5)}$$

Where k is conductivity,

ρ is density and Cp is the specific heat capacity.

Nusselt Number

The average Nusselt Number is defined as the convective heat transfer to Conductive heat transfer. The Nusselt number is commonly used in thermal boundary layer.

$$\text{NuL} = \frac{\text{Convective Heat Transfer}}{\text{Conductive Heat Transfer}} = \frac{\text{hL}}{\text{K}} \qquad \text{Eq(1.6)}$$

Biot Number

Biot number is the measure of conductivity to convective resistance of heat.

$$Bi = h * \frac{L}{K} \qquad \text{Eq(1.7)}$$

Where

h is the thermal conductivity

L Is the characteristic Length of the body and

K is the thermal conductivity of the body

Reynolds Number

Reynolds number is a very important number in the area of fluid mechanics. It is a dimensionless number that helps indicate the property of the fluid. It relates the inertial force to the frictional or viscous force. It determines whether a flow is Laminar of Turbulent. If the Reynolds number is less than the limit (eg around 2300 in pipe flow), the frictional force dominates the flow and the flow is ordered and smooth. This is called a **laminar** flow. On the other hand, if the flow is governed by inertial force, large Reynolds number, the flow becomes unordered, and the property is difficult to be predicted. This flow is categorized as **Turbulent**.

Inertial Force(IF)

$$IF = \rho \vec{a} \qquad \text{Eq(1.8 A)}$$

$$IF = \rho \frac{du}{dx}\frac{dx}{dt} \qquad \text{Eq(1.8.B)}$$

$$IF = \rho u \frac{du}{dx} \qquad \text{Eq(1.8 C)}$$

In dimensional terms,

$$IF = \rho \frac{V^2}{L} \qquad \text{Eq(1.8 D)}$$

Frictional Force (FF)

$$FF = \frac{\partial \tau}{\partial y} = \frac{\partial \left[\mu \frac{\partial u}{\partial y} \right]}{\partial y} \qquad \text{Eq(59 A)}$$

In dimensional terms,

$$FF = \mu \frac{V}{L^2} \qquad \text{Eq(1.9)}$$

Reynolds number can be given as

$$\mathrm{Re} = \frac{IF}{FF} \qquad \text{Eq (1.10 A)}$$

$$\mathrm{Re} = \frac{\rho V^2}{L} * \frac{L^2}{\mu V} = \frac{\rho VL}{\mu}$$ Eq (1.10 B)

$$\mathrm{Re} = \frac{VL}{\nu}$$ Eq (1.11)

Prandtl's Number

Prandtl Number is a dimensionless number in the area of boundary layer theory that relates, or Is described as the ratio of Momentum Diffusivity to thermal diffusivity.

$$P = \frac{\upsilon}{\alpha} = \frac{\mu Cp}{k}$$ Eq (1.12)

The Prandtl Number in boundary layer theory relates the boundary layer of flow and the thermal boundary layer. Prandtl number of one indicates the momentum diffusivity and the thermal diffusivity are equal and hence, the thermal and the boundary layer thicknesses are equal. If it is greater than one, the displacement boundary layer thickness is greater than that of the thermal boundary layer, and if the Prandtl number is less than one, the thermal boundary layer thickness is larger.

Eckert Number

The Eckert number is a dimensionless term in continuum mechanics. It relates flow kinetic energy to enthalpy in a system. The Eckert number is given as

$$Ec = \frac{U^2}{C_p \Delta T^2}$$ Eq (1.13)

Where
U is the local velocity
Cp = specific heat and
$\Delta T = T - T_\infty$ Indicates the temperature difference between wall and ambient fluid

Drag Coefficient

The drag coefficient is the dimensionless number to express the drag force exerted on a body

The relation is given as

$$C_d = \frac{F_d}{\frac{1}{2}\rho U^2 A}$$ Eq (1.14)

Where Fd is the drag force
ρ is the density of the fluid
U is the relative velocity of the body with that of the fluid

A is the reference area

1.1.6. Heat Transfer in fins

A fin is an elongated mechanical device that is used to dissipate heat out of a system. Device function at an optimum temperature and if heat is generated on a device pass that optimum temperature, it causes malfunctioning of the device. We can find fins in cars, computers, and machines and so on.

A fin dissipates heat using the following two basic mechanisms.

Conduction: Conduction in heat transfer is the transfer of heat from one particle to its neighboring particle. In fins, since the distribution of Temperature vertically across a section (vertical) is negligible, we assume a one dimensional analysis and we can assume a section as a particle so the heat is transferred from one section to the next section.

Convection: In addition to the Conduction of heat from one section to the other, heat escapes to the ambient through its perimeter since the heat on the fin is higher than the ambient. This method of heat transfer caused by Temperature gradient is called Convection.

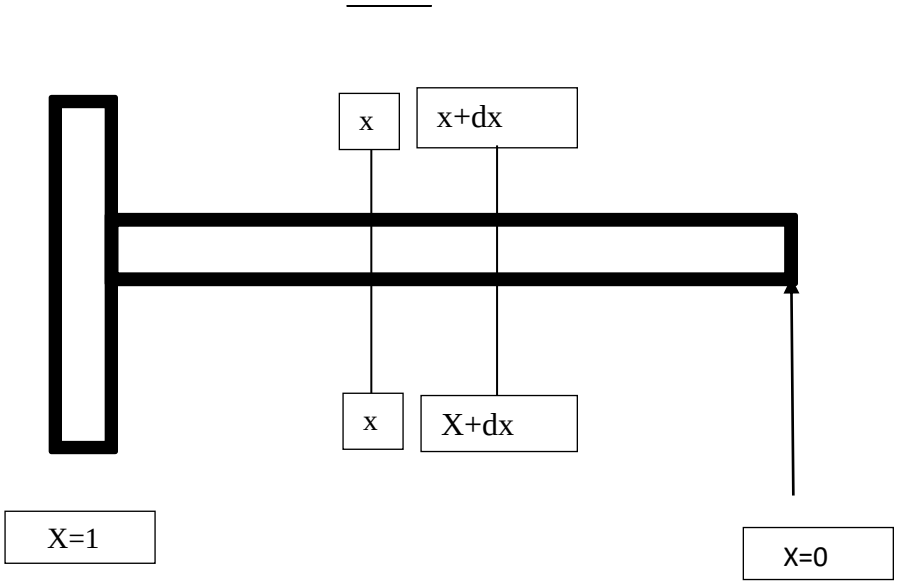

Fig 1.1. Schematic drawing of Fin

The fin is attached at the base to the device(X=1) , and free at the end where X=1.

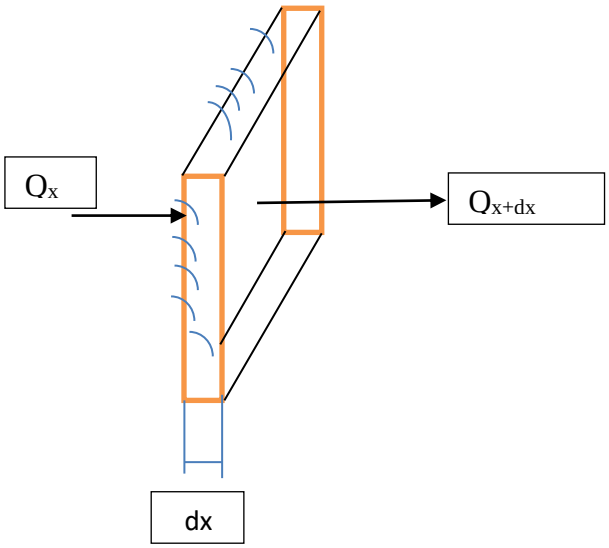

Fig 1.2. Schematic drawing of the cross Section of Fin

From fig 1, we can see that the heat at section x is transferred to the neighboring section (x+dx) through conduction and some are dissipated through the perimeter (convection). In this case, the perimeter with width dx. Therefore,

$$Q_x = Q_{x+dx} + h*\mathrm{p}*dA(T - T\infty)$$

$$-(Q_{x+dx} - Q_x) = h*p*dx(T - T\infty)$$

Eq (1.15)

$$-\frac{dQ}{dx} = h*p(T - T\infty)$$

From Fourier's Law, Q_x can be approximated as $Qx = -KA\frac{dT}{dx}$. Hence,

$$-\frac{dQ}{dx} = h*p(T - T\infty)$$

$$-\frac{d(-KA\frac{dT}{dx})}{dx} = \frac{hp}{}*\theta$$, where θ=T-T∞

Here, h is convective parameter, p is perimeter of the section is the thermal conductivity and A is the cross sectional Area. All these terms are constants and can be built up into one constant.
Let us call it m. Hence,

$$m^2 = \frac{hp}{KA}$$

Therefore, the governing Differential equation will

$$\frac{d^2\theta}{dx^2} = m^2 * \theta$$

Analytically solving the above differential equation, we obtain

$\theta = c_1 * e^{mx} + c_2 * e^{-mx}$. Finding the second derivative of the function yields

$\theta = c_1 * e^{mx} + c_2 * e^{-mx}$

Boundary Conditions are

$\frac{d\theta}{dx} = 0 @ x = 0$ And

$\theta(\mathrm{x}) = 1 @ \mathrm{x} = 1$

Substituting these, we obtain C1 and C2 which are functions of m. But let us assume m=1, we obtain $c_1 = c_2 = \frac{1}{\left[e + \frac{1}{e}\right]}$. Hence, C_1=0.324.

Since M is constant for thermal and geometric parameters, it is commonly called Thermo geometric Parameter.

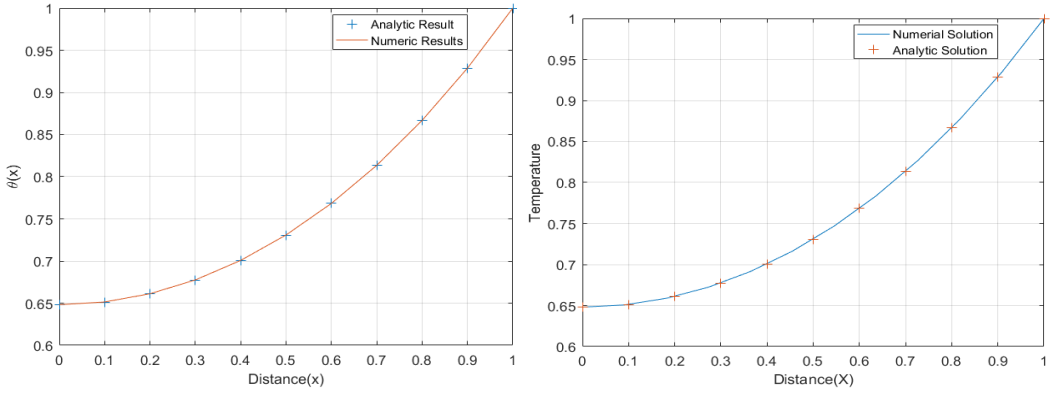

(A) (B)

Fig 1.3. Comparison of analytic and Numeric results of Temperature profile for Numerical results obtained from Finite Difference method and Numerical results obtained from shooting Secant Method

Table 1.1 Comparison for error of Shooting and Finite Difference method

X	ANALYTIC SOLUTION	NUMERICAL SOLUTION			
		SHOOTING SECANT	FINITE DIFFERENCE	ERROR SHOOTING SECANT	ERROR FDM
0	0.648054274	0.648054641	0.648135858	3.67705E-07	8.15845E-05
0.1	0.651297246	0.651297615	0.651392822	3.68645E-07	9.55762E-05
0.2	0.66105862	0.661058983	0.661163715	3.62453E-07	0.000105094
0.3	0.677436092	0.677436441	0.677546244	3.48995E-07	0.000110153
0.4	0.700593571	0.700593899	0.700704236	3.27954E-07	0.000110665
0.5	0.730762826	0.730763125	0.73086927	2.98829E-07	0.000106444
0.6	0.768245801	0.768246062	0.768342997	2.60922E-07	9.71964E-05
0.7	0.813417638	0.813417852	0.813500154	2.13329E-07	8.2516E-05
0.8	0.866730433	0.866730588	0.866792313	1.54928E-07	6.18801E-05
0.9	0.928717757	0.928717841	0.928752394	8.43587E-08	3.46378E-05
1	1	1	1	0	0

1.1.7.FLUIDS

1.1.7.A. BACKGROUND

What are Fluids?

Air is all around us. We drink water every day. We clean ourselves and our environment using water. Almost 71% of the earth is covered with water. Our lives are highly interrelated with fluids. This highly necessitates the study of fluids.[114]

Fluids can be found in liquid or Gaseous state.

Fluids can scientifically be defined as a material that shear constantly in the presence of a very small disturbance. Assume we pour water over a horizontal plate. The water will flow horizontally even if there is no gradient applied until it reaches stable position of a very minimal depth.

1.1.7.B. Scale

Scale is a very important concept when studying natural Science and Engineering.

It helps understand where to position ourselves to look at our study. There are two major categories of scales, namely, microscopic and macroscopic scales.

If we see water with our naked eye, it is continuous and smooth, i.e. macro scale. But when looked under microscope, we see small discontinuity. Zooming it a bit more, it becomes more discontinuous. It somehow looks like a dense crowd in a subway. Again zooming it more, we see groups (large chunks) of circles grouped together and moving along with each other. Finally, if we zoom it enough, we can see

groups with three circles joined and moving together. The three circles joined together are water molecules (H2O), with two hydrogen atoms and one oxygen atom (micro scale).

The scale below molecular level, i.e, molecules, atoms, subatomic particles are microscopic scale. The scale above which can be seen with the naked eye is commonly called macroscopic scale. In fluid mechanics, and also in solid mechanics, macroscopic level of study is performed. In fluid mechanics, as in the case of solid mechanics, materials are continuous and are thought of being composed of macroscopic elements (chunks). A chunk of fluid and solid, called a control volume, is used to study the overall property of fluids and solids respectively.

1.1.7.C. Frame of Reference

In engineering mechanics, there are three types of frame of reference. The lagrangian , Eulerian and the Arbitrary-Lagrangian-Eulerian frame of reference.

- Lagrangian Frame of Reference (L.F.R) :- In the lagrangian frame of reference,properties of material points are studied by tracing individual material elements. Let us assume there is a hypothetical grid of reference aligned with the material element. In the L.F.R., the reference grid is not stationary and deforms together with the domain.

  In fluids, the L.F.R. study can be implemented by using streak lines (dyes). The movement of the dye in the fluid is assumed to be a particle of fluid to be studied. There are some cases that the lagrangian approach can be used. In cases of solid mechanics, since the particles undergo very small deformations, we can allow the reference grid to deform along with the body .Hence, the Lagrangian frame of reference is preferred.

- Eulerian Frame of Reference(EFR):- In the EFR case, we assume a stationary reference grid to monitor properties at a specific point and time. Normally, in fluids, it is impossible to track infinitely many fluid particles. Hence, the lagrangian frame of reference cannot be used.

  Instead, the eulerian frame of reference studies properties of fluids at a specific space and time, which makes it convenient to study fluids. It is performed by tracing properties of the fluid at each stationary grid point.

- Arbitrary Eulerian Lagrangian Frame of Reference(ALE) : We have seen that in case of the Lagrangian Frame of Reference, the reference grid moves independently and in the case of the Eulerian Frame of Reference, the grid is stationary.

  In the case of the Arbitrary Eulerian Lagrangian Frame of Reference, the reference grid moves independently with the material element. This type of frame of reference is called the ALE. The ALE frame of reference is widely used in the study of fluid-structure Interaction problems.

1.1.7.D. Conservation Laws

In fluid mechanics, for convenience, individual fluid particles are called fluid particles. And a set of fluid particles comprise a fluid element or a fluid system. Therefore, one fluid element can comprise of many fluid particles.

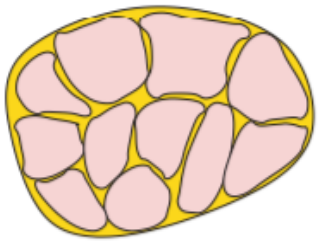

Fig.1.4. Schematic diagram for fluid particle and fluid element

To find answers to different physical problems that arise in fluids, we can simply apply the fundamental laws of physics. But, the problem is that, physical laws are obtained in the Lagrangian frame of reference form. Therefore, it is necessary to customize it to the Eulerian frame of reference. To do that, we use the famous the Reynolds Transport Theorem.

1.1.7.E. Reynold's Transport Equation

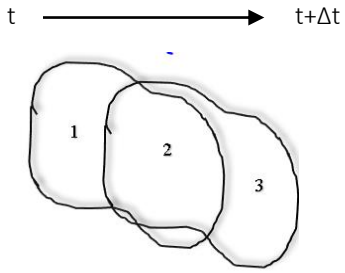

Fig, 1.5. Schematic of fluid particle motion to visualize Renolds transport

The above figure shows a material element(fluid element) in a motion. At time t, the fluid element was at position 1. And after a time increase of Δt ,i.e. at time t+Δt, it moves to position 3. In the moving process, the element t and t+Δt intersected at position 2.

Now, let N be any arbitrary extensive property. Then,

$N_t = (N_1)_t + (N_2)_t$, and

$N_{t+\Delta t} = (N_2)_{t+\Delta t} + (N_3)_{t+\Delta t}$. Eq (1.16)

The rate of change of property N with respect to time t is given as

$$\frac{dN}{dt} = \lim_{\Delta t \to 0} \frac{N_{t+\Delta t} - N_t}{\Delta t} \ , \qquad \text{Eq (1.17)}$$

Solving equation 2, we can obtain

$$\frac{dN}{dt} = \lim_{\Delta t \to 0} \frac{(N_2)_{t+\Delta t} - (N_2)_t}{\Delta t} + (N_3)_{t+\Delta t} - (N_1)_t \qquad \text{Eq (1.18)}$$

Here, region 2 is our control volume. And region 1 is property ready to enter the control volume and region 3 is a region leaving the control volume.

In eq (1.18), the first term on the right hand side iis the rate of change of material property N with respect to time. The second term is the outflow from the control volume and the third term is the inflow to the control volume.

Therefore, eq (1.18) can be read as the rate if change of a material property N with respect to time t is equal to the rate of increase of N in the control volume plus the net flux i.e. Outflow minus the inflow rate of the system.

Rate of change of N = Net rate of change w.r.t. time + Net flux into and out of C.V.

Net flux > 0 if inflow is less than outflow and

Net flux < 0 if inflow is greater than outflow

Now, let us introduce a derived property Φ, which is the rate of N per unit mass.

N = Φ*m.

Flux is written in terms of control surface instead of control volume. Therefore, using divergence theorem

Net Flux = $\int_{cs} \rho\phi u.nds$ Eq (1.19)

Where u is the velocity of the fluids and n is the outward unit normal.

The outward unit normal is normal to the surface since only the normal components of the flux terms enter and leave the control volume.

Hence, the general transport equation of extensive property Φ is

$$\frac{d}{dt}\int_{v}\rho\phi dv = \frac{\partial}{\partial t}\int_{cv}\rho\phi dv + \int_{cs}\rho\phi u.nds \qquad \text{Eq (1.20)}$$

(6)

1.1.7.F. Conservation of mass

The conservation of mass states that mass of fluids in a system in a system is conserved.

Rate of Mass increase in a fluid element = Net rate of flow of mass in the fluid.

So using the transport equation, we can derive the conservation of mass general equation.

Now, let the property N be mass m. Therefore, our desired property Φ be m/m which is equal to 1. Therefore, plugging this into eq(1.20) yields,

$$\frac{d}{dt}\int_{v}\rho dv = \frac{\partial}{\partial t}\int_{cv}\rho dv + \int_{cs}\rho u.nds \qquad \text{Eq (1.21.A)}$$

But, since mass is conserved, the term on the left hand side is zero, i.e. the net rate of change of mass is zero. Therefore,

$$\frac{\partial}{\partial t}\int_{cv}\rho dv + \int_{cs}\rho u.nds = 0 \qquad \text{Eq (1.21.B)}$$

To write equation 8 in compact form, the flux term can be wriiten in the form of control volume, instead of control surface. Hence,

$$\int_{cs}\rho u.nds = -\int_{cv}\nabla.\rho u dv \qquad \text{Eq (1.22)}$$

$$\frac{\partial}{\partial t}\int_{cv}\rho dv + \int_{cv}\nabla.\rho u dv = 0 \qquad \text{Eq (1.23)}$$

Finally, the compact form of conservation of mass is given by

$$\int_{cv}\left[\frac{\partial\rho}{\partial t} + \nabla.\rho u\right]dv = 0 \qquad \text{Eq (1.24)}$$

Physical method of deriving the conservation of Mass Equation

We describe the behavior of the fluid in terms of macroscopic properties, such as velocity, pressure, density and temperature, and their space and time derivatives. These may be thought of as averages over suitably large numbers of molecules. A fluid particle or point in a fluid is then the smallest possible

element of fluid whose macroscopic properties are not influenced by individual molecules. We consider such a small element of fluid with sides δ x, δ y and δ z

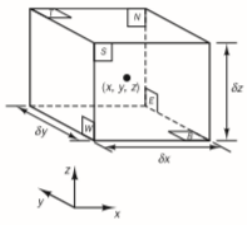

Fig.1.6., Infinitesimal Fluid element

From fig 1.6. , we can see that there are six faces labeled as N, S, W, E, T and B. The positive directions are given in the figure.

We should notice that all properties are functions of space coordinates X, Y,Z and time component t.

The element under consideration is so small that fluid properties at the faces can be expressed accurately enough by means of the first two terms of a Taylor series expansion. Let N be an arbitrary material property, then N at the W and E faces, which are both at a distance of 1 /2 δ x from the element center, can be expressed as

$N - \frac{\partial N}{\partial x} * \frac{1}{2}\delta x$ And $N + \frac{\partial N}{\partial x} * \frac{1}{2}\delta x$.

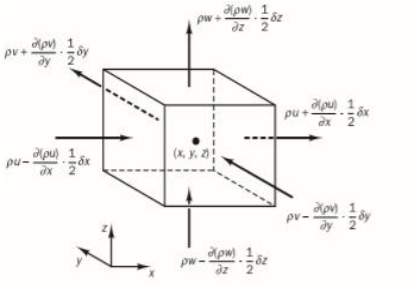

Fig.1.7, Infinitesimal Fluid element of mass transfer

The net rate of increase of fluid element is given by

$$\frac{\partial m}{\partial t} = \frac{\partial(\rho dv)}{\partial t} \qquad \text{Eq(1.25)}$$

$$\frac{\partial(\rho dv)}{\partial t} = \frac{\partial \rho}{\partial t}(\delta x \delta y \delta z) \qquad \text{Eq(1.26)}$$

Assuming inflow to the fluid element to be positive and outflow to be negative

The net flow rate into and out of the fluid element is given as

$$\left[\rho u-\frac{\partial(\rho u)}{\partial x}\frac{\delta x}{2}\right]\delta y\delta z-\left[\rho u+\frac{\partial(\rho u)}{\partial x}\frac{\delta x}{2}\right]\delta y\delta z$$
$$+\left[\rho v-\frac{\partial(\rho v)}{\partial y}\frac{\delta y}{2}\right]\delta x\delta z-\left[\rho v+\frac{\partial(\rho v)}{\partial y}\frac{\delta y}{2}\right]\delta x\delta z \qquad \text{Eq(1.27)}$$
$$+\left[\rho w-\frac{\partial(\rho w)}{\partial z}\frac{\delta z}{2}\right]\delta x\delta y-\left[\rho w+\frac{\partial(\rho w)}{\partial z}\frac{\delta z}{2}\right]\delta x\delta y$$

Therefore, equating equation 13 and 14, we obtain

$$-\left[\frac{\partial(\rho u)}{\partial x}+\frac{\partial(\rho v)}{\partial y}+\frac{\partial(\rho w)}{\partial z}\right]=\frac{\partial\rho}{\partial t} \qquad \text{Eq(1.28)}$$

$$\frac{\partial\rho}{\partial t}+\left[\frac{\partial(\rho u)}{\partial x}+\frac{\partial(\rho v)}{\partial y}+\frac{\partial(\rho w)}{\partial z}\right]=0 \qquad \text{Eq(1.29)}$$

$$\frac{\partial\rho}{\partial t}+\nabla.(\rho u)=0 \qquad \text{Eq(1.30)}$$

Equation 1.29 is an unsteady, three dimensional mass conservation or continuity equation.

In case of incompressible fluids like water, the density do not change with time and space and hence equation (1.29) can be reduced to

$$\nabla.\mathrm{u}=0 \qquad \text{Eq(1.30)}$$

In the long hand notation, the equation becomes

$$\frac{\partial u}{\partial x}+\frac{\partial v}{\partial y}+\frac{\partial w}{\partial z}=0$$

Rates of change following a fluid particle and for a fluid element

Let the value of a property per unit mass be denoted by Φ . The total or substantive derivative of Φ with respect to time following a fluid particle, written as D Φ /Dt, is

$$\frac{D\phi}{Dt}=\frac{d\phi}{dt}+\frac{d\phi}{dx}\frac{dx}{dt}+\frac{d\phi}{dy}\frac{dy}{dt}+\frac{d\phi}{dz}\frac{dz}{dt} \qquad \text{Eq(1.31)}$$

Here, dx/dt=u, dy/dt=v, dz/dt=w. and hence,

$$\frac{D\phi}{Dt} = \frac{d\phi}{dt} + u\frac{d\phi}{dx} + v\frac{d\phi}{dy} + w\frac{d\phi}{dz} \quad \text{Eq(1.32)}$$

$$\frac{D\phi}{Dt} = \frac{d\phi}{dt} + u.grad(\phi) \quad \text{Eq(1.33)}$$

Where u, v and w are velocity in the x, y, and z direction.

$\frac{D\phi}{Dt}$ Is a property that is defined as the property per unit mass. But, we are interested in developing equations of rates of change per unit volume. Therefore. By multiplying the term $\frac{D\phi}{Dt}$ by density, we can obtain rates of change per unit volume.

Therefore,

$$\rho\frac{D\phi}{Dt} = \rho\left[\frac{d\phi}{dt} + u.grad(\phi)\right] \quad \text{Eq(1.34)}$$

The generalization of these terms for an arbitrary conserved property is

$$\frac{\partial(\rho\phi)}{\partial t} + \nabla.\rho\phi u = 0 \quad \text{Eq(1.35)}$$

The above equation eq (1.35) expresses the rate of change in time of Φ per unit volume plus the net flow of Φ out of the fluid element per unit volume. It is now rewritten to illustrate its relationship with the substantive derivative of Φ.

$$\frac{\partial(\rho\phi)}{\partial t} + \nabla.\rho\phi u = \rho\left[\frac{\partial(\phi)}{\partial t} + \nabla.\phi u\right] + \phi\left[\frac{\partial(\rho)}{\partial t} + \nabla.\rho u\right]$$

$$\nabla.\phi u = \frac{\partial(\phi u)}{\partial x} + \frac{\partial(\phi v)}{\partial y} + \frac{\partial(\phi w)}{\partial z} \quad \text{Eq(1.36)}$$

$$\frac{\partial(\phi u)}{\partial x} + \frac{\partial(\phi v)}{\partial y} + \frac{\partial(\phi w)}{\partial z} = \left[u + v + w\right].\left[\frac{\partial(\phi)}{\partial x} + \frac{\partial(\phi)}{\partial y} + \frac{\partial(\phi)}{\partial z}\right]$$

$$\nabla.u\phi = u.\nabla\phi$$

But since the second term on the right hand side is the conservation of mass equation which is zero, therefore

$$\rho\frac{D\phi}{Dt} = \frac{\partial(\rho\phi)}{\partial t} + \nabla.\rho\phi u = \rho\left[\frac{\partial(\phi)}{\partial t} + u.\nabla\phi\right]$$

Eq(1.37)

The rate of increase of Φ In fluid **element**	+	the rate outflow from fluid element	=	The rate of increase of Φ fluid **particle**

1.1.7.G . Conservation of Momentum

The conservation of Momentum states that the sum of the rate of change of momentum on a fluid particle is equal to the sum of forces on the particle. This is basically Newton's second law.

Rate of change of Momentum On a fluid particle	=	Sum of forces on a fluid particle

Our property N is now momentum P. Therefore, P = m*u. Therefore, Φ is the velocity u since momentum is equal to mass times velocity.

From Reynolds's transport theorem, we can obtain

$$\frac{\partial}{\partial t}\int_{cv}\rho u dv + \int_{cs}\rho u.u.nds = 0$$

$$\int_{cv}\left[\frac{\partial(\rho u)}{\partial t} + \nabla.\rho uu\right] = 0 \qquad \text{Eq(1.38)}$$

X-Momentum	U	$\rho \frac{Du}{Dt}$	$\left[\frac{\partial(\rho u)}{\partial t} + \nabla.\rho uu\right]$
Y-Momentum	V	$\rho \frac{Dv}{Dt}$	$\left[\frac{\partial(\rho v)}{\partial t} + \nabla.\rho vu\right]$
Z-Momentum	W	$\rho \frac{Dw}{Dt}$	$\left[\frac{\partial(\rho w)}{\partial t} + \nabla.\rho wu\right]$
Energy	E	$\rho \frac{DE}{Dt}$	$\left[\frac{\partial(\rho E)}{\partial t} + \nabla.\rho Eu\right]$

Eq(1.38), which is the integral form is used for the fluid element.

For fluid particle, we can use the differential form as

$$\left[\frac{\partial(\rho u)}{\partial t} + \nabla.\rho uu\right] = 0 \qquad \text{Eq(1.39)}$$

But equation (1.39) deals with the rate of change of Momentum. Now we shall see the force components of the equation.

Types of Forces on Fluid particles

There are generally two types of forces on fluids.

Surface Forces: Are type of forces that are applied on surfaces(area). Some of the Surface forces pressure forces, viscous and the like.

Body Forces: Are type of forces that are applied on volumes. Some of the Body forces gravity forces, electromagnetic forces, centrifugal forces.

There are nine viscous stress terms as state of stress and one pressure term as can be seen on figure 1.8..

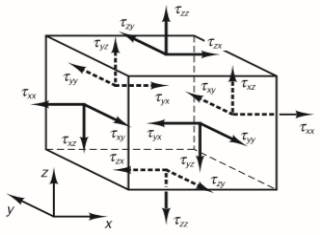

Fig.1.8 Infinitesimal Fluid element of momentum transfer with shear stress

The pressure, a normal stress, is denoted by p. Viscous stresses are denoted by τ . The usual suffix notation τ_{ij} is applied to indicate the direction of the viscous stresses. The suffices i and j in τ_{ij} indicate that the stress component acts in the j direction on a surface normal to the i-direction.

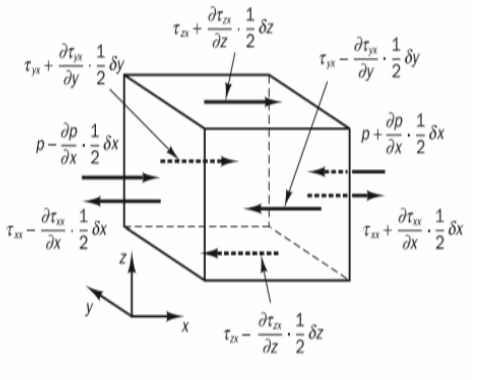

Fig.1.9 Infinitesimal Fluid element of momentum transfer with shear stress

Therefore, the summation of forces in the X direction is given below.

Summation for the Pressure term is given as

$$\left[\left[P-\frac{\partial P}{\partial x}\frac{\delta x}{2}\right]-\left[P+\frac{\partial P}{\partial x}\frac{\delta x}{2}\right]\right]\delta y\delta z \qquad \text{Eq(1.40)}$$

Equation 1.40 can be reduced to

$$-\frac{\partial P}{\partial x}\delta x\delta y\delta z \qquad \text{Eq(1.41)}$$

Similarly, for the viscous shear stress along the X-direction at the east and west sides is given as

$$\left[\left[\tau_{xx}+\frac{\partial \tau_{xx}}{\partial x}\frac{\delta x}{2}\right]-\left[\tau_{xx}-\frac{\partial \tau_{xx}}{\partial x}\frac{\delta x}{2}\right]\right]\delta y\delta z \qquad \text{Eq(1.42)}$$

$$\frac{\partial \tau_{xx}}{\partial x}\delta x\delta y\delta z \qquad \text{Eq(1.43)}$$

Similarly, for the viscous shear stress along the X-direction at the North and South sides is given as

$$\left[\left[\tau_{yx}+\frac{\partial \tau_{yx}}{\partial y}\frac{\delta y}{2}\right]-\left[\tau_{yx}-\frac{\partial \tau_{yx}}{\partial y}\frac{\delta y}{2}\right]\right]\delta x\delta z \qquad \text{Eq(1.44)}$$

$$\frac{\partial \tau_{yx}}{\partial y}\delta x\delta y\delta z \qquad \text{Eq(1.45)}$$

Again for the viscous shear stress along the X-direction at the Top and Bottom sides is given as

$$\left[\left[\tau_{zx}+\frac{\partial \tau_{zx}}{\partial z}\frac{\delta z}{2}\right]-\left[\tau_{yx}-\frac{\partial \tau_{zx}}{\partial z}\frac{\delta z}{2}\right]\right]\delta x\delta y \qquad \text{Eq(1.46)}$$

$$\frac{\partial \tau_{zx}}{\partial z}\delta x\delta y\delta z \qquad \text{Eq(1.47)}$$

Therefore, the Total net force per unit volume along the X-axis is given as

$$\frac{\partial(-P+\tau_{xx})}{\partial x}+\frac{\partial \tau_{yx}}{\partial y}+\frac{\partial \tau_{zx}}{\partial z} \qquad \text{Eq(1.48)}$$

Finally, the General Conservation of Momentum Equation is given as

$$\frac{\partial(-P+\tau_{xx})}{\partial x}+\frac{\partial \tau_{yx}}{\partial y}+\frac{\partial \tau_{zx}}{\partial z}=\rho\frac{Du}{Dx} \qquad \text{Eq(1.49)}$$

And the Final equation for X-Momentum is

$$\frac{\partial(-P+\tau_{xx})}{\partial x}+\frac{\partial \tau_{yx}}{\partial y}+\frac{\partial \tau_{zx}}{\partial z}+S_x=\frac{\partial(\rho u)}{\partial t}+\nabla.(\rho uu) \qquad \text{Eq(1.50)}$$

Similarly, Total Y-Momentum

$$\frac{\partial(\tau_{xy})}{\partial x}+\frac{\partial(-P+\tau_{yy})}{\partial y}+\frac{\partial \tau_{zy}}{\partial z}+S_y=\frac{\partial(\rho v)}{\partial t}+\nabla.(\rho uv) \qquad \text{Eq(1.51)}$$

And for the Z-Momentum

$$\frac{\partial(\tau_{xz})}{\partial x}+\frac{\partial(\tau_{yz})}{\partial y}+\frac{\partial(-P+\tau_{zz})}{\partial z}+S_z=\frac{\partial(\rho w)}{\partial t}+\nabla.(\rho uw) \qquad \text{Eq(1.52)}$$

The sign of the Pressure term is opposite to the stress term in the same direction because, normally, the sign convention for the normal tensile stress is positive. But, since the pressure term is compressive, their signs are opposite.

1.1.7.H. Energy Equation in three dimension

The energy equation is derived from the first law of thermodynamics, which states that the rate of increase of energy on a particle is equal to the sum of the net rate of heat addition on to the fluid particle and the work done on the particle.

Rate of Energy on a fluid particle = Net rate of heat added + Work done on a fluid particle

The rate of increase of Energy of fluid per unit volume is given as

$$\left[\frac{\partial(\rho E)}{\partial t}+\nabla.\rho Eu\right] = \rho\frac{DE}{Dt}$$

Work done on a Fluid Particle

Work done by the surface forces per unit volume are equal to the stress and pressure terms multiplied by the velocity. The sum of these terms (work done) can be obtained multiplying the terms we derived by the Momentum equation with the velocity components.

Pressure terms:-

$$-\left[\frac{\partial(pu)}{\partial x}+\frac{\partial(pv)}{\partial y}+\frac{\partial(pw)}{\partial z}\right]=-\nabla.(pu) \qquad \text{Eq(1.53)}$$

The work done due to the stresses is given as

Total surface stress = Stress in X-direction + Stress in the Y Direction + Stress in the Z Direction

$$\left[\frac{\partial(u.\tau_{xx})}{\partial x}+\frac{\partial(u.\tau_{yx})}{\partial y}+\frac{\partial(u.\tau_{zx})}{\partial z}\right]+\left[\frac{\partial(\mathrm{v}.\tau_{xy})}{\partial x}+\frac{\partial(\mathrm{v}.\tau_{yy})}{\partial y}+\frac{\partial(\mathrm{v}.\tau_{zy})}{\partial z}\right]+\left[\frac{\partial(\mathrm{w}.\tau_{xz})}{\partial x}+\frac{\partial(\mathrm{w}.\tau_{yz})}{\partial y}+\frac{\partial(\mathrm{w}.\tau_{zz})}{\partial z}\right] \qquad \text{Eq(1.54)}$$

Therefore, the total work done on a fluid particle can be given as

$$-\nabla.(pu)+\left[\frac{\partial(u.\tau_{xx})}{\partial x}+\frac{\partial(u.\tau_{yx})}{\partial y}+\frac{\partial(u.\tau_{zx})}{\partial z}\right]+\left[\frac{\partial(\mathrm{v}.\tau_{xy})}{\partial x}+\frac{\partial(\mathrm{v}.\tau_{yy})}{\partial y}+\frac{\partial(\mathrm{v}.\tau_{zy})}{\partial z}\right]+\left[\frac{\partial(\mathrm{w}.\tau_{xz})}{\partial x}+\frac{\partial(\mathrm{w}.\tau_{yz})}{\partial y}+\frac{\partial(\mathrm{w}.\tau_{zz})}{\partial z}\right] \quad \text{Eq (1.55)}$$

Energy Flux due to heat Conduction

The second component that contributes to the rate of Energy addition is the rate of heat flux.

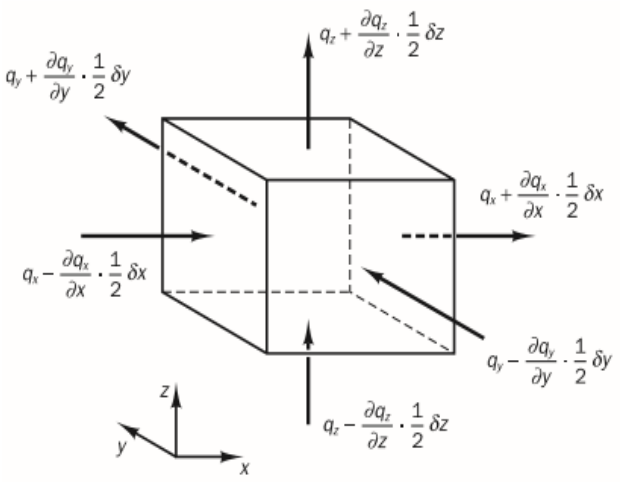

Fig.1.10 Infinitesimal Fluid element of heat energy

From fig(1.10), we can see the relation

$$-\frac{\partial q_x}{\partial x}-\frac{\partial q_y}{\partial y}-\frac{\partial q_z}{\partial z}=-\nabla.q \quad \text{Eq (1.56)}$$

But from Fourier's series, we can relate heat conduction to the temperature gradient as

$$q=-k\nabla T \quad \text{Eq (1.57)}$$

Therefore, the energy addition due to heat is given as

$$div(k.grad.T) \quad \text{Eq (1.58)}$$

Total Energy Equation

The energy equation mostly deals with the heat transfer analysis of a given system.

There are three main forms of energy namely, kinetic energy per unit mass $1/2(u^2+v^2+w^2)$, Internal (thermal) energy (i), and gravitational potential Energy. The gravitational potential energy can be regarded as a source term as it does work when the fluid pass through a gravitational field.

As derived earlier, the energy equation is given as

$$\rho\frac{DE}{Dt} = -\nabla.(pu) + \left[\frac{\partial(u.\tau_{xx})}{\partial x} + \frac{\partial(u.\tau_{yx})}{\partial y} + \frac{\partial(u.\tau_{zx})}{\partial z}\right] + \left[\frac{\partial(\mathrm{v}.\tau_{xy})}{\partial x} + \frac{\partial(\mathrm{v}.\tau_{yy})}{\partial y} + \frac{\partial(\mathrm{v}.\tau_{zy})}{\partial z}\right] + \left[\frac{\partial(\mathrm{w}.\tau_{xz})}{\partial x} + \frac{\partial(\mathrm{w}.\tau_{yz})}{\partial y} + \frac{\partial(\mathrm{w}.\tau_{zz})}{\partial z}\right] + div(k.grad.T) + \mathrm{SE} \quad \text{Eq (1.59)}$$

The mass and momentum conservation equations are solved for flow equations. Alongside them, energy equation is solved for heat transfer problems.

1.1.7.I. Navier-Stokes Equation

The Navier- Stokes equation is a general equation that is used to solve properties of fluid flow. It is basically the general conservation of momentum equation with the force (stress terms) are more complicated and include viscosity terms as the viscosity induce stress on fluid particles.

One basic assumption here is that the fluid is considered isotropic. It does not behave differently at different points in nature.

In many fluid flows the viscous stresses can be expressed as functions of the local deformation rate or strain rate. In three-dimensional flows the local rate of deformation is composed of the linear deformation rate and the volumetric deformation rate.

And hence, the deformations can be found as

$$S_{xx} = \frac{\partial u}{\partial x},\ S_{yy} = \frac{\partial v}{\partial y} \text{ and } S_{zz} = \frac{\partial w}{\partial z} \quad \text{Eq (1.59)}$$

These are the main stress terms.

For the linear shearing terms, which we have six of them, we have

$$S_{xy} = S_{yx} = \frac{1}{2}\left[\frac{\partial u}{\partial y} + \frac{\partial v}{\partial x}\right],\ S_{yz} = S_{zy} = \frac{1}{2}\left[\frac{\partial v}{\partial z} + \frac{\partial w}{\partial y}\right], \text{ and } S_{xz} = S_{zx} = \frac{1}{2}\left[\frac{\partial u}{\partial z} + \frac{\partial w}{\partial x}\right] \quad \text{Eq (1.60)}$$

The volumetric deformation can be obtained by

$$\frac{\partial u}{\partial x}+\frac{\partial v}{\partial y}+\frac{\partial w}{\partial z}=div(u)$$ Eq (1.61)

In fluid flow, there are two viscous term constants of proportionality, namely the linear viscous term (μ), and the volumetric viscous constant (λ). But the volumetric viscosity constant can be considered negligible.

$$\tau_{xx}=\left[2\mu\left[\frac{\partial u}{\partial x}\right]\right]+\lambda\nabla.u \;,\; \tau_{yy}=\left[2\mu\left[\frac{\partial v}{\partial y}\right]\right]+\lambda\nabla.u \text{ and } \tau_{zz}=\left[2\mu\left[\frac{\partial w}{\partial z}\right]\right]+\lambda\nabla.u$$ Eq (1.62)

And for the linear shearing viscous stresses, we obtain

$$\tau_{xy}=\tau_{yx}=\mu\left[\frac{\partial u}{\partial y}+\frac{\partial v}{\partial x}\right], \tau_{yz}=\tau_{zy}=\mu\left[\frac{\partial v}{\partial z}+\frac{\partial w}{\partial y}\right] \text{ and } \tau_{xz}=\tau_{zx}=\mu\left[\frac{\partial u}{\partial z}+\frac{\partial w}{\partial x}\right]$$ Eq (1.63)

Inserting the general terms into the Navier stokes equation in the three dimensions yields,

$$\rho\frac{Du}{Dt}=-\frac{\partial p}{\partial x}+\left[\frac{\partial}{\partial x}\left[2\mu\frac{\partial u}{\partial x}+\lambda\nabla.u\right]\right]+\frac{\partial}{\partial y}\left[\mu\left[\frac{\partial u}{\partial y}+\frac{\partial v}{\partial x}\right]\right]+\frac{\partial}{\partial z}\left[\mu\left[\frac{\partial u}{\partial z}+\frac{\partial w}{\partial x}\right]\right]+S_x$$

$$\rho\frac{Dv}{Dt}=-\frac{\partial p}{\partial y}+\frac{\partial}{\partial x}\left[\mu\left[\frac{\partial u}{\partial y}+\frac{\partial v}{\partial x}\right]\right]+\left[\frac{\partial}{\partial y}\left[2\mu\frac{\partial v}{\partial y}+\lambda\nabla.u\right]\right]+\frac{\partial}{\partial z}\left[\mu\left[\frac{\partial v}{\partial z}+\frac{\partial w}{\partial y}\right]\right]+S_y$$ Eq (1.64)

$$\rho\frac{Dw}{Dt}=-\frac{\partial p}{\partial z}+\frac{\partial}{\partial x}\left[\mu\left[\frac{\partial u}{\partial z}+\frac{\partial w}{\partial x}\right]\right]+\frac{\partial}{\partial y}\left[\mu\left[\frac{\partial w}{\partial y}+\frac{\partial v}{\partial z}\right]\right]+\left[\frac{\partial}{\partial z}\left[2\mu\frac{\partial w}{\partial z}+\lambda\nabla.u\right]\right]+S_z$$

Therefore, from this equation, we can rearrange the terms to obtain

$$\frac{\partial}{\partial x}\left[\mu\frac{\partial u}{\partial x}\right]+\frac{\partial}{\partial y}\left[\mu\frac{\partial u}{\partial y}\right]+\frac{\partial}{\partial z}\left[\mu\frac{\partial u}{\partial z}\right]$$

$$+$$ Eq (1.65)

$$\frac{\partial}{\partial x}\left[\mu\frac{\partial u}{\partial x}\right]+\frac{\partial}{\partial y}\left[\mu\frac{\partial v}{\partial x}\right]+\frac{\partial}{\partial z}\left[\mu\frac{\partial w}{\partial x}\right]+\lambda\nabla.u=[S_x]$$

Equation 1.65 can be summarized as

$$=\nabla.(\mu\nabla U)+Sx$$ Eq (1.66)

Therefore, the general Navier Stokes equations in three dimensions can be written as

$$\rho\frac{Du}{Dt}=-\frac{\partial P}{dx}+\nabla.(\mu\nabla U)+S_x$$

$$\rho\frac{Dv}{Dt}=-\frac{\partial P}{dy}+\nabla.(\mu\nabla V)+S_y \qquad \text{Eq (1.67)}$$

$$\rho\frac{Dw}{Dt}=-\frac{\partial P}{dz}+\nabla.(\mu\nabla W)+S_z$$

1.1.7.J. The Transport Equation

The Transport equation traces the transport of a flow property Φ, which can be pollutants or temperature. The differential form of the Transport Equation can be written as

$$\frac{\partial(\rho\phi)}{\partial t}+\nabla.(\rho\phi u)=\nabla.(\Gamma\nabla\phi)+\mathrm{S_x} \qquad \text{Eq (1.68)}$$

The first term, $\frac{\partial(\rho\phi)}{\partial t}$ mentions the rate of increase of ϕ in a fluid element. The second term is a convective term that represents convective outflow transport. The third term to the right of the equality sign is a diffusive transport term to mean rate of increase of ϕ due to diffusion.

The last term is the increase of ϕ in a fluid element due to production from the source.

The vorticity stream function is a method of reducing unknowns and solving the Navier-Stokes equation.

Generally, for a two dimensional flow, we usually use three equations, two momentum equations in X and Y directions and one is Conservation of mass (Continuity equation) for case of incompressible flow.

$$\frac{\partial u}{\partial x}+\frac{\partial v}{\partial y}=0 \qquad \text{Eq (1.69 A)}$$

$$\frac{du}{dt}+u\frac{\partial u}{\partial x}+v\frac{\partial u}{\partial y}=-\frac{1}{\rho}\frac{\partial P}{dx}+\nu\frac{\partial^2 u}{\partial x^2}+\nu\frac{\partial^2 u}{\partial y^2}+S_{mx} \text{ and} \qquad \text{Eq (1.69 B)}$$

$$\frac{dv}{dt}+u\frac{\partial v}{\partial x}+v\frac{\partial v}{\partial y}=-\frac{1}{\rho}\frac{\partial P}{dy}+\nu\frac{\partial^2 v}{\partial x^2}+\nu\frac{\partial^2 v}{\partial y^2}+S_{my} \qquad \text{Eq (1.69 C)}$$

Here, in Eq 1.69, we have three equations and three unknowns namely u,v and P. But, we can reduce the number of equations and the number of unknowns.

To do that, we can introduce a vorticity term.

$$\omega=\nabla\times U \qquad \text{Eq (1.70)}$$

$$U=f_n(u,v,w,t)$$

The vorticity term has three components,

$$\omega_x = \frac{\partial w}{\partial y} - \frac{\partial v}{\partial z}, \omega_y = -\left[\frac{\partial u}{\partial z} - \frac{\partial w}{\partial x}\right], \text{and } \omega_z = \frac{\partial v}{\partial x} - \frac{\partial u}{\partial y} \quad \text{Eq (1.71)}$$

Here, ω_x and ω_y contain terms varying with respect to Z, which we are not considering. Therefore, we shall take ω_z since it is valid and have variations X and Y, and not Z.

Therefore, differentiating the whole Y momentum equation with respect to X and the X momentum equation with respect to Y,

$$\frac{\partial(\mathrm{x}-momentum)}{\partial y} - \frac{\partial(\mathrm{y}-momentum)}{\partial x} \quad \text{Eq (1.72)}$$

and finally subtracting it yields,

$$\frac{dw}{dt} + u\frac{\partial w}{\partial x} + v\frac{\partial w}{\partial y} = \nu\frac{\partial^2 w}{\partial x^2} + \nu\frac{\partial^2 w}{\partial y^2} + S_{mx} \quad \text{Eq (1.73)}$$

Now let us introduce stream function to reduce the number of equations and unknowns. The Stream function combines velocity components u and v into one variable ψ. Let

$$u = \frac{\partial \psi}{\partial y} \text{ and } v = -\frac{\partial \psi}{\partial x} \quad \text{Eq (1.74)}$$

Substituting equation (1.74) into (1.73), we obtain a single equation

$$\frac{\partial(\nabla^3\psi)}{\partial t} + \frac{\partial \psi}{\partial y}\frac{\partial(\nabla^2\psi)}{\partial x} - \frac{\partial \psi}{\partial x}\frac{\partial(\nabla^2\psi)}{\partial y} = \nu\left[\nabla^4\psi\right] \quad \text{Eq (1.75)}$$

Which is a final vorticity stream function.

1.1.7.K. BOUNDARY LAYER THEORY

When a fluid is flowing over a body, or when a solid is passing through a stationary fluid like in the case of a plane wing moving through air, two regions show themselves. One is the outer region, where viscosity and friction are negligible. The other region is found in a very close vicinity to the solid wall, called the Boundary layer, and is dominated by viscosity and friction.

The Boundary layer is very important area of study in areas of aerodynamics, drag and lift on automobiles, planes and aircrafts, wind blades and so on. Computing drag and lift helps the industry of automobiles especially, to determine the number of cylinders that can overcome the drag to attain a certain maximum velocity. There are so many applications for the Boundary layer flow.

One thing to note is that, practically in Boundary layer flow, is that velocity of the fluid particles at the surface of the solid is zero, if the fluid is stationary, and takes the velocity of the plate if the plate is moving.

Reynolds number is a very important parameter in the study of Boundary Layer. It relates the inertial term to the viscous term. Below is the derivation of the Reynolds's Number parameter.

Simplified Navier-Stokes Equation

Prandtl, in his paper presented in 1904, suggested that most of the Navier Stokes equation can be neglected in the boundary layer theory. The simplified Navier-Stokes equation is

$$u\frac{\partial u}{\partial x}+v\frac{\partial u}{\partial y}=\nu\frac{\partial^2 u}{\partial y^2} \qquad \text{Eq (1.76)}$$

Besides the simplified Navier Stokes equation, we use the Conitnuity equation in 2-D

$$\frac{\partial u}{\partial x}+\frac{\partial u}{\partial y}=0 \qquad \text{Eq (1.77)}$$

And the thermal boundary layer equation which shall be discussed I later

$$\rho Cp\left[u\frac{\partial T}{\partial x}+v\frac{\partial T}{\partial y}\right]=k\frac{\partial^2 T}{\partial y^2}+\mu\left[\frac{\partial u}{\partial y}\right]^2 \qquad \text{Eq (1.78)}$$

With accompanying Boundary Conditions

$u = v = 0, \partial T/\partial y = 0$ at $y = 0$ Eq (1.79)

$u/U \rightarrow 1$, $T0/T \rightarrow 1$ as $y \rightarrow \infty$

Boudary Layer Thickness

As seen previously, the Boundary Layer Thickness is a region on a Boundary layer where the viscous and frictional forces are dominant. Here, we consider the fluid velocity to be the free stream velocity U_∞ and the depth Y to be the Boundary Layer thickness (δ) for the frictional component.

Exactly at the boundary layer where the boundary and external layers meet, the frictional and the inertial forces are very close. So

IF ~ FF

$\frac{\rho U_\infty{}^2}{L}=\frac{\mu U_\infty}{\delta^2}$, and finally we obtain Eq (1.80)

$$\delta=\sqrt{\frac{\mu L}{\rho U_\infty}} \qquad \text{Eq (1.81)}$$

Replacing L with a horizontal distance x where L=max(X), we obtain

$$\delta = \sqrt{\frac{\upsilon x}{U_\infty}}$$ Eq (1.82)

Self-Similar Boundary Layer Equation for Flow

At high Reynolds number, in a very thin flat plate flow, Viscosity is confined within a thin boundary layer next to the body surface. Here the governing equations are derived from the famous Navier-Stokes equation assuming a very small δ in relation to L. We now introduce a similarity variable η to non dimensinalize y, which is y/δ, such that

$$\eta = y\sqrt{\frac{U_\infty}{\nu x}}$$ Eq (1.83)

The value of stream function ψ can be obtained by integrating the continuity equation as follows

$$\psi = \sqrt{\upsilon x U_\infty}\, f(\eta)$$ Eq (1.84)

Where f(η) denotes the stream function.

Therefore, the velocity components U and V are given by

$$u = \frac{\partial \psi}{\partial y} = \frac{\partial \psi}{\partial \eta}\frac{\partial \eta}{\partial y} = U_\infty f'(\eta)$$ and Eq (1.85)

$$v = -\frac{\partial \psi}{\partial x} = \frac{1}{2}\sqrt{\frac{U_\infty \upsilon}{x}}\left[\eta f'(\eta) - f(\eta)\right]$$ Eq (1.86)

Inserting U and V into equation (1.76), we obtain

$$-\frac{U_\infty^{\,2}}{2x}\eta f' f'' + \frac{U_\infty^{\,2}}{2x}\eta(f' - f) f'' = \upsilon\frac{U_\infty^{\,2}}{xv} f'''$$ Eq (1.87)

After simplification, we obtain the Blasius equation

$$ff'' + 2f''' = 0$$ Eq (1.88)

1.1.7.L. Thermal Boundary Layer

Let us consider a flow over a flat plate. Frictional forces between the plate (Solid Body) and the fluid arise, which in turn cause heat and gives rise to a thermal boundary layer.

The temperature profile (heat dissipation) in the boundary layer resembles that of fluid flow. It maintains the same shape as of the flow boundary layer. The thermal boundary, unlike that if the flow boundary, at the plate, the temperature is higher.

The governing equations for the flow and thermal boundary layer is given as

$$\frac{\partial u}{\partial x} + \frac{\partial v}{\partial y} = 0$$

$$u\frac{\partial u}{\partial x} + v\frac{\partial u}{\partial y} = \nu\frac{\partial^2 u}{\partial y^2} \qquad \text{Eq (1.89)}$$

$$\rho cp\left[u\frac{\partial T}{\partial x} + v\frac{\partial T}{\partial y}\right] = k\frac{\partial^2 T}{\partial y^2} + \mu\left[\frac{\partial u}{\partial y}\right]^2$$

$$u = v = \frac{\partial T}{\partial y} = 0 \; at \; y = 0 \qquad \text{Eq (1.90)}$$

$$u \to U \; , \; T \to T_1 \; as \; y \to \infty$$

To solve the energy equation we first obtain expressions for velocity components from the Blasius solution, subject to their three boundary conditions stated above. Substituting u and v into (1.89 C) in terms of the similarity variables η and f, and introducing a dimensionless temperature difference θ (η) defined by

$$\theta = \frac{T - T_1}{U^2 / 2cp} \qquad \text{Eq (1.95)}$$

And we obtain

$$\frac{d^2\theta}{d\eta^2} + 0.5Pr * f * \frac{d\theta}{d\eta} = -2Pr\left(f''\right)^2 \qquad \text{Eq (1.96)}$$

Subjected to dimensionless Boundary Conditions given as

$$\frac{d\theta}{d\eta} = 0 \; at \; \eta = 0$$

$$\theta \to 0 \; at \; \eta \to \infty \qquad \text{Eq (1.97)}$$

1.2. Literature Review

The study of heat transfer analysis of fins has been seen to catch attention of many researchers.

Various studies have been and are being conducted to create the most convenient, effective , efficient and economical fins. Practically, various fins with different thermal and geometric properties (Thermo-Geometric properties) are used.

Aziz and Enamul-Huq [1] were able applied perturbation expansion in order to examine pure convection fin with temperature reliant on thermal conductivity. Later on, a research done by Aziz [2] was able to extend the study to comprise uniform internal heat generation within the fin.

Chowdhury and Hashim[3], in their research, employed the Adomian decomposition technique in order to assess the temperature circulation of a straight rectangular fins with temperature reliant on surface flux for all plausible transfers of heat.

Khani and Aziz[4] contemplated a trapezoidal fin which comprises both the convection heat transfer coefficient and the thermal conductivity in which there occurs an alteration as a function of temperature and were able to convey a diagnostic solution engendered by using the homotopy analysis method (HAM). Another notable finding came through Hosseini et al.[6] in which the application of HAM was put to use to provide a ballpark estimate to heat transfer in fins and temperature-dependent internal heat generation and thermal conductivity. Moitsheki et al [7] was able to employ lie symmetry analysis to deliver precise solutions to the problems concerning fin with a power-law temperature-dependent thermal conductivity. Inadequate researches were fundamentally focused to the analysis of heat transfer within fins with a temperature-dependent internal heat generation, and also heat transfer coefficient and thermal conductivity are not widely stated in literatures as well.

Dynamical Analysis for stability study has been done on finding asymptotic answers for heat transfers through a rectangular longitudinal fin. Among the few, the researches done by Harley and Motikeshi [8] and Motikeshi and Harley [9] have been able to mention the influence of thermo geometric parameter(M) with the length of the fin(L) which is observed to be directly proportional($M \propto L$).

M.G. Sobamowo[10] studied the thermal properties of lingitudinal fins with a source term (Internal Heat generation parameter) using Galerkin's method.

Since convection is the main heat dissipation mechanism of Heat Sinks, many previous investigations focused primarily on the convective parameters around the heat sink. For example, in recent studies [11-14], because of their higher cooling capabilities, Nano fluids are used as ambient fluids dissipation in order to increase the rate of convective heat transfer from the heat sink to coolant fluid of the heat sinks. In addition, some studies [15-18] considered properties of conventional airflow and features of channel cross section. Further studies were conducted on the Effects of various geometric parameters on the performance of the heat sink are studied [19-23]. The main idea of this research revolves around the effects of using FGMs (impact of Heterogeneity) on the performance of Heat sinks in comparison to the traditional (conventional) heat sinks. In computers, either Longitudinal or pin-shape fins of heat sinks are generally used.

To enhance the thermal performance of heat sinks, using heterogeneous material or functionally graded materials (FGM) is suggested in some literatures. In FGM, different materials are used to enhance the performance of the heat sinks, with varying materials along a specific axis.

Since the application of first type, namely longitudinal fin is more common in comparison to the pin type heat sinks, this study deals to study on such heat sinks, which are made by longitudinal fins. In fact, in the present research, the conventional homogeneous fin material of heat sink is replaced with Functionally Graded Material (FGM).

Japan was the first country to use the concept of FGM to enhance thermal performance in 1984 for a space plane project. When entering the earth's atmosphere from an outer space, there is a large thermal increment in the temperature which can cause thermal explosion. Therefore, due to the continuous demand to enhance thermal performance in this area, Japan used FGM to address this difficulty. Since then, FGM has been used in different areas like heat shielding of satellites, engines, nuclear and so on.

FGM are also used in thermal stress control of curved geometries for Linear, power and exponential functions [25-26].

FGM is considered for devices with higher thermal sensitivity like heat sinks are considered in [27]. Their thermal property and energy saving are also studied analytically for Linear and Power Law.

Different and many studies have been conducted in the area of entropy generation on Boundary layer flow.

In 1908, Henrich Blasius [28], doctoral student of Prandtl, used Power series method to solve Boundary layer problem. Howarth[29] used numerical method of Runge-Kutta to solve the Blasius equation by hand.

Following these breakthrough, numerous studies have been conducted like [30-31].

Impacts of thermal radiation on the Boundary layer flow is an important concept and has numerous application areas like in Nuclear Power plants, Thermal Energy storages etc.

Hossain et al [32,33] studied the impact if thermal radiation on free convection over a porous vertical plate. He approximated the thermal radiation using Rosseland's approximation. Cortell [35] also studied the impact of Radiation on Blasius flow. Raptis et al [34] analyzed radiation in Magneto -Hydrodynamic flows.

In Thermodynamic analysis, it is important to avoid the energy loss or irreversibility of energy in order to enhance the thermal performance of the system. This can numerically be quantified as Entropy generation. Entropy is the measure of destructed energy that cannot be used to do work. Therefore, the main focus of engineering in relation to this area is to reduce the entropy generated in the system. This is called the Entropy Generation Minimization.

Enropy generation in fluid flow was initially studied by Bejan[36]. Yilbas et al [37] studied entropy generation in a semi-blocked pipe including the swirling effect. Arpaci [38] studied entropy generation due to radiation. Abu–Hijleh et al [39] studied entropy generation due to natural convection from a heated horizontal isothermal cylinder in oil. In his paper, Mahmud [40] applied second law analysis to basic convective heat transfer problems in non-Newtonian fluid flow through a channel made of two parallel plates.

Adnaan Saeed Butt [42] studied Entropy generation in the Blasius flow under thermal radiation. In this paper, modification to [42] has been made with an altered Boundary condition for the thermal aspect of the boundary layer flow.

Moving Boundary flow is a famous field of study and is important in metal and plastic industries as can be seen in [43-44]. Sakiadis [45] carried out a pioneering work in in boundary layer flow on a stretching surface with a constant speed. Tsou et al. [46] extended the work by experimentally verifying it. Several studies have been conducted using the boundary conditions [47-55]. Most solutions use boundary layer assumptions and are not exact solutions except for [47].

Miklavcic and Wang [56] investigated flow over a shrinking sheet. This solution is an exact solution of the Navier-Stokes equation.

The shrinking sheet problem was also extended to power-law shrinking velocity or other fluids [21–23].

Magneto-Hydrodynamic flow over a shrinking sheet was studied by Sajid [60]. Tiegang Fang * and Ji Zhang studied the closed form exact solution of Magneto hydrodynamics viscous flow over a shrinking sheet.

Boundary layer flow of a conducting incompressible viscous fluid due to deformation of an elastic surface in uniformly applied magnetic field is studied by Pavlov [62]. Andersson [63] studied MHD viscous flow over a stretching plate and demonstrated the effect of magnetic field having the same effect as of viscoelasticity. Heat and mass transfer of viscous fluid in an electrically conducting fluid demonstrating that MHD decreases the boundary layer thickness has been show in studies. [64-67].

Hayata et al.[68] studied two dimensional magneto hydrodynamic boundary layer flow in a porous media using Homotopy Analysis Method (H.A.M.) to solve the governing ODEs.

Xu et al. [69] employed Homotopy Analysis Method to study the Boundary Layer Flow and Heat transfer of viscous flow of an electrically conductive flow. The paper demonstrated application of magnetic field reduces the Boundary layer thickness but reduces the Thermal Boundary layer.

The study of fluid flows and mass transfer problems has significant applications in a wide variety of geophysical and engineering application such as flow of ground water energy storage and chemical reactors (Nield and Bejan [70])

Ramesh B. Kudenatti,1 Shreenivas R. Kirsur,2 Achala L. Nargund,3 and N. M. Bujurke4 [71] studied

Similarity Solutions of the MHD Boundary Layer Flow Past a Constant Wedge within Porous Media.

Numerous studies have been conducted in the area of stagnation point flow and Nano fluids.

Hiemenz [72] is considered the first to study the two dimensional stagnation point flow over a stationary plate. He use the Similarity method to reduce the Navier Stokes into nonlinear ODEs. Homann [73] extended the problem to axisymmetric stagnation point flow. Mahapatra and Gupta [74] studied stagnation point flow past a stretching sheet.

Wang [76] investigated two-dimensional axisymmetric stagnation flow towards a shrinking sheet in a viscous fluid. This research became an eye opening to the area of stagnation point flow towards stretching/shrining sheet and many researches were produced afterwards, [77, 80] to mention a few.

All of the above fluids mentioned above are Newtonian and viscous. Most fluids like water, ethylene glycol, and engine oil have limited heat transfer properties. Therefore, in order to enhance the thermal conductivity, studies have been conducted to introduce nanoparticles. Solids, such as metals, on the other hand have higher thermal conductivity to that of liquids. Therefore, it was obvious to introduce solid nanoparticles at create suspension Nano fluids which have superior to the base fluids alone.

Background of Nano fluids has many industrial application in the areas of engine cooling systems, electronics, nuclear cooling systems and biomedical applications.

Nano fluids are widely studied in various literatures [77-91]. . The paper by Khan and Pop [28] is the first which considered the problem on stretching sheet in Nano fluids.

Another model have been used in the study conducted by in several papers [92-101]. Norfifah Bachok1, Anuar Ishak2* and Ioan Pop [102] used this model to study stagnation point flow of Cu, Al2O3 and TiO2 over a stretching/shrinking sheet

Norfifah Bachok1, Anuar Ishak2* and Ioan Pop [102] studied Stagnation-point flow over a stretching/shrinking sheet in a Nano fluid with Pr=6.2.

Some studies have been conducted in the area of thermal explosion. Evaluation of criticality of explosiveness of chemical reactions mathematically has been conducted in [103] and [104].

Formulation of the problem was first introduced by Frank-Kamenetskii ([104]).Reactant consumption is neglected in the formulation. Analytical methods of solving thermal explosion problem are indicated in previous studies [105-107].

O.D. Makinde [108] employed Analytical and Dynamical Analysis of thermal explosion to solve for the criticality of thermal explosion.

This study uses Numerical method and Dynamical systems analysis to solve the problems.

1.3. Statement of the Problem

Modelling single physics and multi physical problems in the area of fluid mechanics and heat transfer problems usually ends up in higher order nonlinear differential equations.

Obtaining solutions for these resulting differential equations and describing solutions in accordance to the physics of the problems is considered the problem of this thesis.

1.4. Aim of the Study

The aim of this study is to employ numerical solutions, and in case of second order ODEs, dynamical systems analysis for higher order ODEs resulting from modelling of single physics and multi physical problems in the realm of fluid mechanics and heat transfer problems.

1.5. Methodology

For the numerical study, the Shooting secant method is used together with the Fourth order Runge-kutta method for problems in the following chapters to solve the resulting nonlinear BVPs.
The Shooting method coverts the BVP into IVPs by using guesses for the unknowns and iterating the process to obtain end boundary condition until a specific convergence criteria is reached between the end condition obtained from the guess and the actual end condition from the Boundary condition.
Assume the following second order BVP,

$$y'' = f(x, y, y'), y(a) = \alpha \text{ and } y(b) = \beta \qquad \text{Eq (1.94)}$$

In domain [a, b] where $a < b$
Assume the following Boundary value problem.

Taking initial guess ρ for $y'(a)$, the converted IVP will have the form

$$y''(x) = f(x, y, y'), y(a) = \alpha, y'(a) = \rho \quad \text{Eq (1.95)}$$

Assuming by applying the Runge-Kutta to obtain end condition using ρ as an initial condition as δ (b), check convergence criterion as

$$\varepsilon = \beta - \delta(b) \text{ and } \varepsilon <= Error\_Tolerance \quad \text{Eq (1.96)}$$

The method of Fourth order Runge-Kutta is used as a root finding technique and is given as

$$y_{n+1} = y_n + \frac{h}{6}\left[k_1 + 2k_2 + 2k_3 + k_4\right], \quad \text{Eq (1.97)}$$

Where

$$\begin{aligned} k_1 &= f(x_n, y_n), \\ k_2 &= f\left(x_n + \frac{h}{2}, y_n + \frac{hk_1}{2}\right), \\ k_3 &= f\left(x_n + \frac{h}{2}, y_n + \frac{hk_2}{2}\right), \\ k_4 &= f(x_n + h, y_n + hk_3). \end{aligned} \quad \text{Eq (1.98)}$$

A MATLAB code (script) by the author has been developed to solve the BVPs in the following Chapters.

Steps taken

Using the above nomenclature,

Step 1: Make an Initial Guess for the Unknown condition to obtain an IVP guess1 (ρ).

Step 2: Apply the method of RK4 to obtain an end condition 'Strike_1' to obtain a second guess 'guess2', Note that the secant method has been employed to fine tune the guess and the secant method requires two initial guesses

For the entire domain with some grid spacing.

Step 3: Use Linear interpolation to obtain guess2.

Guess2 = guess1 + (β- Strike_1)/ (b-a)

Step 4: Start Loop since the third guess is an iteration process

Step 5: Having two guesses, end condition (strike_2) can be predicted again by using RK4 method

Step 6: After obtaining strike_2, a secant method is used to obtain the third guess, guess3

guess3= guess2 – (Strike_2 – β)*(guess2-guess1) /(Strike_2 – Strike_1)

Step 7: Assign guess3 to guess2 and guess2 to guess1 and Strike_3 to Strike_2 and Strike_2 to Strike_1

Step 8: Convergence check, Check if abs (Strike_2- β) < tolerance, if so break the loop, else break.

Tools Used

For solving problems numerically in this Thesis, MATLAB software has been used. For the Dynamical analysis, PPlane 9 i.e. a MATLAB external package prepared for dynamical study has been used.

MATLAB app designer has been used to make the GUI for fins. MS Excel and MS Word have been used for the tables and the whole documentation.

Chapter Two:

Numerical and Qualitative Features of a Longitudinal Fin with Temperature – Dependent Properties with Internal Heat Generation

2.1. Background

Mechanical devices such as air conditioner,cylinders in automobiles, processors in computers,electronic chips,oil pipelines and such generate a high amount of heat which can result in inefficiency and decrease in performance. Therefore, heat generated wiithin these equipments need to dissipate the heat inorder for them to work properly. So they use surface extensions, ussually called fins, to dissipate the heat into another fluid medium, be it air or liquid, mainly through convection.

Various studies have been and are being conducted to create the most convinient, effective , efficient and economical fins.practically, various fins with different thermal and geometric properties (Thermo-Geometric properties) are used. Fins can be circular or rectangular in shape, they can be made of Aluminum and Copper in thermal properties. But due to its convinience, economy and larger convective area, the Rectangular longitudinal fin is favored over the Circular one.

In the study of fins, in problems where temperature between the Tip of the fin and the base of the fin is not large, linear approach is generally used. But if large,the thermal parameters (Convective and conductive heat transfer coefficients) shall be functions of temperature, rather than constants as in the case mentioned earlier.Two approaches(Linear and Power Law) dependencies exist. In this case, It can be difficult to obtain an analytical results.

Internal heat generation is of a practical importance in cases where other forms of energy are present, in cases of electrical current carrying conductors,nuclear rods or any other heat generating electrical equipments. It is useful to analyze where conversion of energy from one form of energy to thermal energy is present, which is considered as a source term for heat.

During the previous years, the results of the highly nonlinear differential equations were partaken by means of diverse procedures. Aziz and Enamul-Huq [1] were able to apply regular perturbation expansion in order to examine pure convection fin with temperature reliant on thermal conductivity. Later on, a research done by Aziz [2] was able to extend the study to comprise uniform internal heat generation within the fin.

Chowdhury and Hashim[3], in their research, were able to apply the Adomian decomposition technique in order to assess the temperature circulation of a straight rectangular fins with temperature reliant on surface flux for all plausible transfers of heat.

Khani and Aziz[4] contemplated a trapezoidal fin which comprises both the convection heat transfer coefficient and the thermal conductivity in which there occurs an alteration as a function of temperature and were able to convey a diagnostic solution engendered by using the homotopy analysis method (HAM). Another notable finding came through Hosseini et al.[6] in which the application of HAM was put to use to provide a ballpark estimate to heat transfer in fins and temperature-dependent internal heat generation and thermal conductivity. Moitsheki et al [7] was able to employ lie symmetry analysis to deliver precise solutions to the problems concerning fin with a power-law temperature-dependent thermal conductivity. Inadequate researches were fundamentally focused to the analysis of heat transfer within fins with a temperature-dependent internal heat generation, and also heat transfer coefficient and thermal conductivity are not widely stated in literatures as well.

With regards to the Qualitative analysis (dynamical analyses) diminutive work has been done on finding asymptotic answers for heat transfers through a rectangular longitudinal fin. Among the few, the researches done by Harley and Motikeshi [8] and Motikeshi and Harley [9] have been able to mention the influence of thermo geometric parameter(M) with the length of the fin(L) which is observed to be directly proportional(M∝L).

M.G. Sobamowo[10] studied the thermal properties of lingitudinal fins with a source term (Internal Heat generation parameter) using Galerkin's method. In this chapter, I have tried to implement the Shooting Secant method [5] to verify the results from [10]. I have also implemented dynamical systems further understand the stability of the system[10（2）].

2.2. Problem Formulation

Assumptions used for this chapter are

1.The heat flow in the fin is dependent on one dimensional spatial domain. Properties donot vary with time.

2. The temperature of the base of the fin and the ambient are constant.

3. No resistance between fin base and prime surface.

4. Thickness of the fin is neglibible as compared to width and length

5. The fin at the tip is insulated (flux at the tip is zero)

Using the above assumptions, consider a temperature dependent Thermal conductivity K(T),convective heat transfer h(T), base temperature(TB), Ambient Temperature(T ∞), thickness(δ), internal heat generation parameter q(T), as shown in fig 1.1. For the horizontal dimension X, the distance starts at zero which I steh Fin Tip and goes to one, which is the base of the fin.

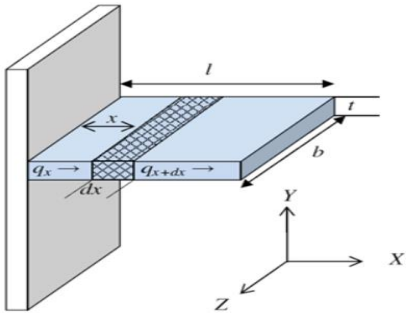

Fig 2.1.A Schematic drawing for a rectangular longitudinal Fin

$$\frac{d}{dx}\left[k(T)\frac{dT}{dx}\right]-\frac{h(T)}{A}P(T-T_{\infty})+q(T)=0 \qquad \text{eq (2.1)}$$

The Boundary Conditions are

$$X=0;\frac{dT}{dx}=0 \text{ and } X=\infty;T=T_B \qquad \text{eq (2.2)}$$

Temperature dependent thermal properties are

$$K(T) = K_0(1+\lambda(T-T_0)) \text{ and} \qquad \text{eq (2.3)}$$

$$h(T) = h_b\left[\frac{T-T_\infty}{T_b-T_\infty}\right]^n \qquad \text{eq (2.4)}$$

Internal heat generation parameter can be given as

$$q(T) = q_0[1+\psi(T-T_\infty)] \qquad \text{eq (2.5)}$$

The exponent constant n practically varies between -3 and 3, and represent different modes of convection. Eg, for n=-1/4 and n=1/4, it represents natural boiling and condensation respectively. ,nucleate boiling when n=2, thermal +radiation for n=0 for constant heat transfer and n=1 for linear heat distribution.

Inserting equations (2.3-2.5) into equation 2.1, we obtain

$$\frac{d}{dx}\left[k_0[1+\lambda(T-T_\infty)]\frac{dT}{dx}\right] - \frac{h_b P(T-T_\infty)^{n+1}}{A(T_b-T_\infty)^n} + q_0[1+\psi(T-T_\infty)] = 0 \qquad \text{eq(2.6)}$$

Non dimensinalizing terms,we obtain

$$X = \frac{x}{l}, \theta = \left[\frac{T-T\infty}{T_b-T\infty}\right], H = \frac{h}{h_b}, M^2 = \frac{Ph_bL^2}{AK_a} \qquad \text{eq(2.7)}$$

$$Q = \frac{q_0 A}{h_b P(T_b-T_\infty)}, \gamma = \psi(T_b-T_\infty), and, \beta = \lambda(T_b-T_\infty)$$

Using the above non dimensional equations, we obtain

$$\frac{d^2\theta}{dx^2} + \beta\theta\frac{d^2\theta}{dx^2} + \beta\left[\frac{d\theta}{dx}\right]^2 - M^2\theta^{n+1} + M^2Q(1+\gamma\theta) = 0 \qquad \text{eq(2.8)}$$

We have the following nondimensional Boudary Conditions

$$X = 0, \frac{d\theta}{dx} and$$
$$X = 1, \theta = 1 \qquad \text{eq (2.9)}$$

2.3. Method of Solution

To Solve the second order nonlinear and nondimensional differential equation given on eq (2.8), with the given Boundary Condition of eq(2.9), I employed the Shooting method and a secant method to refine the solutions to an acceptable and tolerable Convergence tolerance.

But primarily, eq(2.8), has to be rearranged as

$$\frac{d}{dx}\left[(1+\beta\theta)\frac{d\theta}{dx}\right] = m^2\theta^{n+1} - m^2Q(1+\gamma) \qquad \text{eq (2.10)}$$

Rearranging eq (2.10), we obtain a refined second order ODE,

$$\frac{d^2\theta}{dx^2} = \frac{-\beta\left[\frac{d\theta}{dx}\right]^2 + M^2\theta^{n+1} - M^2Q(1+\gamma)}{1+\beta\theta} \qquad \text{eq(2.11)}$$

Decomposing eq (2.11) into two first order nonlinear ODEs, we obtain

$$T = \theta, and$$

$$S = \frac{dT}{dx} = \frac{-\beta\left[\frac{d\theta}{dx}\right]^2 + M^2\theta^{n+1} - M^2Q(1+\gamma)}{1+\beta\theta} \qquad \text{eq(2.12)}$$

Here after, eq (2.12) is used to employ the Shooting Secant method for the two first order ODEs for the Numerical solution aspect of the problem.

As for the Dynamical analysis aspect , the following decomposition were used.

$$\frac{du}{dx} = (1+u\beta)v \qquad \text{eq (2.13)}$$

$$\frac{dv}{dx} = M^2u^{(n+1)} - M^2Q(1+\gamma) - \beta v^2 \qquad \text{eq (2.14)}$$

2.3.1. Total Heat Flux

The total heat flux of the fin is given by

$$q_b = k(T)A\frac{dT}{dx}$$

Non-dimensional heat transfer at the base of the fin is given by

$$q_T = \frac{q_b}{kA(T)(\mathrm{T}-\mathrm{T_b})} = (1+\beta\theta)\frac{d\theta}{dx} \qquad \text{eq(2.15)}$$

$$q_T = \frac{1}{Bi}(1+\beta\theta)\theta^{-n}\frac{d\theta}{dx} \qquad \text{eq(2.16)}$$

2.3.2. Fin Efficiency

Efficiency of a fin is defined as a heat transfer rate of a fin to the maximum heat transfer rate possible, which is equal to the heat transfer rate of equaling the base of the fin.

The heat transfer rate is given by

$$Q_f = \int_0^1 ph(T)(T-T_b)dX \quad \text{and} \qquad \text{eq(2.17)}$$

The maximum heat transfer rate is given by

$$Q_{\max} = ph_b\,\mathrm{L}(T_b - T_\infty)dX\ .$$

Therefore, the efficiency Is given by

$$\eta = \frac{Q_f}{Q_{\max}} = \frac{\int_0^1 ph(T)(T-T_b)dX}{ph_bL(T_b-T_\infty)}\ .$$

Simplifying the above equation yields

$$\eta = \int_0^1 \theta^{n+1}dX$$

2.3.3. Fin Effectiveness

Effectiveness of a fin can be defined as the ratio of heat transfer rate of the fin to the rate of fin to the rate of heat transfer if the fin is not there.

$$\varepsilon = \frac{Q_f}{Q_{fb}}$$

Q_{fb} is the amount of heat dissipation from the area of the Fin base and is given by

$$Q_{fb} = \int_0^1 ph_b \frac{\delta}{2}(T_b - T_\infty)dX \ .$$

$$\varepsilon = \frac{\int_0^1 2ph(T)(T - T\infty)}{ph_b\delta(T_b - T_\infty)dX}$$

Therefore, the dimensionless effectiveness is given as

$$\varepsilon = 2a_r \int_0^1 \theta^{n+1} dX$$

Where a_r is the aspect ratio given as the dimensionless length (L) to the thickness of the fin (δ).

2.4. Results and Discussion

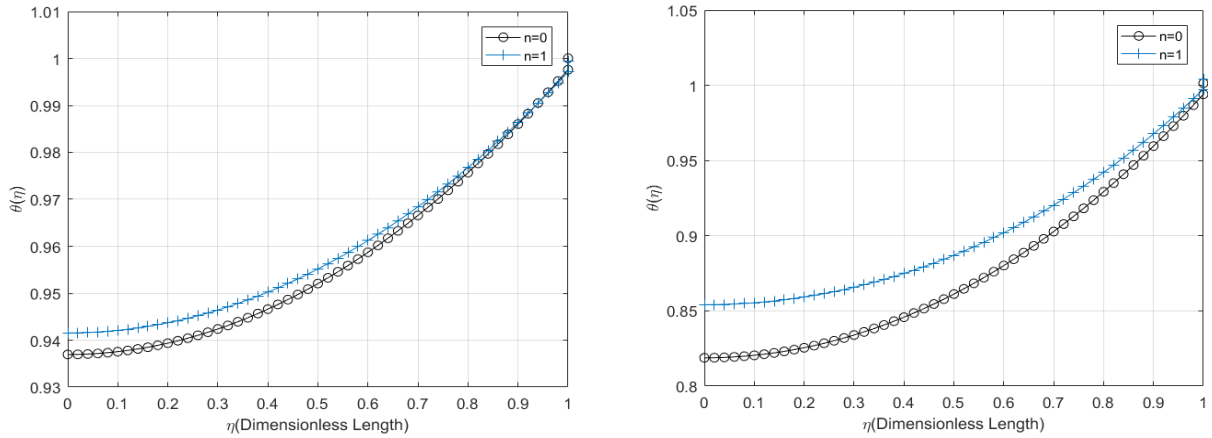

(B)

Fig(2.1) Temperature profile for (A)M=0.5,β=1,Q=0.8,γ=0.1 and (B)M=1,β=1,Q=0.8,γ=0.1

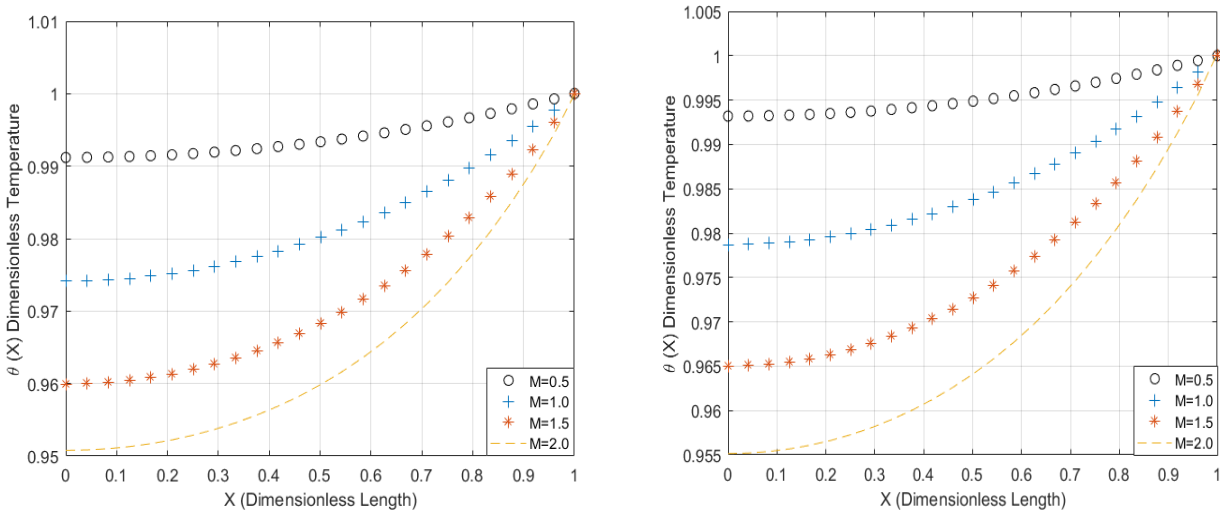

Fig 2.2. Temperature profile for (A)β=0.5,Q=0.8,γ=0.1 and (B) β=1,Q=0.8,γ=0.1

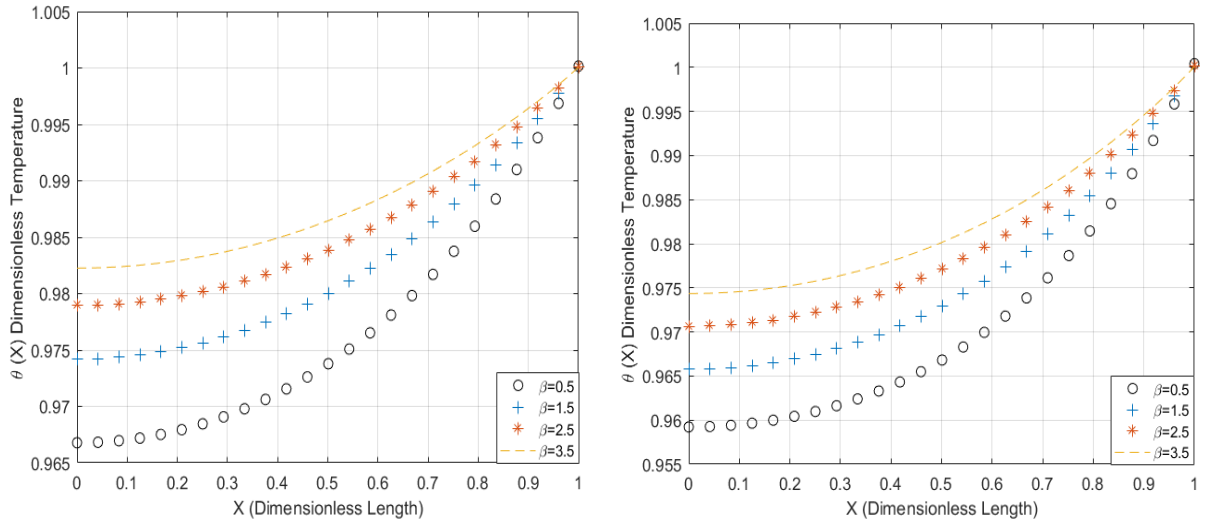

(A) (B)

Fig 2.3. Temperature profile for (A) M=1.5, n=1, Q=0.8, γ=0.1 and (B) M=2.0, n=1, Q=0.8, γ=0.1

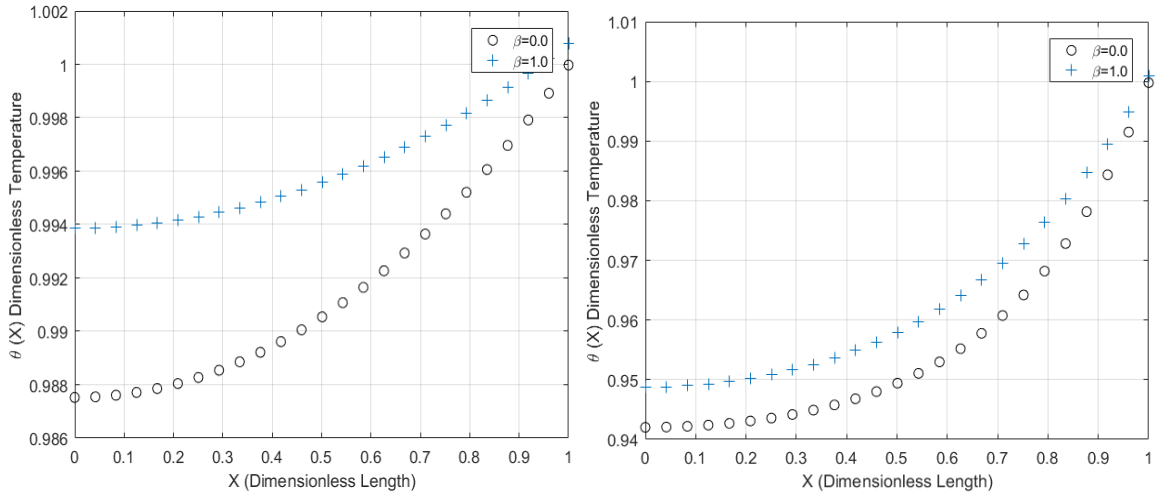

Fig 2.4. Temperature profile for (A) M=0.5, n=1, Q=0.8, γ=0.1 and (B) M=2.5, n=1, Q=0.8, γ=0.1

Figures 2.1-2.4 represent the temperature profile over a dimensionless length(X) as it varies, , from the base to the tip of the fin, for parameters M,β,γ and Q.

The Biot number in this analysis is taken to be between 0 and 1. If the Biot number is greater than 0.1, one dimensional analysis is insufficient and two dimensional analysis is required.

Figure 2.1 shows constant and linear cases of Convective heat transfer coefficients. The linear convective coefficient has a higher initial fin temperature than that of the constant convective coefficient.

In figures 2.1 and 2.2, we can notice the impact of thermo-geometric parameter (M) on the temperature profile with dimensionless length (X). Increase in M would increase the change in temperature, lower Tip Temperature and vice versa.

Figures 2.1, 2.2 and also2.9-2.10, the Efficiency and the Effectiveness of the fin is reduced with an increase in M. This makes sense that fins are said to perform well if it absorbs much heat without large temperature difference between fin's base and tip (larger tip temperature). The most effective and Efficient fin is a fin with constant temperature for the whole fin equaling the base temperature.

An increase in thermal conductivity helps spread heat better and increases the tip temperature as can be demonstrated from figures 2.3 and 2.4.

In relation to M, M is proportional to biot number (h δ/K). Large conductivity parameter results smaller Biot number, and smaller M, which can guarantee good performance. This again can be proved with efficiency and effectiveness relation from figure 2.9, that the efficiency and effectiveness increases as the thermal conductivity increases.

As can be seen from figure 2.4, when thermo geometric parameter (M) increases highly, we can notice that the effect of nonlinearity vanishes.

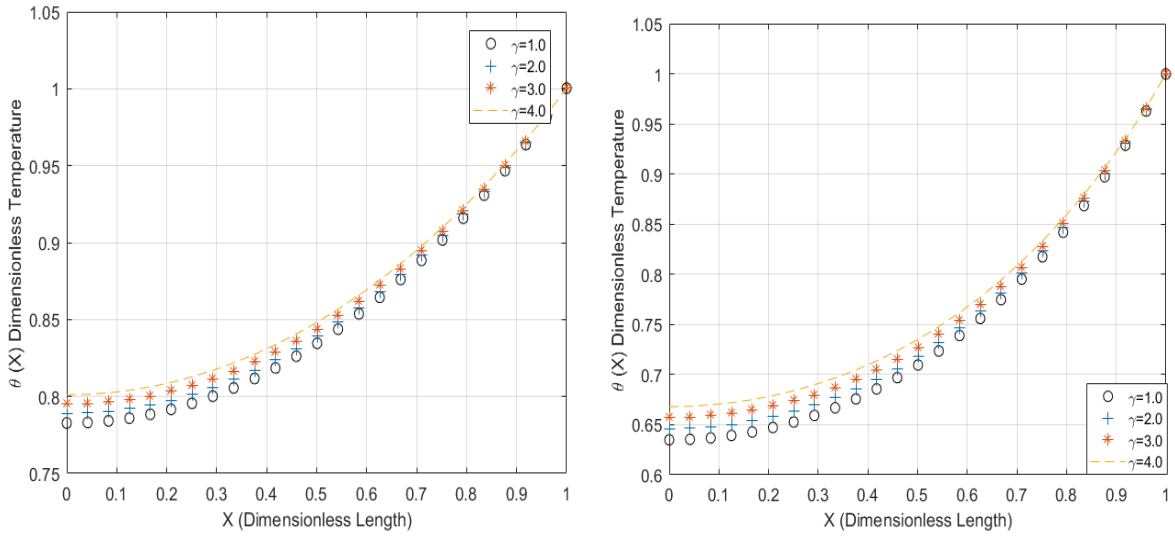

Fig 2.5. Temperature profile for (A) M=1.5, n=1, Q=0.6, β=1.5 and (B) M=2.0, n=1, Q=0.6, β=0.5

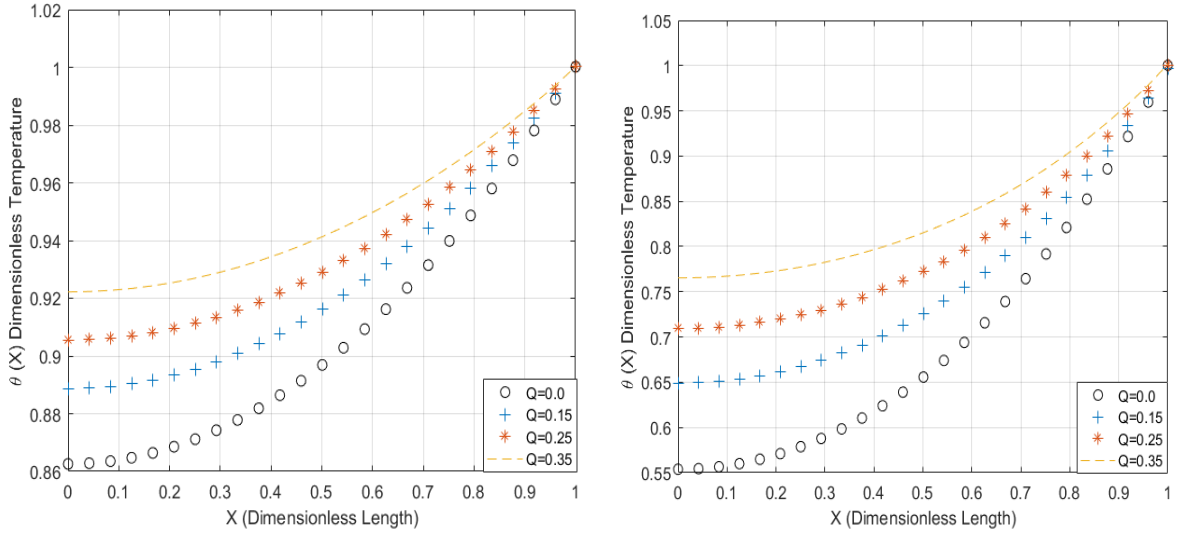

Fig 2.6. Temperature profile for (A) M=1, n=1, γ=0.2, β=2.0 and (B) M=2.0, n=1, γ=0.2, β=1.0

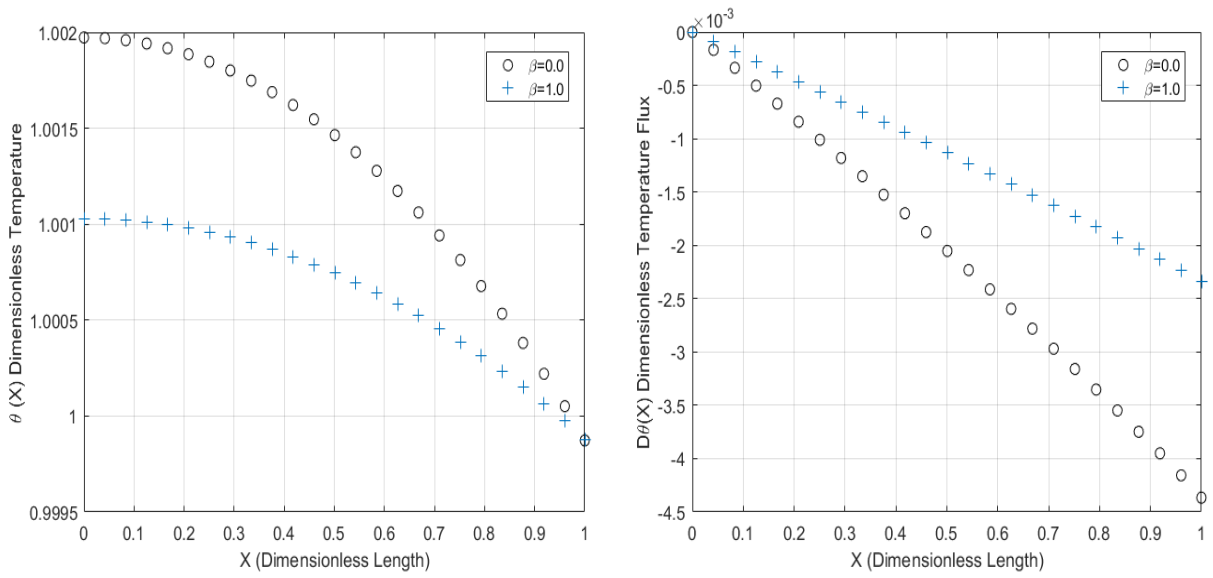

Fig 2.7. (A) Temperature profile for M=0.5, n=1, γ=0.7, Q=0.6 and
(B)Temperature Flux profile for (A) M=0.5, n=1, γ=0.7, Q=0.6

The impact of internal heat generation on temperature profile is shown in figures 2.5-2.7. It can be seen that the internal heat generation, up to a certain extent, could help in balancing the energy, and results in higher performance.

But after a threshold value of internal heat generation parameters Q and γ, Q=0.7 and γ=0.6 as indicated in figure 2.7, the temperature gradient at the base is reversed and instead of dissipating heat to the external surface, heat ends up flowing over the surface, and the fin is forced to gain heat instead of losing heat. This is an undesirable situation that reverses the primary purpose of the fin.

In practice, With regards to the material, Copper and Aluminum are the two most commonly used materials to produce fins because of their good thermal conductivity. The Thermal conductivity of Copper is higher than that of Aluminum. Aluminum has a thermal conductivity of 136 BTU/(hr-ft-F) and that of Copper is 231 BTU/(hr-ft-F). BTU/(hr-ft-F) is an imperial unit and is equal to 1.731 W/m-k. But Aluminum is favored and mostly used over copper because Aluminum has lighter weight per unit volume and cost wise, Aluminum is cheaper. The density of Aluminum is about 2712 kg/m3 and of Copper is about 8940. This is a very large number (more than three folds) which makes Copper vary heavy and is not desired. According to London Metals Exchange, the price of Copper is about 6939 USD/Metric ton and that of Aluminum is about 2463. Therefore, due to reasons of weight and Cost, Aluminum is greatly favored over Copper. Some illustration is presented in the Appendix section with an app I developed intended to help with simple preliminary engineering study.

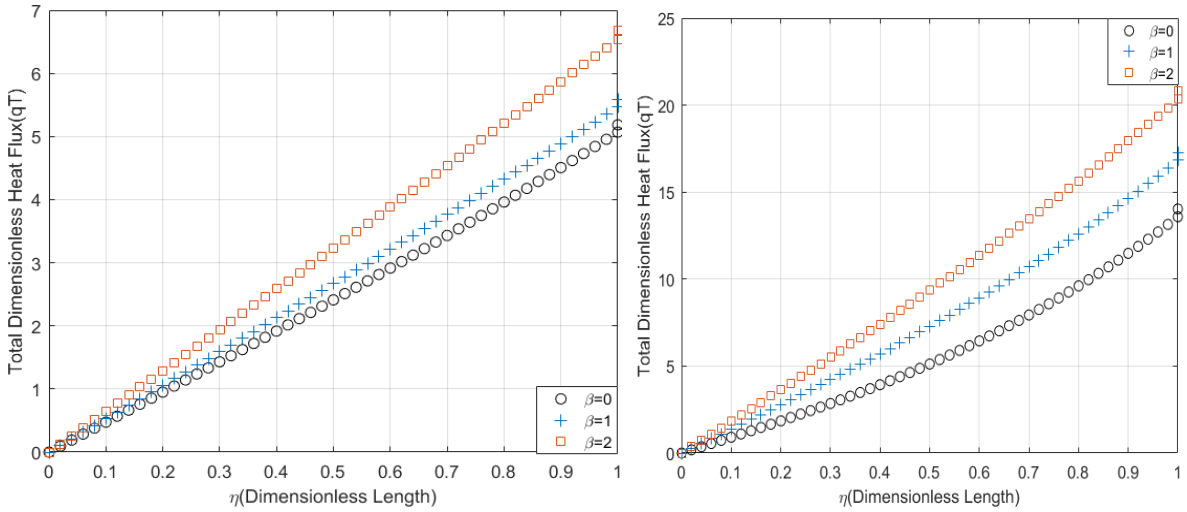

Fig 2.8. (A) Dimensionless Total heat flux profile for M=1.0, n=1, γ=0.6, Q=0.2 and Bi=0.08
(B) Dimensionless Total heat flux profile for M=2.0, n=1, γ=0.6, Q=0.2 and Bi=0.08

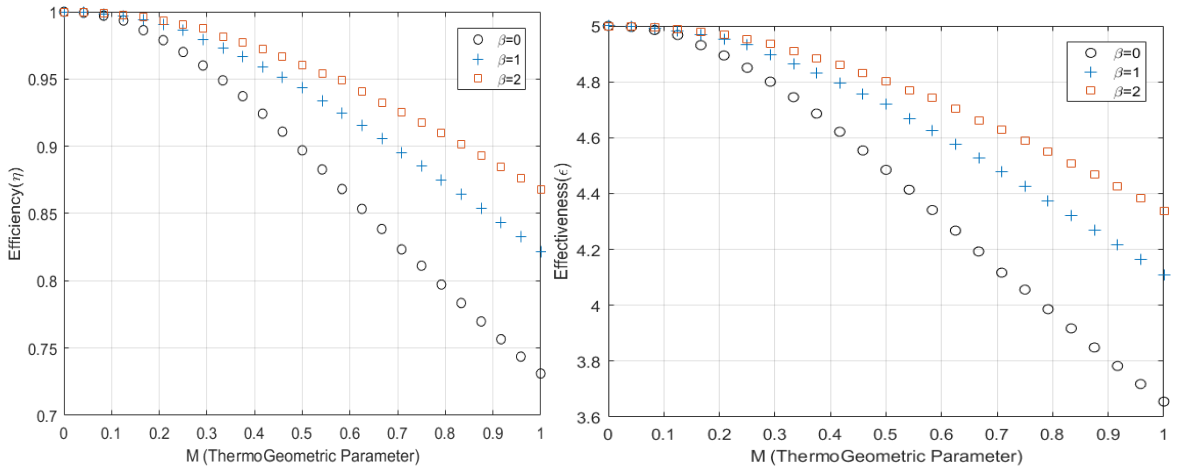

(A) (B)

Fig 2.9. (A) Efficiency vs. dimensionless length(X) n=1, γ=0.2, Q=0.2

B) Effectiveness vs. dimensionless length(X) n=1, γ=0.2, Q=0.2 and ar=2.5.

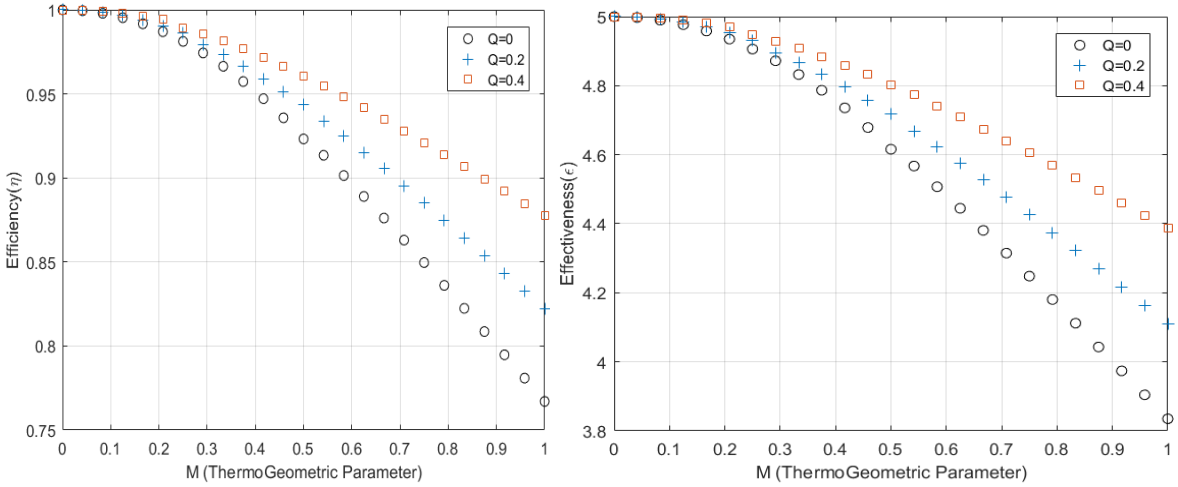

Fig 2.10. (A) Efficiency vs. dimensionless length(X) n=1, γ=0.2, β=1.0

B) Effectiveness vs. dimensionless length(X) n=1, γ=0.2, β=1.0and ar=2.5.

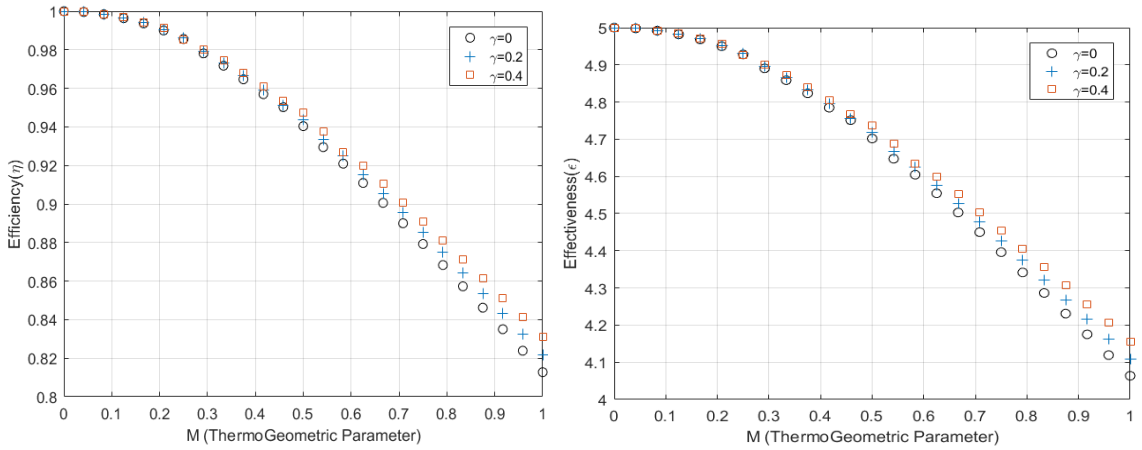

Fig 2.11. (A) Efficiency vs. dimensionless length(X) n=1, Q=0.2, β=1.0

B) Effectiveness vs. dimensionless length(X) n=1, Q=0.2, β=1.0 and ar=2.5.

Figures 2.9, 2.10, 2.11 deal with efficiency and effectiveness plotted against thermo-geometric parameter of varying parameters of β, Q and γ.

An effective fin is a fin with small Thermo-geometric parameter (M) as shown above. This is a short and thick fin and a good thermal conductivity parameter, and a non-effective fin is a long and slender fin with

poor thermal conductivity. Therefore, in design of fins, it is recommended to use shorter and multiple fins.

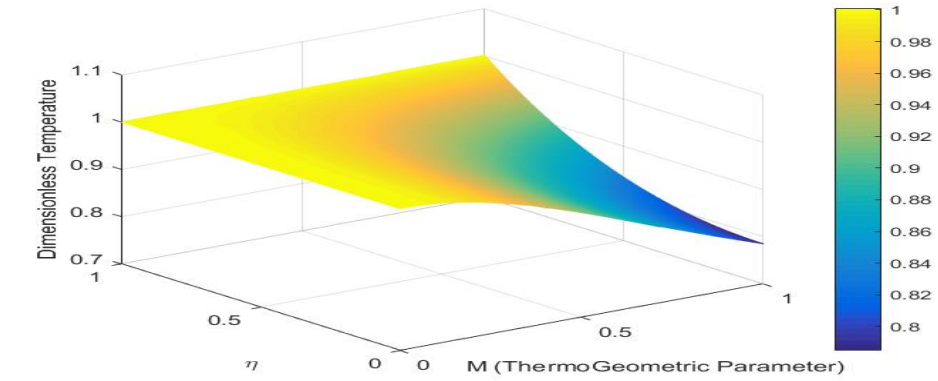

Fig 2.12. (A) Three dimensional plot for β=0

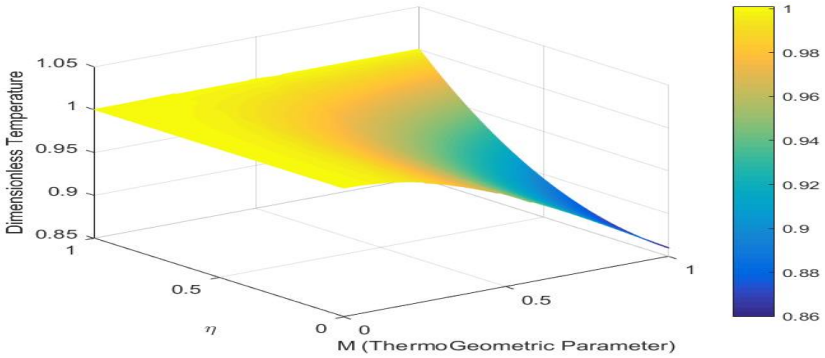

Fig 2.12. (B) Three dimensional plot for β=1

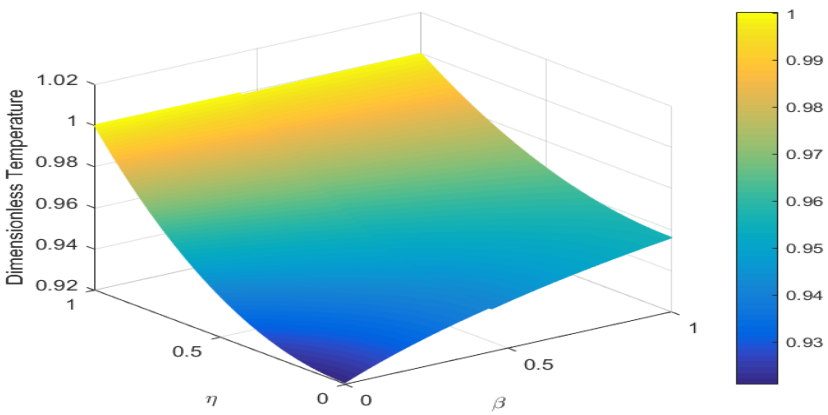

Fig 2.12. (C) Three dimensional plot for varying β and m= 0.5

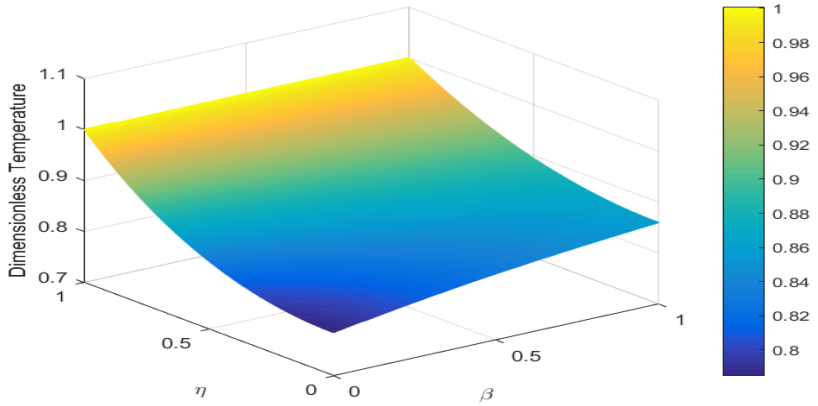

Fig 2.12. (D) Three dimensional plot for varying β and m= 1.0

The three dimensional plots help capture dimensionless temperature as a function of dimensionless distance (η), which s equal to x, and the thermo-geometric parameter M, for figures 2.12(A-D)

As can be seen in Fig 2.12, at η=1, which is the base of the fin, θ is one for all values of M and β. This is given as a boundary condition in our problem.

For fig 2.12(A-B), M=0 corresponds to an ideally perfect fin, and goes to decrease with an increasing M, which perfectly agrees with the physics of the problem.

In Fig 2.12(C-D), as β increases horizontally, so does the dimensionless temperature, which again agrees with the physics. Comparing 2.12 (C and D), as M raises from 0.5 to 1.0, the temperature at the tip of the fin is reduced from 0.93 to 0.8, which backs up our theory.

2.5. Dynamical Analysis

Below is presented the dynamical systems analysis for this specific problem. This helps us understand how the system behaves around equilibrium points. It shall be noted that practically, dimensionless temperature of positive values are of main interest since we are assuming that the temperature of the fin is higher than the ambient, and heat is convected to the surrounding fluid, air or liquids.

The dynamical analysis is conducted by varying parameters Q,γ,β and n.

Case 1: Varying n and β parameters holding other parameters Constant.

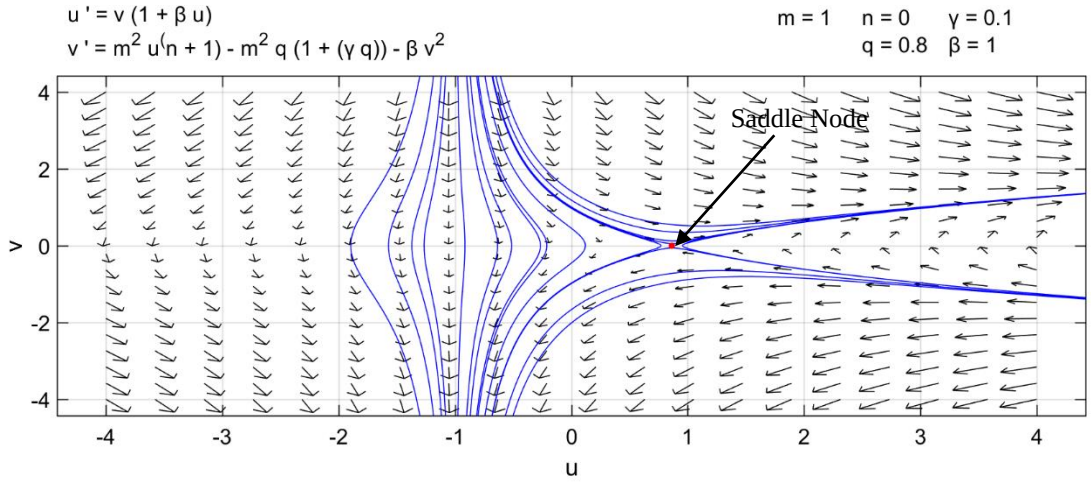

Fig 2.13.A Dimensionless temperature Phase plane for m=1,β=1,Q=0.8,γ=0.1 and n=0

From Fig 2.13.A, we can see that we have one equilibrium point at (0.86, 0). Eigenvalue for this equilibrium point is -1.36 and 1.36, which can be understood that the equilibrium point is unstable saddle point.

a

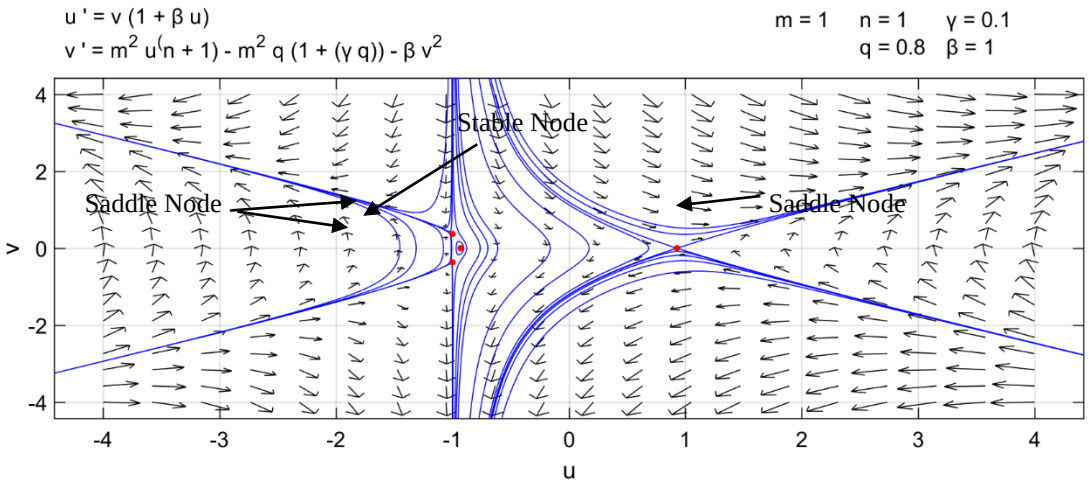

Fig 2.13.B Dimensionless temperature Phase plane for m=1,β=1,Q=0.8,γ=0.1 and n=1

From Fig 2.13.B, we can see that that we have equilibrium point at (0.92, 0),(-1,0.37), (-0.92,0),(-1,-0.37). Their corresponding Eigenvalues are (1.89,-1.89), (-0.74,0.37), (0.74,-0.37) and (-5.13*10^-7 + 0.36 i, -5.13*10^-7 - 0.36 i) respectively, which can be understood that the first three equilibrium points is unstable saddle and the last is Stable spiral node, since it has an Eigenvalue that has both real and Imaginary components. For the spiral node, it can be said that the solution approaches the equilibrium point in an oscillatory mode.

Another thing to note here is that, as the value of n changes from zero to one, the equilibrium points increased from one saddle point to three saddle and one stable point. Hence, we can say that the system has undergone a Subcritical Pitchfork bifurcation. Again, by keeping all the rest of the parameters in fig2.13.A constant and setting β to zero converts the equilibrium points from saddle to neutral equilibrium points with eigenvalue of real part equal to zero and an Imaginary part of 0.36 i. So the equilibrium point is spiral center.

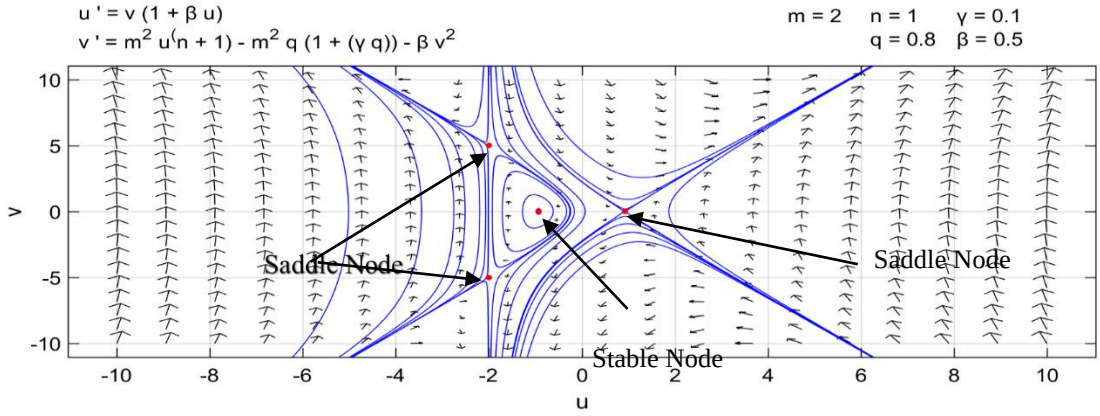

Fig 2.14.A Dimensionless temperature Phase plane for m=2,β=0.5,Q=0.8,γ=0.1 and n=0

From Fig 2.14.A, we can see that that we have equilibrium points at (0.92, 0),(-2,5), (-1,-0.37) and (-0.92,0), Their corresponding Eigenvalues are (3.3,-3.3), (-5,2.5), (5,-2.5) and (-5.13*10^-7 + 0.36 i, -5.13*10^-7 - 0.36 i) respectively, which can be understood that the first three equilibrium points is unstable saddle and the last is Stable spiral node, since it has an Eigenvalue that has both real and Imaginary components.

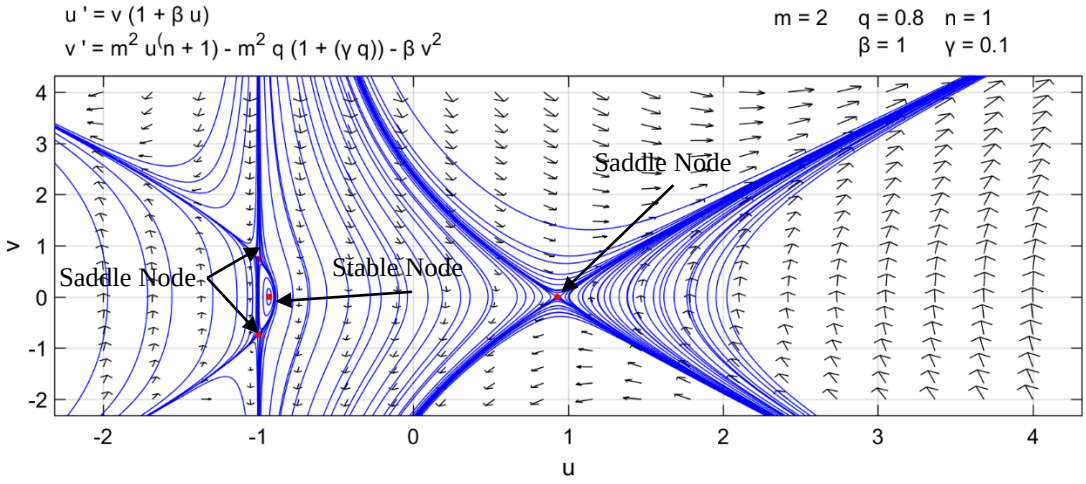

Fig 2.14.B Dimensionless temperature Phase plane for m=2,β=1,Q=0.8,γ=0.1 and n=1

From Fig 2.14.B, we can see that that we have equilibrium points at (0.92, 0),(-1,0.74), (-1,-0.74) and (-0.92,0), Their corresponding Eigenvalues are (3.79,-3.79), (-0.74,1.47), (0.74,-1.47) and (-5.13 *10^-7 + 0.723 i, -5.13*10^-7 - 0.723 i) respectively, which can be understood that the first three equilibrium points is unstable saddle and the last is Stable spiral node, since it has an Eigenvalue that has both real and Imaginary components.

For case 1, Figures 2.13 A and 2.13 B, we tried to vary the n parameter (convective power parameter). For n being 0, we obtain one critical point, which is saddle and Unstable. As we increase the value of n to 1, we get four equilibrium points, which three of them are saddle and one is a stable node. As n goes from 0 to 1,a Supercritical Pitchfork bifurcation occurs since come across two saddle node, which changes to a stable and then a saddle critical points.

Again, for Figure 2.14 A and 2.14 B, for both values of β, we obtain a Supercritical Pitchfork bifurcation. We can see that as we increase the value for β, the equilibrium points get closer to each other.

Case 2: Varying β and M parameters holding other parameters Constant.

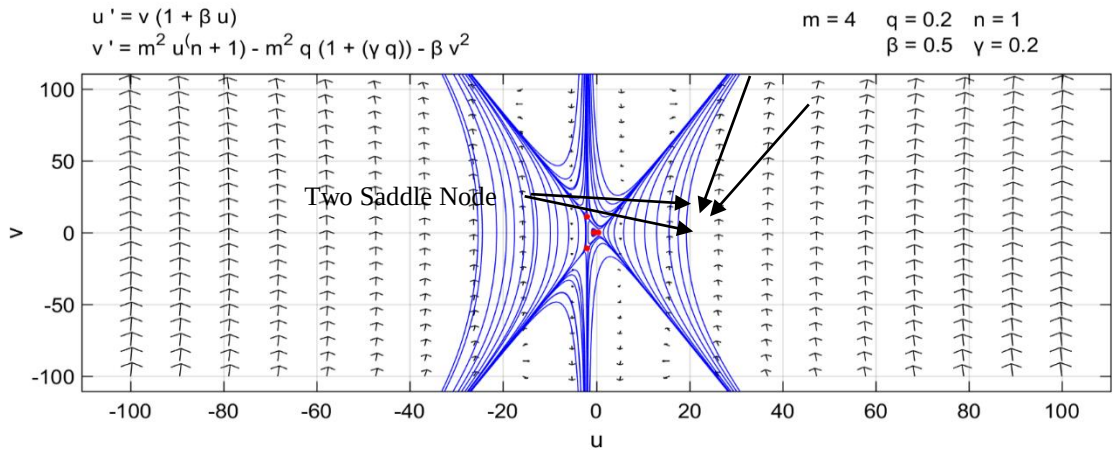

Fig 2.15.A

Dimensionless temperature Phase plane for m=4,β=0.5,Q=0.2,γ=0.2 and n=1

From Fig 2.15.A, we can see that that we have equilibrium points at (0.456, 0),(-2,11).(-2,-11) and (-0.456,0), Their corresponding Eigenvalues are (4.23,-4.23), (5.5,-11) , (-5.5,11) and (-2.5 *10^-7 + 3.35 i, -2.5 *10^-7 – 3.35 i) respectively, which can be understood that the first three equilibrium points are unstable saddle and the last is Stable spiral node, since it has an Eigenvalue that has both real and Imaginary components.

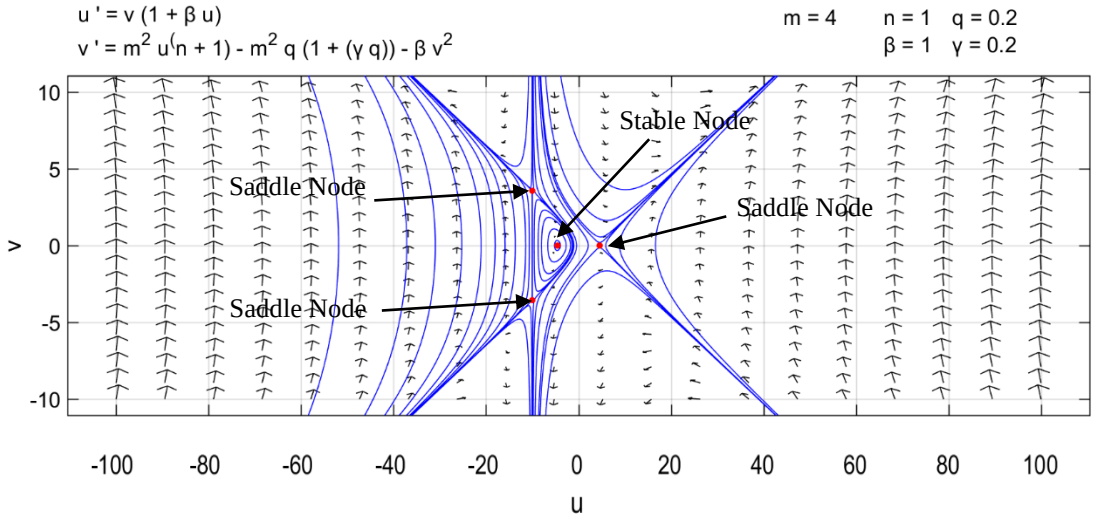

Fig2.15.B Dimensionless temperature Phase plane for m=4,β=1,Q=0.2,γ=0.2 and n=1

From Fig 2.15.B, we can see that that we have four equilibrium point at (0.456, 0),(-1,3.56), (-1,-3.56) and (-0.456,0), Their corresponding Eigenvalues are (4.6,-4.6), (-7.12,3.56), (7.12,-3.56) and (-5 *10^-7 + 2.82 i, -5 *10^-7 – 2.82i) respectively, which can be understood that the first three equilibrium points is unstable saddle and the last is Stable spiral node, since it has an Eigenvalue that has both real and Imaginary components.

Case 3: Varying β and Q parameters holding other parameters Constant.

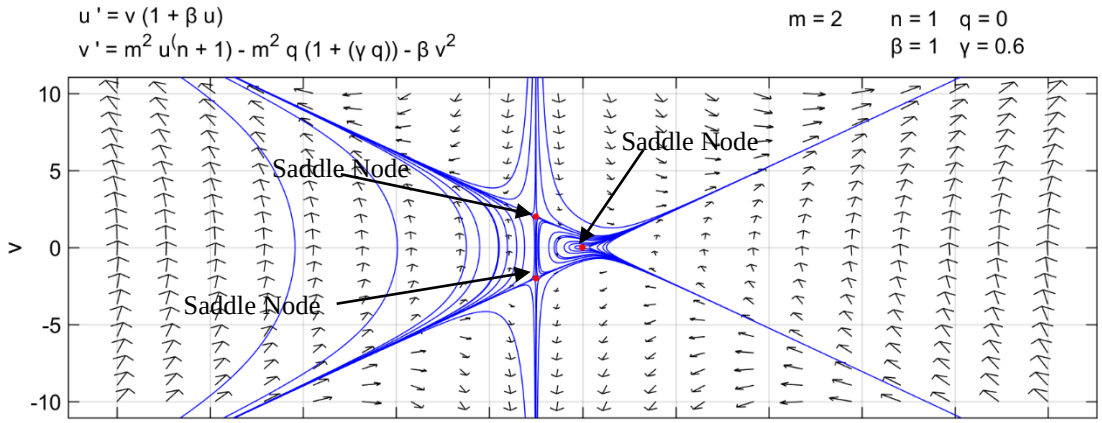

Fig 2.17.A Dimensionless temperature Phase plane for m=2,β=1,Q=0,γ=0.6 and n=1

From Fig 2.17.A, we can see that that we have three equilibrium point at (-1, 2),(-1,-2) and (0,0) . Their corresponding Eigenvalues are (-4,2), (4,-2), (0.03,-0.03) respectively, which can be understood that the all three equilibrium points are unstable saddle node.

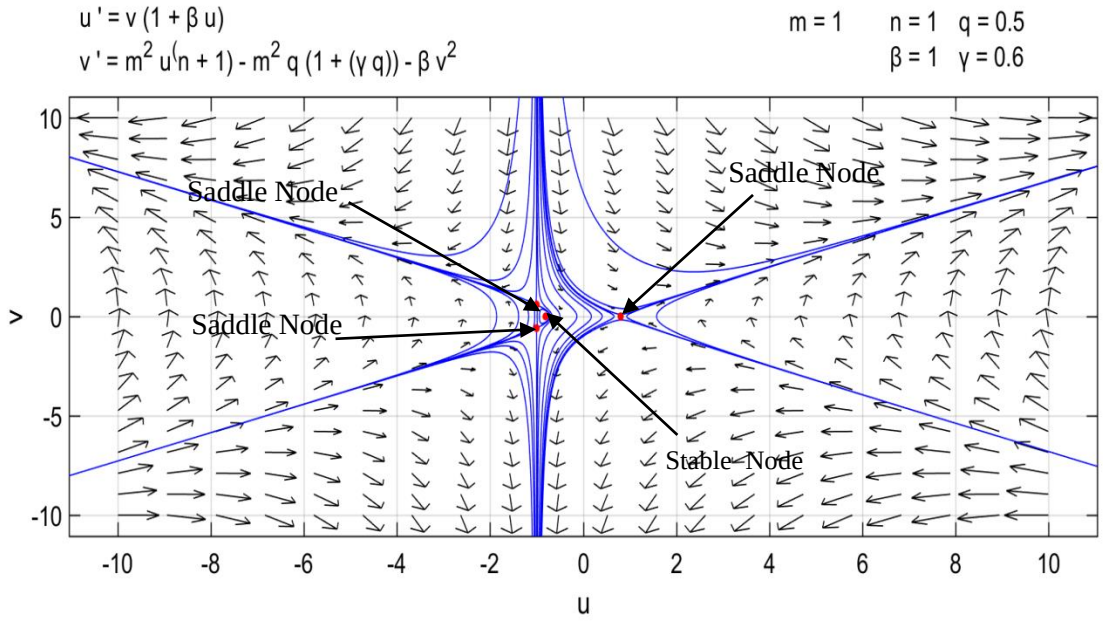

Fig 2.17.B Dimensionless temperature Phase plane for m=1,β=1,Q=0.5,γ=0.6 and n=1

From Fig 2.17.B, we can see that that we have four equilibrium point at (0.81, 0),(-1,0.59), (-1,-0.59) and (-0.81,0), Their corresponding Eigenvalues are (1.71,-1.71), (-1.18,0.59), (1.18,-0.59) and (-5.07 *10^-7 + 0.56 i , -5.07 *10^-7 – 0.56 i) respectively, which can be understood that the first three equilibrium points is unstable saddle and the last is Stable spiral node, since it has an Eigenvalue that has both real and Imaginary components.

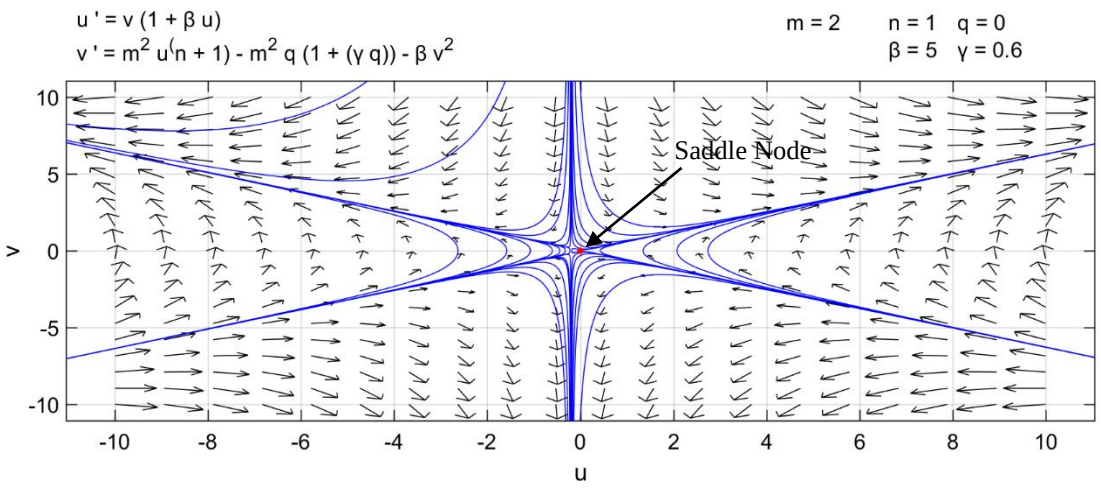

Fig 2.18.A Dimensionless temperature Phase plane for m=2,β=5,q=0,γ=0.6 and n=1

From Fig 2.18.A, we can see that that we have one saddle node equilibrium point at (0,0).Its corresponding Eigenvalues (-0.025 , 0.025) respectively,

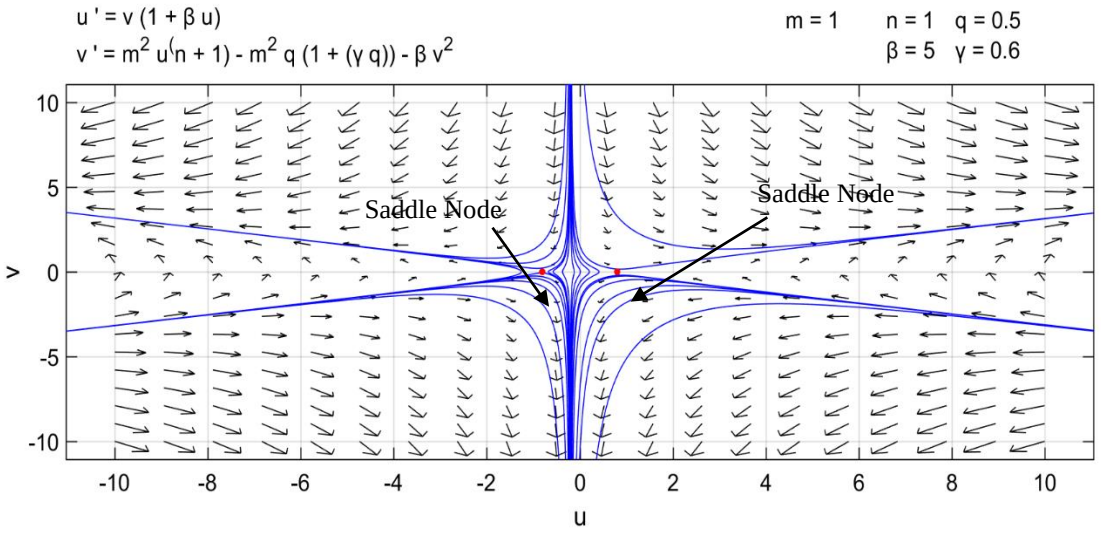

Fig 2.18.B Dimensionless temperature Phase plane for m=1,β=5,Q=0.5,γ=0.6 and n=1

From Fig 2.18.B, we can see that that we have two saddle node equilibrium points at (-0.81,0) and (0.81,0).Its corresponding Eigenvalues (-2.21 , 2.21) and (-2.842 , 2.842) respectively,

In case 3, we tried to consider varying β and Q values. In figure 2.17.A, for M=2 and β=1 and Q=0, we have three equilibrium points which one on the right is saddle and one on the left is stable center and in fig 2.17.B,we can see the transition from three Unstable node to three unstable and one Stable node. Transition from 2.17.B to 2.18.A shows the stable node ghosts into a saddle node even for the same M=1 instead of M=2, which indicates a Saddle node Bifurcation.

In figure 2.18.A, and also in Figure 2.17.A, we can see that increasing the nonlinear conductivity parameter β results in merging of equilibrium points. Which shows that the Fin exhibits somewhat closer property to Linear. Figure 2.18.A and 2.18.B exhibits unstable properties since the equilibrium points are saddle points. So, we have tried keeping the parameters at fig 2.18.A constant including M and change the value of q, we get an additional Saddle point and hence, a Saddle node bifurcation has taken place. Another thing we notice here is that for an increase of Q, which is dimensionless heat transfer parameter, the number of equilibrium point's increase.

Case 4: Varying β,γ and M parameters holding other parameters Constant.

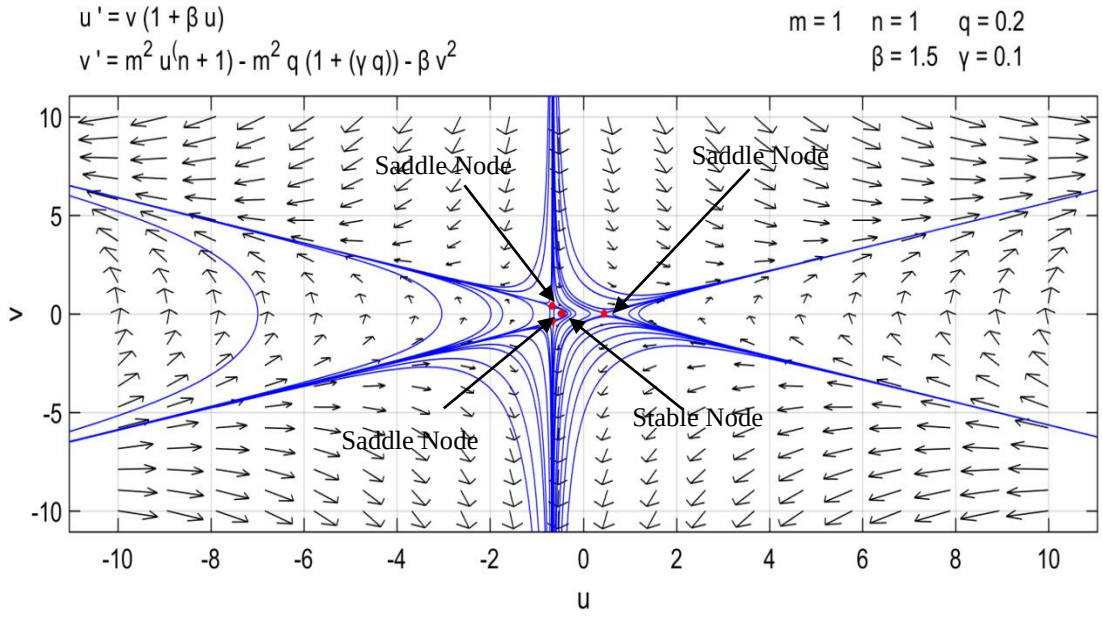

. Fig 2.19.A Dimensionless temperature Phase plane for m=1,β=1.5,Q=0.2,γ=0.1 and n=1

From Fig 2.19.A, we can see that that we have four equilibrium points at (-0.667, 0.4),(-0.667,-0.4), (0.452,0) and (-0.452,0), Their corresponding Eigenvalues are (-1.2,0.6), (1.2,-0.6), (1.23,-1.23) and (-7.5 *10^-7 + 0.53 i, -7.5 *10^-7 – 0.53 i) respectively, which can be understood that the first three equilibrium points is unstable saddle and the last is Stable spiral node, since it has an Eigenvalue that has both real and Imaginary components.

The two saddle points are all found clustered around the stable node. We have set the value of m to zero and the resulting plot showed that the two saddle points ghosts into the stable point. So, we can say that we can have a Saddle node bifurcation at the bifurcation point m=0 and m=1.

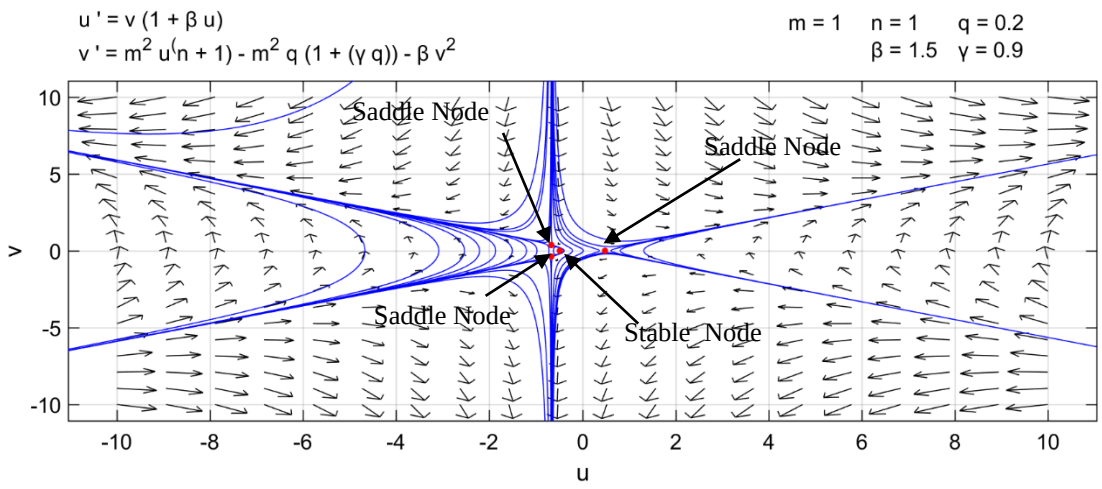

Fig 2.19.B Dimensionless temperature Phase plane for m=1,β=1.5,Q=0.2,γ=0.9 and n=1

From Fig 2.19 B, we can see that that we have four equilibrium points at (-0.667, 0.37),(-0.667,-0.37), (0.486,0) and (-0.486,0), Their corresponding Eigenvalues are (-1.12,0.56), (1.12,-0.56), (1.296,-1.296) and (-7.5 *10^-7 + 0.513 i, -7.5 *10^-7 – 0.513 i) respectively, which can be understood that the first three equilibrium points is unstable saddle and the last is Stable spiral node, since it has an Eigenvalue that has both real and Imaginary components.

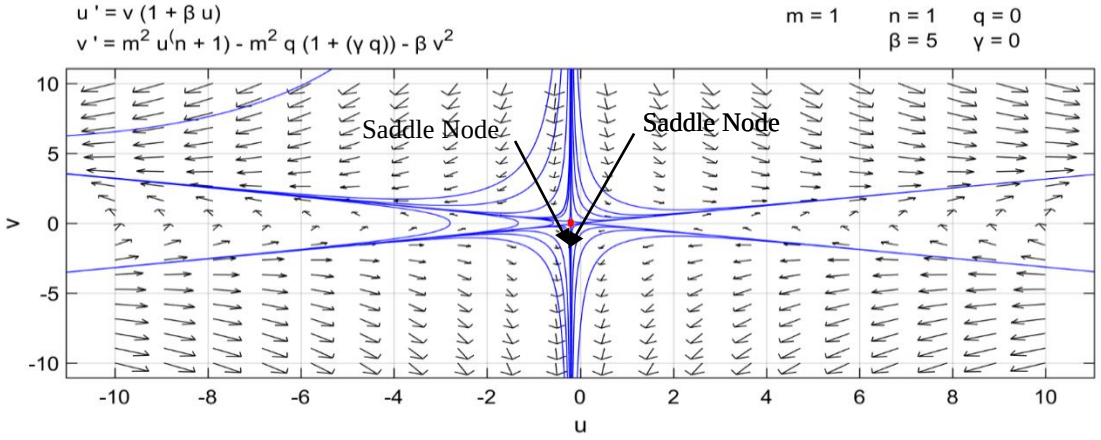

Fig 2.19.C Dimensionless temperature Phase plane for m=1,β=5,Q=0,γ=0 and n=1

From Fig 2.19.C, we can see that that we have two equilibrium points at (-0.2,-0.08) and (0,0). Their corresponding Eigenvalues are (-0.45,0.89) and (-2.5 *10^-7 + 0.01 i, -2.5 *10^-7 – 0.01 i) respectively, which can be understood that the first three equilibrium points is unstable saddle and the last is Stable spiral node, since it has an Eigenvalue that has both real and Imaginary components.

This case somehow seems relatively good for the design of the fin since for positive values of u, when the fin is serving its purpose and the temperature of the fin is large in comparison to the ambient temperature, we have stable equilibrium point which indicates a stable heat transfer.

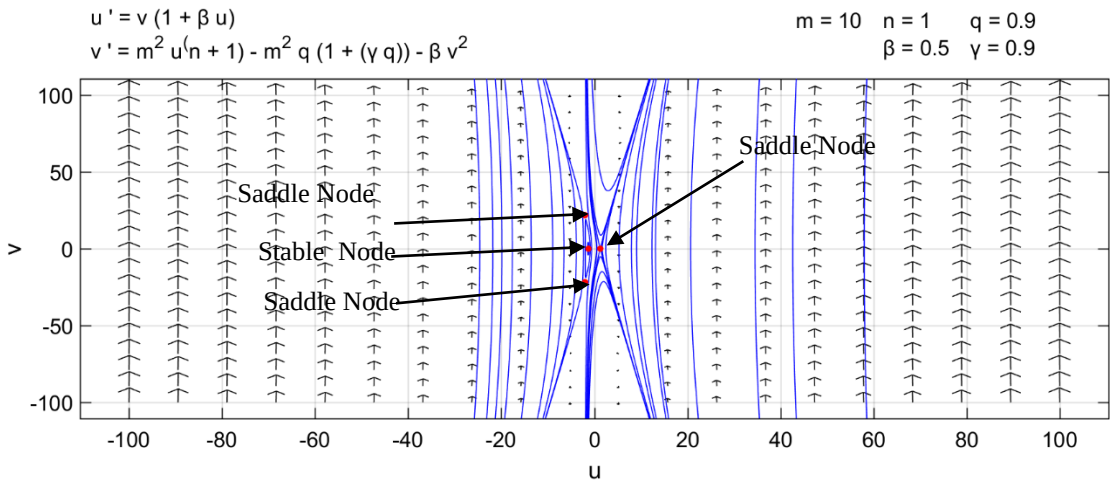

Fig 2.19.D Dimensionless temperature Phase plane for m=10,β=5,Q=0.2,γ=0.9 and n=1

From Fig 2.19.D, we can see that that we have four equilibrium points at (1.28,0), (-2,21.8), (-2,-21.8), and (-1.28,0). Their corresponding Eigenvalues are (20.45,-20.45), (-21.8,10.9) , (21.8,-10.9) and (-3.2 *10^-7 + 9.6 I , -3.2 *10^-7 – 9.6 i) respectively, which can be understood that the first three equilibrium points is unstable saddle and the last is Stable spiral node, since it has an Eigenvalue that has both real and Imaginary components.

Here again, as can be seen in Figure 2.19.A and Figure 2.19.B, we can see that of all the equilibrium points, there is one spiral node at equilibrium point (-0.45, 0) on all two plots, we can classify it as a stable spiral node. The rest of the equilibrium points are saddle in all cases. We can deduce that the impact of Q is negligible for the given conditions. The equilibrium points remained the same for an increase on Q from 0.1 to 0.9.

Here again, for increasing in γ and M, the equilibrium points got split further. One of the equilibrium points located at -1.276, 0, which is a stable equilibrium point and at equal span at 1.276,0, we find a saddle node.

From all the four cases, we have found that most of the equilibrium points are of saddle node type, and the remaining are stable.

In all cases, the real part of the eigenvalues are positive and negative for the equilibrium points, which tells us it is a saddle node.

Looking at the arrows around the equilibrium points, we can say that some of the arrows are going into the equilibrium point, which indicates stable, and some are going out of the same equilibrium points, which indicates instability.

When both the eigenvalues are negative in an equilibrium point, we can say that the equilibrium point is stable.

In practice, our condition usually is when the temperature of the fin is less than the base of the fin and both fin and base temperature are greater than the ambient, since heat dissipates from the fin to the ambient through convection. Therefore, for positive Temperature U, The equilibrium points are saddle.

This intuitively makes sense since heat is injected into the fin at higher gradient from the base which indicates the inward arrows and leaves the system at higher gradient to the ambient as well indicating outward arrows.

Chapter Three:

The Effects of Heterogeneity on the Thermal Efficiency of a Computer Heat Sink

3.1. Background

In the previous chapter, we have seen a heat dissipating extension (fin) with Conductivity and convective parameters which are functions of temperature (dependent variable). In this chapter, we shall try to extend our study to heterogeneity, where the extensions (heat sinks)' conductivity are functions the independent variable (X),since it varies along a specific spatial axis, and the computer heat sinks are made of different materials with variable conductivity parameters.

Heat sinks are surface extensions, composed of plate fins, which are used to dissipate heat into the surrounding fluids. Heat sinks are mostly used in electronic components, semiconductor devices and the like.

Improving the performance of heat sinks are helpful mainly because it enables energy saving by using small sized fans.

At higher temperatures, using homogeneous materials would be inefficient or costly in some cases. Therefore, Functionally Graded Materials (FGM), a heat sink made of different materials varying along a specific axis is designed to produce an efficient and effective fin.

In this study, we mainly focus on improving the efficiency of a longitudinal heat sinks using numerical and qualitative schemes. Comparison is made between homogeneous case and functionally graded materials. We assume that the FGMs fin material is graded as the linear and power-law functions. Internal heat generation is not considered in this study.

Several studies have been conducted regarding the heat transfer analysis of heat sinks.

Since convection is the main heat dissipation mechanism of Heat Sinks, many previous investigations focused primarily on the convective parameters around the heat sink. For example, in recent studies [11-14], because of their higher cooling capabilities, Nano fluids are used as ambient fluids dissipation in order to increase the rate of convective heat transfer from the heat sink to coolant fluid of the heat sinks. In addition, some studies [15-18] considered properties of conventional airflow and features of channel cross section. Further studies were conducted on the Effects of various geometric parameters on the performance of the heat sink are studied [19-23]. The main idea of this research revolves around the effects of using FGMs (impact of Heterogeneity) on the performance of Heat sinks in comparison to the traditional (conventional) heat sinks. In computers, either Longitudinal or pin-shape fins of heat sinks are generally used.

This study deals with the longitudinal types of heat sinks as it is commonly.

To enhance the thermal performance of performance, using heterogeneous material or functionally graded materials (FGM) is suggested in some literatures. In FGM, different materials are used to enhance the performance of the heat sinks, with varying materials along a specific axis.

Since the application of first type, namely longitudinal fin is more common in comparison to the pin type heat sinks, this study deals to study on such heat sinks, which are made by longitudinal fins. In fact, in the present research, the conventional homogeneous fin material of heat sink is replaced with Functionally Graded Material (FGM).

Japan was the first country to use the concept of FGM to enhance thermal performance in 1984 for a space plane project. When entering the earth's atmosphere from an outer space, there is a large thermal increment in the temperature which can cause thermal explosion. Therefore, due to the continuous demand to enhance thermal performance in this area, Japan used FGM to address this difficulty. Since then, FGM has been used in different areas like heat shielding of satellites, engines, nuclear and so on. FGM are also used in thermal stress control of curved geometries for Linear, power and exponential functions [25-26].

FGM is considered for devices with higher thermal sensitivity like heat sinks are considered in [27]. Their thermal property and energy saving are also studied analytically for Linear and Power Law.

In this chapter, I have used a numerical technique to verify results on [27] using numerical technique of the Shooting Secant method [5] for FGM for the power and Linear laws. Comparison of results between Numerical and Analytical solutions are compared. In addition, to further study on dynamical systems analysis has been conducted.

3.2.Problem Formulation

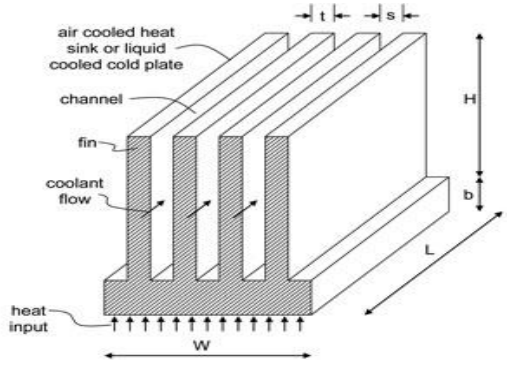

Fig 3.1. Schematic drawing of heat sink

$$\frac{d}{dx}\left[k\frac{dT}{dx}\right]-\frac{h}{t}(T-T_{\infty})=0 \qquad \text{eq (3.1)}$$

The Boundary Conditions are

and $X = 0; T = T_B$ $\qquad X = L; \frac{dT}{dx} = 0$ eq (3.2)

Non dimensinalizing terms,we obtain

$$\xi = \frac{x}{l}, \theta = \left[\frac{T - T\infty}{T_b - T\infty}\right], M^2 = \frac{h}{K_0 t}, \Gamma = mL \qquad \text{eq(3.3)}$$

Here, K0 is the thermal conductivity of Homogeneous fin, m is dimensional and Γ is dimensionless thermo geometric parameter. Therefore, the dimensionless boundary condition is]

$\xi = 0; \theta(\xi) = 1$ and

$$\xi = 1; \frac{d\theta}{d\xi} = 0 \qquad \text{eq(3.4)}$$

Case of Homogeneous heat sink

In case of Homogeneous sinks, the thermal conductivity is constant is given as

$$\frac{d^2\theta}{d\xi^2} - \Gamma^2\theta = 0 \qquad \text{eq(3.5)}$$

Case of Functionally Graded Material

There are two cases for the heterogeniety of the heat sink

3.2.1. Linear Law case

In this case, a linear relation of ξ and β is considered for thermal conductivity. Therefore,

$k = k_0[1 + \beta\xi]$, eq(3.6)

Where β is the inhomogenity index.

The goverining equation of the Linear Class case is given as

$$\frac{d\left[k\frac{d\theta}{d\xi}\right]}{d\xi} - \Gamma^2\theta = 0 \text{ ,} \qquad \text{eq(3.6)}$$

But since $k = (1 + \beta\xi)$, we obtain

$$k\frac{d^2\theta}{d\xi^2}+k'\frac{d\theta}{d\xi}-\Gamma^2\theta=0 \qquad \text{eq(3.7)}$$

$$(1+\beta\xi)\frac{d^2\theta}{d\xi^2}+\beta\frac{d\theta}{d\xi}-\Gamma^2\theta=0 \qquad \text{eq(3.8)}$$

$$(1+\beta\xi)=\frac{1}{1-0}\int_0^1(1+\beta\xi)d\xi=1+\frac{\beta}{2} \qquad \text{eq(3.9)}$$

$$(1+\beta/2)\frac{d^2\theta}{d\xi^2}+\beta\frac{d\theta}{d\xi}-\Gamma^2\theta=0 \qquad \text{eq(3.10)}$$

3.2.2. Power Law case

In this case, a power relation of ξ and β is considered for thermal conductivity. Therefore,

$k=k_0\xi^{-\beta}$, we obtain

$$k\frac{d^2\theta}{d\xi^2}+k'\frac{d\theta}{d\xi}-\Gamma^2\theta=0 \qquad \text{eq(3.11)}$$

$$(\xi^{-\beta})\frac{d^2\theta}{d\xi^2}-\beta\xi^{-\beta-1}\frac{d\theta}{d\xi}-\Gamma^2\theta=0 \qquad \text{eq(3.12)}$$

$$f(\xi)=\xi=\frac{1}{1-0}\int_0^1\xi d\xi=\frac{1}{2} \qquad \text{eq(3.13)}$$

The efficiency of a fin ,which is a main indicator of performane as indicated earlier.

The equation for efficiency is given as

$$\eta=\int_0^1\theta(\xi)d\xi \qquad \text{eq(3.14)}$$

for both homogenioius and FGM cases.

The effective efficiency is defined as the ratio of fin efficiency enhancement of FGM to that of the HM case. It can also be considered as the energy saving of the heat sink.The equation can be given as

$$\eta_{eff}=\frac{\eta_{FGM}-\eta_{HM}}{\eta_{HM}}*100 \qquad \text{eq(3.15)}$$

3.3. Results and Discussions

3.3.1. Linear Law case

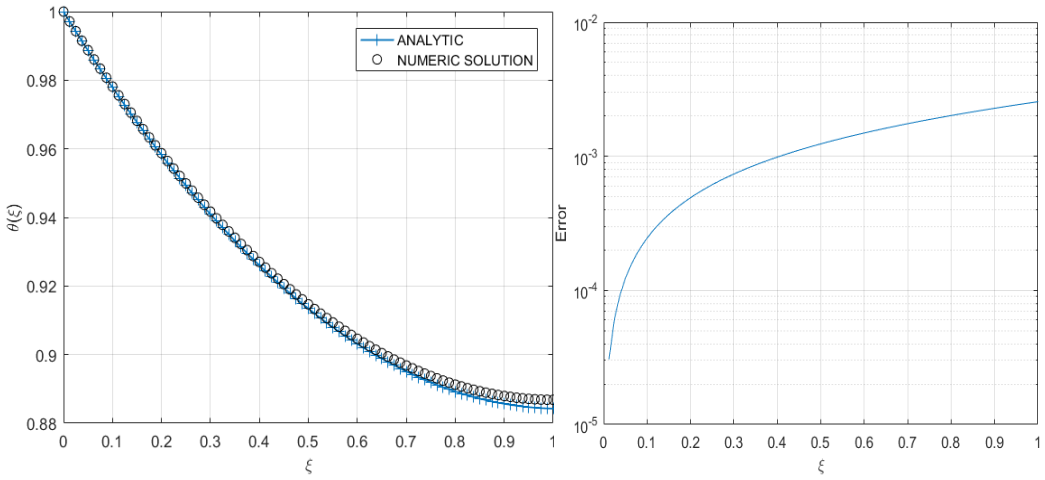

Fig 3. (A) (B)

Fig 3.3.A. Analytic and numeric results for Homogeneous case (β=0) and $\Gamma = 0.5$

Fig 3.3.B. Semilog plot for Error vs dimensionless length results for Homogeneous case (β=0) and $\Gamma = 0.5$

Table 3.1. Comparison for Homogeneous Material (Inhomogeneity index (β =0) for Analytic vs Numeric Solution

NUMBER OF ITERATION = 4			
ξ	ANALYTIC	NUMERIC	ABSOLUTE_ERROR
0	1	1	0
0.1	0.97789	0.978134774	0.000245156
0.2	0.958224	0.958715394	0.000490925
0.3	0.940955	0.941693302	0.000737922
0.4	0.926039	0.927025934	0.000986764
0.5	0.913439	0.914676614	0.001238073
0.6	0.903122	0.904614462	0.001492478

0.7	0.895064	0.896814317	0.001750615
0.8	0.889244	0.891256675	0.00201313
0.9	0.885647	0.887927639	0.002280678
1	0.884265	0.886818884	0.002553929

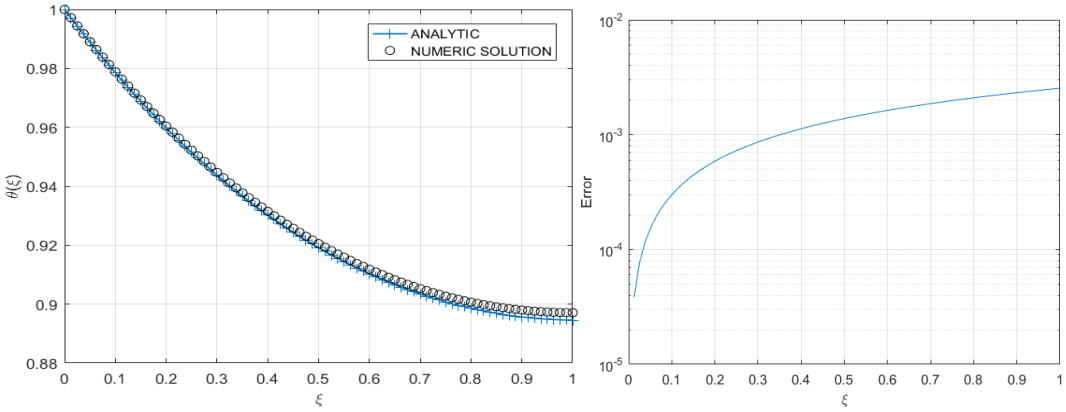

(A) (B)

Fig 3.4.A. Analytic and numeric results for Homogeneous case(β=0.6) and $\Gamma = 0.5$

Fig 3.4.B. Semilog plot for Error vs dimensionless length results for Homogeneous case (β=0.6) and $\Gamma = 0.5$

Table 3.2. Comparison for FGM (Inhomogeneity index (β =0.6) for Analytic vs Numeric Solution

NUMBER OF ITERATION = 4			
ξ	ANALYTIC	NUMERIC	ABS._ERROR
0	1	1	0
0.1	0.978523799	0.97882386	0.000300062
0.2	0.959855586	0.960442739	0.000587153
0.3	0.943833619	0.944696018	0.000862399
0.4	0.930308422	0.931435272	0.00112685
0.5	0.919141955	0.920523447	0.001381492
0.6	0.910206838	0.911834084	0.001627245
0.7	0.903385632	0.905250605	0.001864972

0.8	0.898570167	0.900665649	0.002095482
0.9	0.895660923	0.897980457	0.002319534
1	0.894566451	0.89710429	0.002537839

We shall begin by verifying the numerical results with that of the analytic by using the relation given from [27].

Figures 3.3.A. and 3.3.B show the analytic versus numerical results for a homogeneous case for Γ=0.5 where 3.3A show the numeric vs. analytic results throughout the longitudinal axis and 3.3B shows the Error semi log plot throughout the longitudinal axis. Table 1. Shows the numerical, analytical and absolute error in tabular form for the homogeneous case. The absolute error is to a 3rd decimal place but the error can further be reduced by decreasing the step size.

Figures 3.4.A. and 3.4.B show the analytic versus numerical results for a heterogeneous case for FGM of β=0.6 and Γ=0.5 where 4.A show the numeric vs. analytic results throughout the longitudinal axis and 3.3.B shows the Error semi log plot throughout the longitudinal axis. Table 2. Shows the numerical, analytical and absolute error in tabular form for the heterogeneous case of FGM of β=0.6 and Γ=0.5 . The absolute error is to a 3rd decimal place but the error can further be reduced by decreasing the step size.

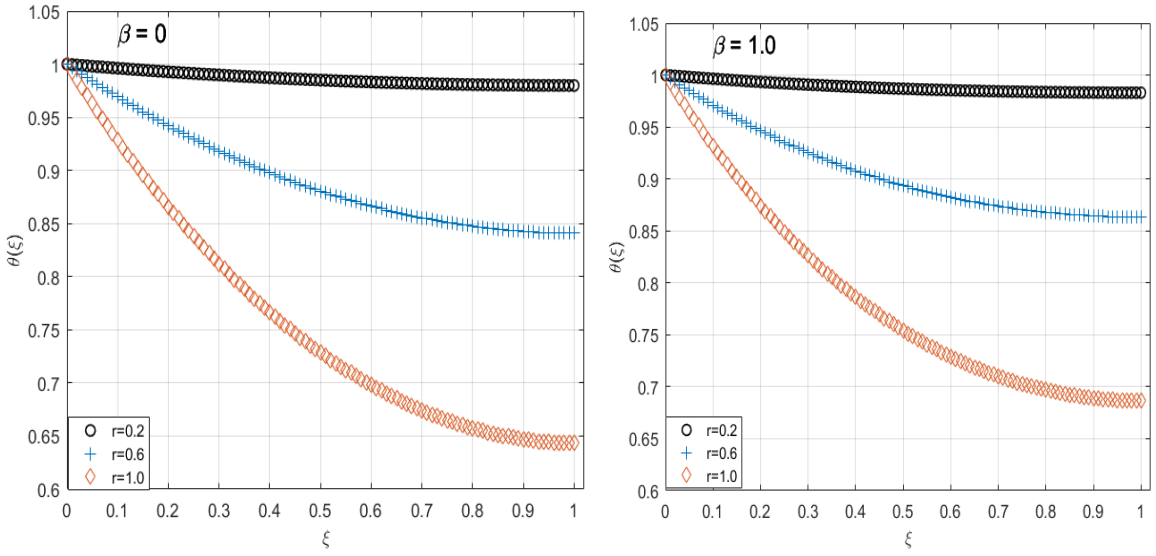

(A) (B)

Fig 3.5.A Temperature profile for various values of thermo geometric parameters for HM (β=0.0)

Fig 3.5.B Temperature profile for various values of thermo geometric parameters for FGM (β=1.0)

Table 3.3. Temperature for homogeneous (HM) case for Γ=0.2, 0.6 and 1.0.

NUMBER OF ITERATION = 10			
ξ	Γ(0.2)	Γ (0.6)	Γ (1.0)
0	1	1	1
0.1	0.996214	0.969303	0.9283
0.2	0.992826	0.942096	0.865891
0.3	0.989836	0.918282	0.812148
0.4	0.987241	0.897774	0.766534
0.5	0.985041	0.8805	0.728591
0.6	0.983236	0.866396	0.69794
0.7	0.981823	0.855413	0.674274
0.8	0.980804	0.847509	0.657357
0.9	0.980176	0.842658	0.647019
1	0.979941	0.840841	0.643156

Table 3.4. Temperature for heterogeneous (FGM) case of β=1 for Γ=0.2,0.6 and 1.0.

NUMBER OF ITERATION = 10			
ξ	r(0.2)	r(0.6))	r(1.0)
0	1	1	1
0.1	0.996459	0.971097	0.931978
0.2	0.993404	0.946313	0.874357
0.3	0.990802	0.925325	0.826094
0.4	0.988623	0.90784	0.786275
0.5	0.98684	0.89359	0.754097
0.6	0.985427	0.882334	0.728861
0.7	0.984359	0.873854	0.709956
0.8	0.983613	0.867949	0.696851
0.9	0.98317	0.864441	0.689088
1	0.983009	0.863167	0.686272

Figure 3.5.A shows the temperature profile for a homogeneous case for varying thermo geometric parameter and 5.B shows the temperature profile for the heterogeneous case of β=1.0.

From figure 3.5.A and table 3, the HM case (β=0), as we have seen in chapter one, the temperature of the Tip of the heat sink (or fin as shown in chapter one) is small for a larger value of thermo geometric parameter and large for smaller thermo geometric parameter, implying larger efficiency, as can be implied from figure (3.8) since a high performing fin is the one that absorbs more heat with a small change in temperature. The same is true for the FGM case, as can be seen from Figure 5.B and table 4.

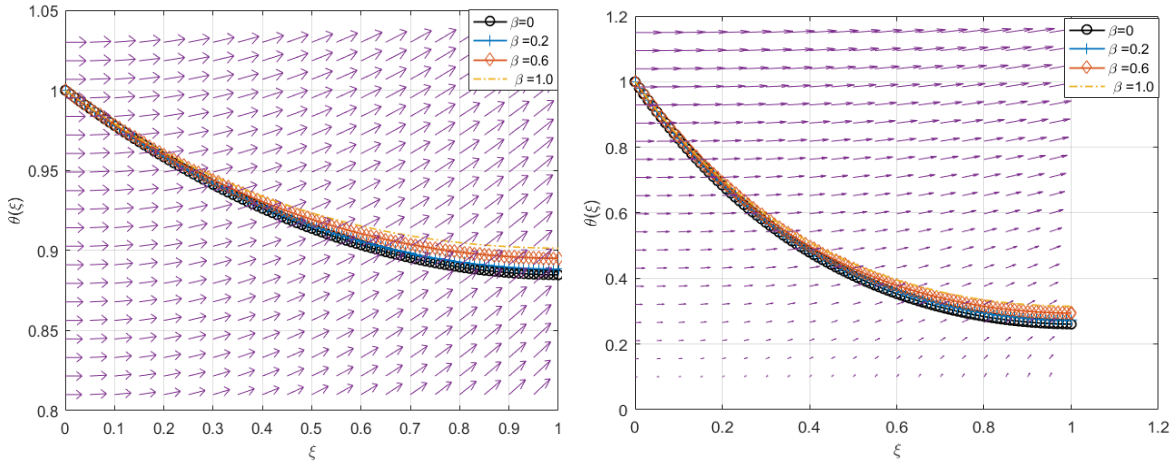

Fig 3.6.A Temperature profile for comparison of HM and FGM of different β for Γ (0.5)

Fig 3.6.B Temperature profile for comparison of HM and FGM of different β for Γ (2.0)

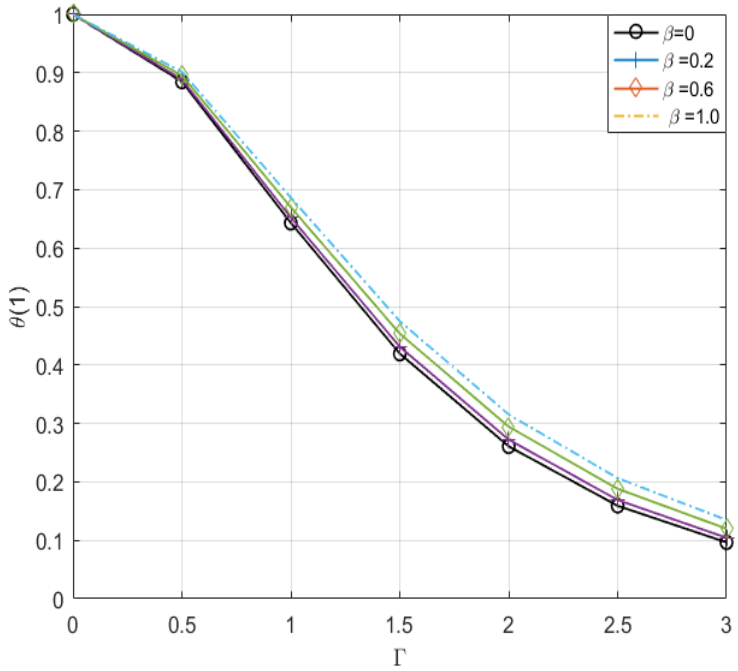

Fig 3.7. Plot for temperature at the tip Vs thermo geometric parameter

From figure 3.6A and 3.6.B compare temperature profile for HM and three different FGM sinks for thermo geometric parameter of 0.5 and 2.0 respectively for linear cases. And Figure 3.7 shows relation between the temperature at the tip and the thermo geometric parameter for linear cases. In a similar manner, figures 3.9A and 3.9B, compare temperature profile for HM and three different FGM sinks for thermo geometric parameter of 0.5 and 2.0 respectively for power law cases. And Figure 3.8A shows relation between the temperature at the tip and the thermo geometric parameter for power law.

As the thermo geometric parameter increases, the temperature at the tip decreases thereby reducing performance and efficiency, which can be seen from figure 3.7 for linear case and figure 3.10.A for power law case. Also in figure 3.6A, with thermo geometric parameter 0.5 has a higher tip temperature than that with thermo geometric parameter of 2.0.Similarly, for power law case, tip temperature for 3.9.A with Γ=0.5 is higher than that of figure 3.9.B with Γ=2.0.

From figures 3.6.A and 3.6.B from linear case and figure 3.9.A and 3.9.B for power law case, we can see that the temperature at the tip for HM is lower than to that of the FGM. It can be noted that as the value for inhomogeneity index β increases, the temperature at the tip increases, and hence the efficiency of the fin increases as the thermal conductivity parameter increases, which is only logical. The FGM with β=1 has a higher efficiency than that of the FGM with β=0.2, which shall be proved in efficiency diagram fig (3.8).

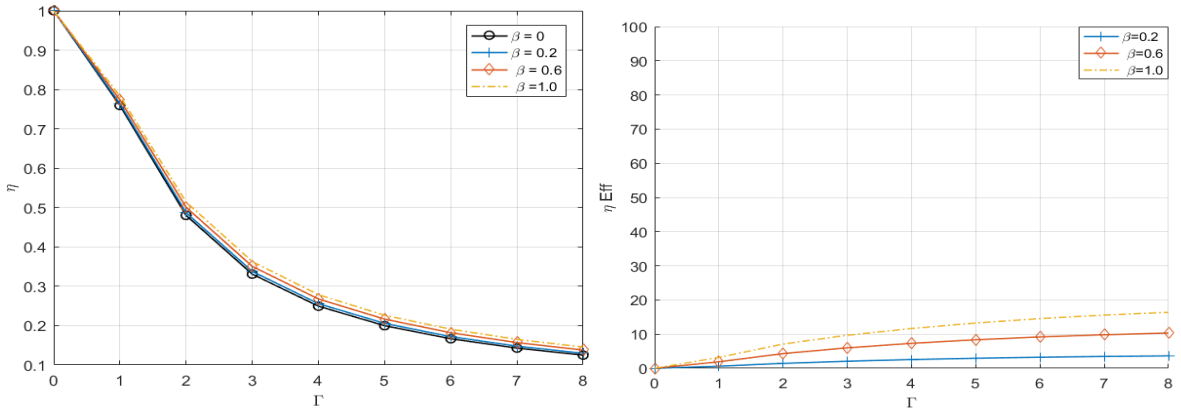

Fig 3.8.A Efficiency vs Thermo geometric parameter and 3.8.B Effective Efficiency vs Thermo geometric parameter

Previously, we have defined the effective efficiency as a rate of increase of energy saving by using functionally graded material with that of a homogeneous one. From figure 3.8(B) for linear case and figure 3.11 for power law case, we can see that as the inhomogeneity index increase, the effective efficiency increases.

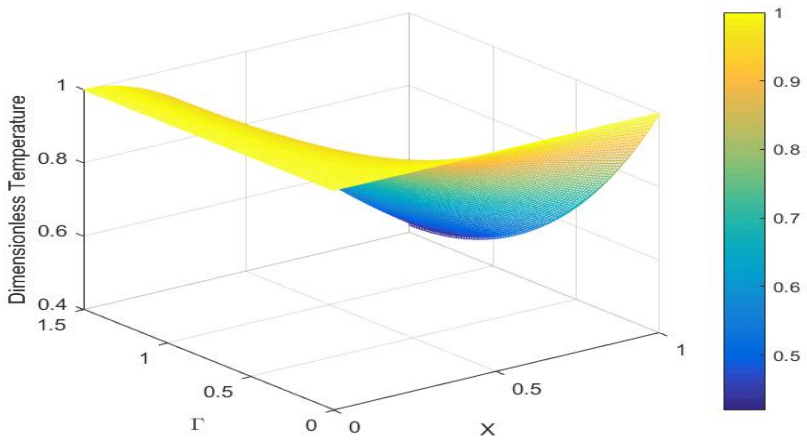

Fig 3.8.C. Three dimensional Plot for β = 0

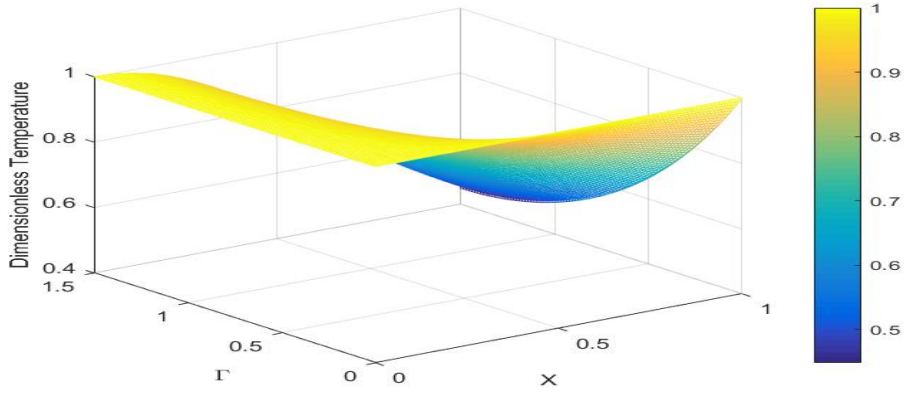

Fig 3.8.D. Three dimensional Plot for β = 0.5

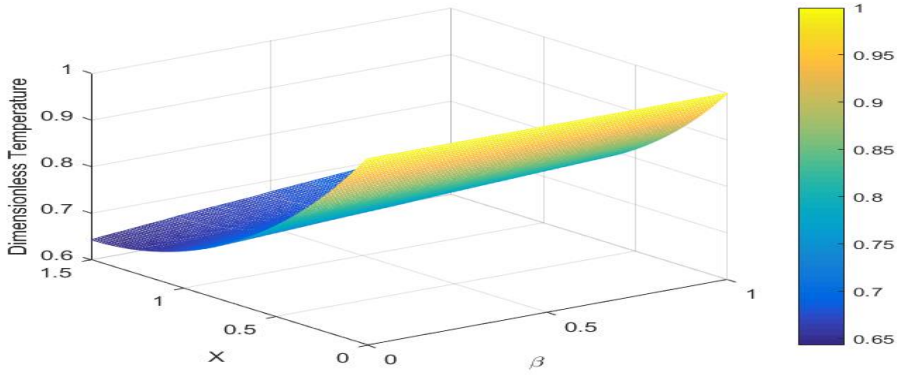

Fig 3.8.E. Three dimensional Plot for r = 1.0

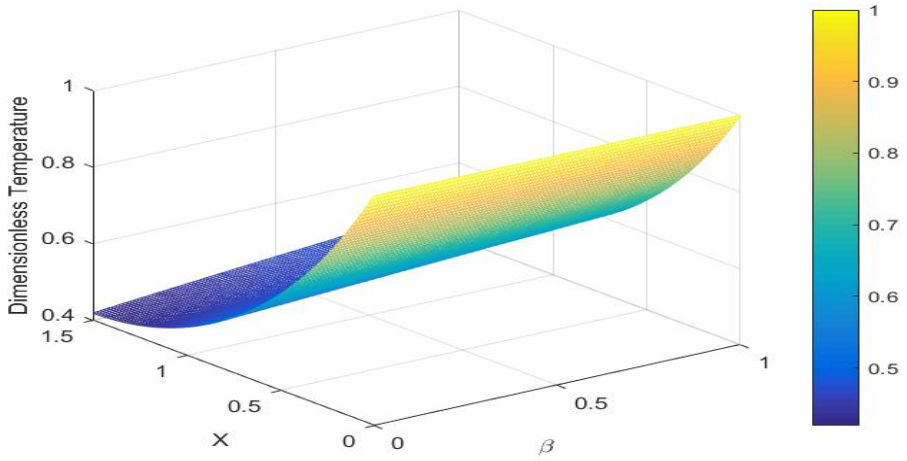

Fig 3.8.F. Three dimensional Plot for r = 1.5

3.3.2. Power Law case

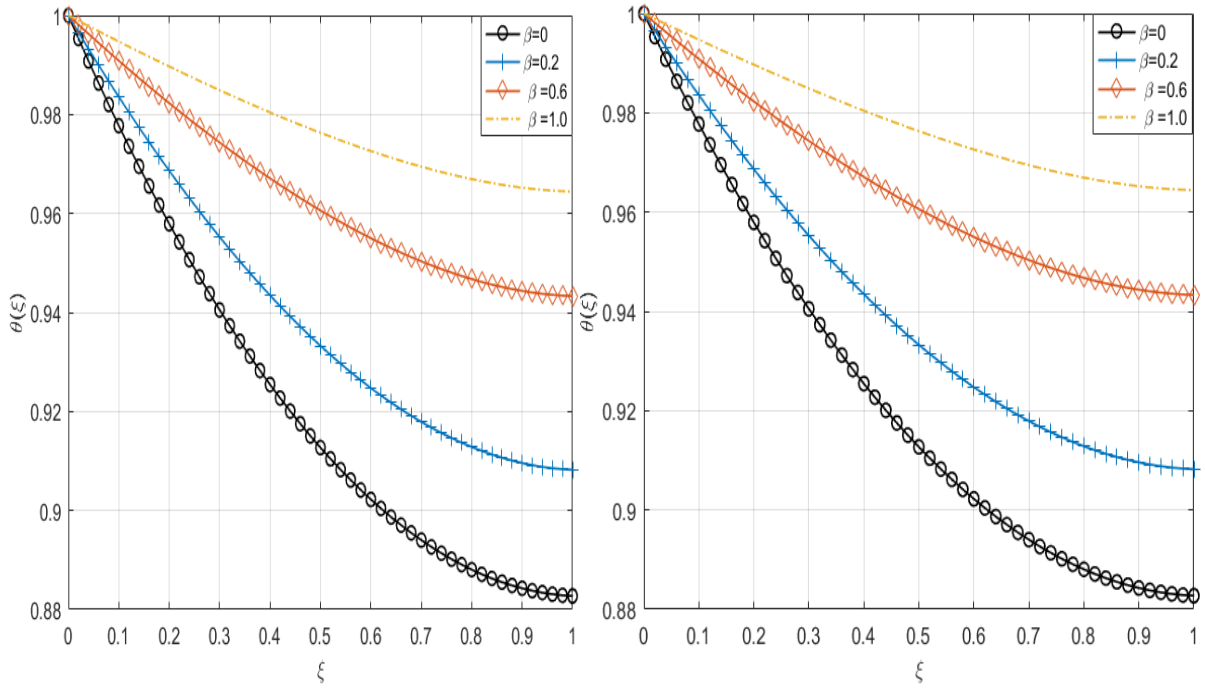

(A) (B)

Fig 3.9. Temperature profile for HM and FGM Thermo geometric parameter for A) Γ=0.5 and B) Γ=2.0

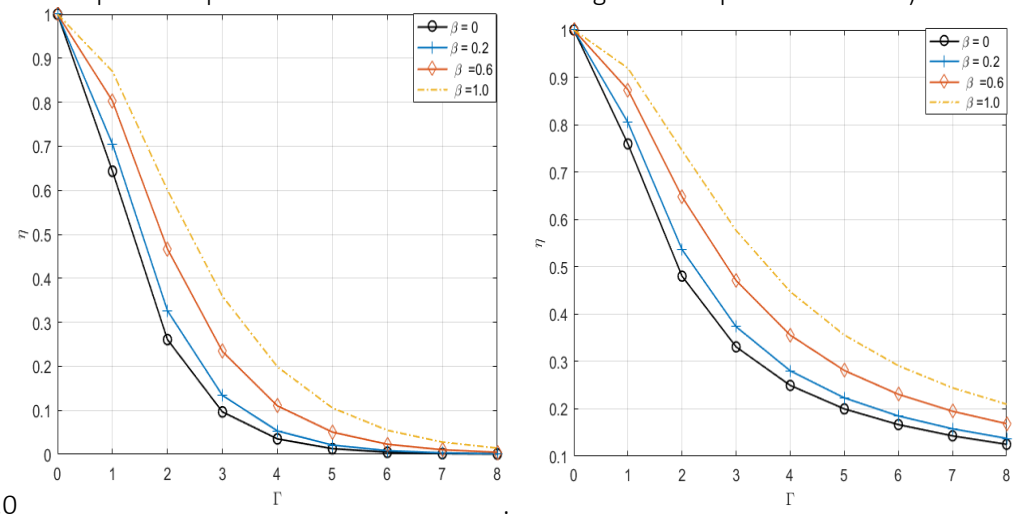

(A) (B)

Fig 3.10.A Temperature at the tip of the fin for HM and FGM vs thermo geometric parameter

Fig 3.10.B Efficiency of the fin for HM and FGM vs thermo geometric parameter

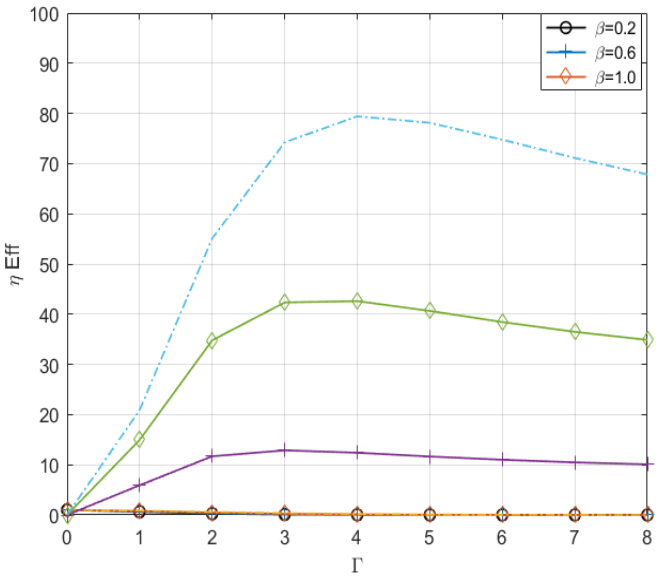

Fig 3.11 Plot for Effective Efficiency plot versus thermo geometric parameter

3.4. Dynamical Analysis

3.4.1. Problem Definition

Considering the Second Order BVP

$$\frac{d^2\theta}{d\xi^2} = \frac{-\beta}{(1+\beta\xi)}\left[\frac{d\theta}{d\xi}\right] + \frac{\Gamma^2\theta}{1+\beta\xi} \qquad \text{eq (3.16)}$$

A) Break in to system of first order nonlinear ODEs

B) Try different scenarios to determine the bifurcation parameter and find the equilibrium points u.

C) Find the Jacobean Matrix of each system

D) Find the Linearization at each equilibrium points and determine the eigenvalue and corresponding stability.

E) Determine the bifurcation point and bifurcation type if any

F) Do a Phase Plane analysis on the system and do a numerical experiment on a parameter(s). A routine (Program) called PPlane9 is used to obtain phase diagrams for this paper.

Steps for Qualitative Analysis First-Order System of ODEs

After breaking of a second order nonlinear ODE in to system of first order nonlinear ODEs we follow the following steps to find the stability information of the system.

STEP 1: Find all the equilibrium points. The equilibrium points are obtained by setting the derivatives of the dependent variables to zero.

STEP 2: Find the Jacobian matrix of the system

STEP 3: Compute the Jacobian matrix at each equilibrium points

STEP 4: Find the eigenvalue of the Jacobian matrix at each equilibrium points to check stability of the System.

STEP 5: Give information about stability based on the eigenvalue and plot the phase portrait

STEP 6: Do a phase plane analysis on the system

STEP 7: Do a numerical experiment on a parameters

3.4.2. Eigenvalues and Stability of Linear ODEs

Based on the above steps we will show how compute and determine using a hand computation and then we will confirm and experiment on MATLAB using PPlane9 and in-built functions.

3.4.3. Solution to Fin Problem

Before doing stability analysis we have to be breaking the second order ODE in to first order system of ODE, we do this through the following steps:

Step 1: Rewrite the original equation in to the following form

$$\frac{d^2\theta}{d\xi^2} = \frac{-\beta}{(1+\beta\xi)}\left[\frac{d\theta}{d\xi}\right] + \frac{\Gamma^2\theta}{1+\beta\xi} \qquad \text{eq (3.17)}$$

Step 2: Introduce new variables T and S.

We denote T = θ, and S = θ'.

Derivation of both T and S yields

$$T' = S$$

$$S' = \frac{-\beta}{(1+\beta\xi)}\left[\frac{d\theta}{d\xi}\right] + \frac{\Gamma^2\theta}{1+\beta\xi} \qquad \text{eq (3.18)}$$

Step 3: Determine the equilibrium points by setting

T' = 0 and

S' = 0 eq (3.19)

and

$$\frac{\Gamma^2 T}{1+\beta\xi} = 0 \qquad \text{eq (3.20)}$$

Hence, $T = 0$

Therefore, we have an Equilibrium point (0,0)

Step 4: Determine the Jacobian of the system.

$$J(T,S) = \begin{bmatrix} 0 & 1 \\ \dfrac{\Gamma^2}{1+\beta\xi} & \dfrac{-\beta}{1+\beta\xi} \end{bmatrix} \qquad \text{eq (3.21)}$$

Step 5: Calculate the jacobian at each equilibrium point to compute the Eigenvalues and Eigenvectors.

Here below, pplane9 is used to undertake the phase plane analysis. Two cases are shown in the Phase Plane analysis since we have two main parameters. First, we will see a case for varying Inhomogeneity index (β). Then, we shall vary and see how the system behaves for varying Thermo geometric parameter (r). Properties including the Jacobian and the Eigenvalues as well as the Eigenvectors are presented.

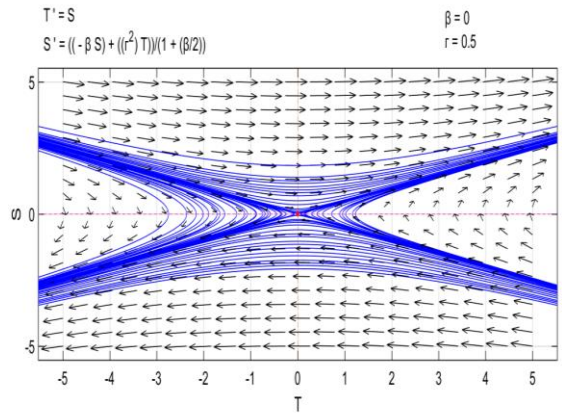

There is a saddle point at (0, 0).

The Jacobian is:

0 1

0.25 0

The eigenvalues and eigenvectors are:

0.5 (0.89443, 0.44721)

-0.5 (-0.89443, 0.44721)

Fig 3.12. Phase plane diagram for β=0 and r = 0.5

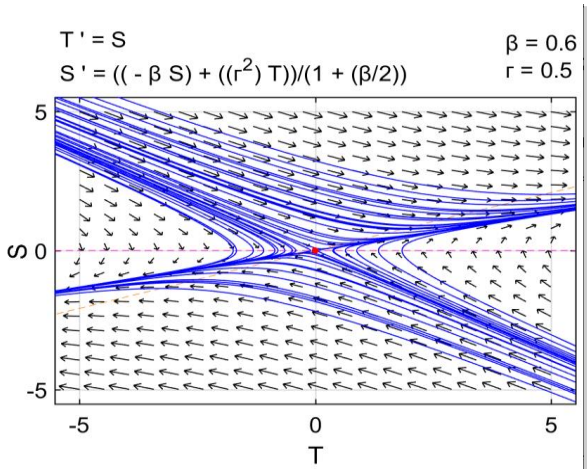

There is a saddle point at (0, 0).

The Jacobian is:

0 1

0.19231 -0.46154

The eigenvalues and eigenvectors are:

0.26477 (0.96669, 0.25595)

-0.72631 (-0.80911, 0.58766)

Fig 3.13.A Phase plane diagram for β=0 and r = 0.5

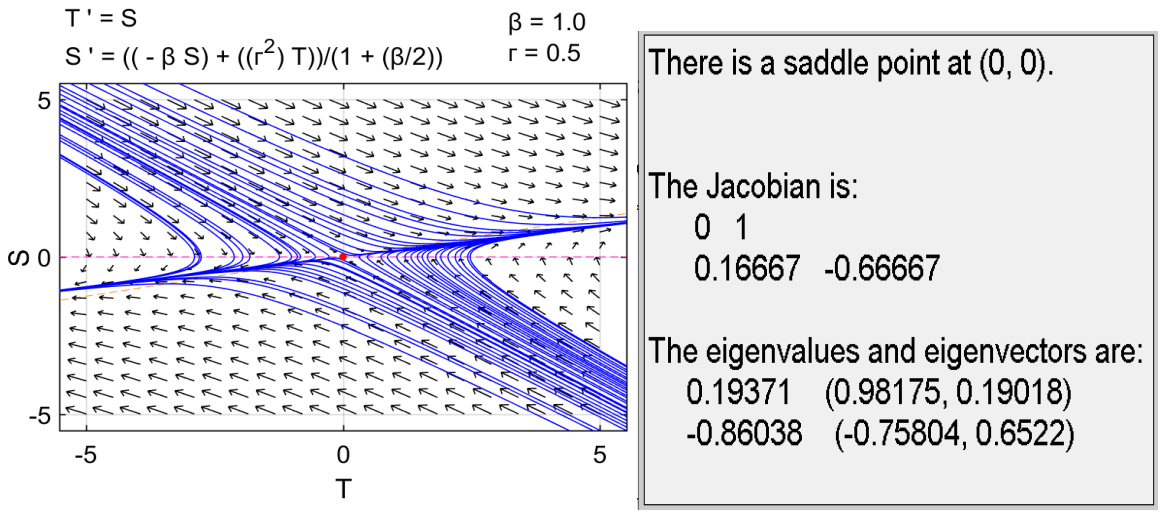

Fig 3.13.B Phase plane diagram for β=0 and r = 0.5

It can be seen from the above figures that the Heat transfer property of the fin does not as such vary for varying (**β).** There is one equilibrium point as been tried to show in the computation of the Equilibrium point earlier. From the phase plane diagrams, one equilibrium point obtained for T=0. As can be seen here, one positive and one negative Eigenvalues are obtained making the equilibrium point saddle. The directional derivatives prove that as some arrows try to get into the equilibrium point whereas some try to leave.

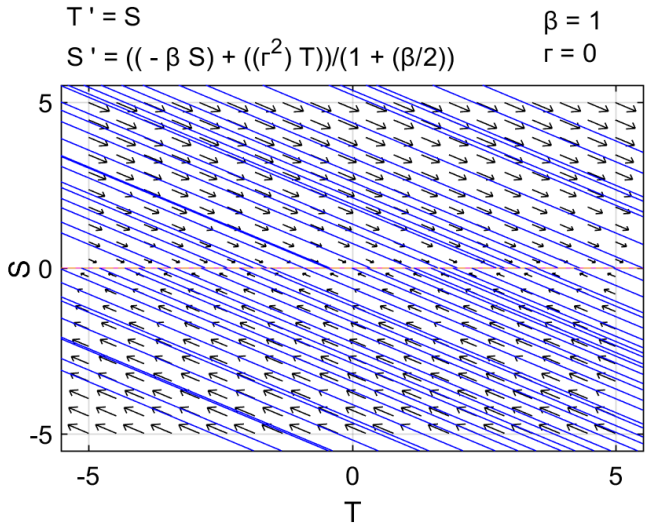

(A)

Fig 3.14.A. Phase plane diagram for β=1 and r = 0

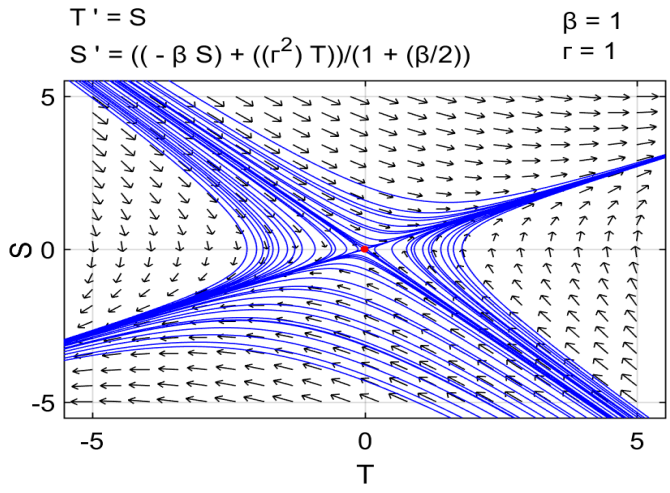

There is a saddle point at (0, 0).

The Jacobian is:

0 1

0.66667 -0.66667

The eigenvalues and eigenvectors are:

0.54858 (0.87674, 0.48097)

-1.2153 (-0.63541, 0.77218)

(B) (C)

Fig 3.14.B-C. Phase plane diagram for β=1 and r = 0

It can be seen from the above figures that the Heat transfer property of the fin vary for varying thermo geometric parameter (**r**). Starting from figure B, There is one equilibrium point as been tried to show in the computation of the Equilibrium point earlier. From the phase plane diagrams, one equilibrium point obtained for T=0. As can be seen here, one positive and one negative Eigenvalues are obtained making the equilibrium point saddle. The directional derivatives prove that as some arrows try to get into the equilibrium point whereas some try to leave.

In Figure 3.14 A, when the thermo geometric parameter goes from one to zero, we can see that the equilibrium point vanishes, which tells us that a saddle node Bifurcation has taken place. As can be observed from the phase plane, the directional derivative arrows tend to get into the horizontal null cline. This tells us that the system is stable for very small values of thermo geometric parameter.

From an intuitive point of view, the equilibrium point is zero. The dimensionless temperature is zero if the temperature of the fin is equal to the ambient temperature. If we slightly increase (perturb) the temperature of the fin, we can see that the heat of the fin dissipates to the ambient, and temperature from the base conducts to the fin to maintain balance for the heat lost to the ambient. We consider the equilibrium point a saddle node since heat from the fin dissipates heat to the ambient and gains heat from the base of the fin, and also the temperature gradient is relatively high throughout the fin.

Chapter Four:

Blasius Flow and Entropy Generation under Thermal Radiation

4.1. Background

The study of the Boundary layer over a flat plate is applied in most engineering fields such as chemical, mechanical, aerodynamic and industrial engineering.

In 1908, Henrich Blasius [28], doctoral student of Prandtl, used Power series method to solve Boundary layer problem. Howarth[29] used numerical method of Runge-Kutta to solve the Blasius equation by hand.

Following these breakthrough, numerous studies have been conducted like [30-31].

Impacts of thermal radiation on the Boundary layer flow is an important concept and has numerous application areas like in Nuclear Power plants, Thermal Energy storages etc.

Hossain et al [32,33] studied the impact if thermal radiation on free convection over a porous vertical plate. He approximated the thermal radiation using Rosseland's approximation. Cortell[35] also studied the impact of Radiation on Blasius flow. Raptis et al [34] analysed radiation in Magneto -Hydrodynamic flows.

In Thermodynamic analysis, it is important to avoid the energy loss or irreversibility of energy inorder to enhance the thermal performance of the system. This can numerically be quantified as Entropy generation. Entropy is the measure of destructed energy that cannot be used to do work. Therefore, the main focus of engineering in relation to this area is to reduce the entropy generated in the system. This is called the Entropy Generation Minimization.

Enropy generation in fluid flow was initially studied by Bejan[36]. Yilbas et al [37] studied entropy generation in a semi-blocked pipe including the swirling effect. Arpaci [38] studied entropy generation due to radiation. Abu–Hijleh et al [39] studied entropy generation due to natural convection from a heated horizontal isothermal cylinder in oil. In his paper, Mahmud[40] applied second law analysis to basic convective heat transfer problems in non-Newtonian fluid flow through a channel made of two parallel plates.

Adnaan Saeed Butt [42] studied Entropy generation in the Blasius flow under thermal radiation. In this paper, modification to [42] has been made with an altered Boundary condition for the thermal aspect of the boundary layer flow.

Blasius flow of Boundary layer under thermal radiation is studied in this paper. In [42], the effect of thermal radiation over a flat plate has been seen by using dirichilet boundary condition for both temperature and flow Boundary Conditions at the plate. But in this paper, a Newman condition for temperature whereby gradient of temperature at the solid surface is assumed to be zero has been employed. This can be interpreted to mean that heat does not flow from the plate to the fluid but rather friction between the plate and the fluid induces frictional heat.

In this paper, emphasis is given to the effect of thermal radiation on entropy generation in entropy generation of boundary layer flow. The shooting Secant method [5] is employed to solve the resulting nonlinear ODEs. Entropy generation, Average Entropy generation, and Bejan number are computed and plotted for in the following sections.

4.2. Mathematical Model

Here, we shall derive the governing differential equation of heat and flow equations are given as follows.

$$\frac{\partial u}{\partial x}+\frac{\partial v}{\partial y}=0 \qquad \text{eq(4.1)}$$

$$u\frac{\partial u}{\partial x}+v\frac{\partial v}{\partial y}=\upsilon\frac{\partial^2 u}{\partial y^2} \qquad \text{eq(4.2)}$$

$$u\frac{\partial T}{\partial x}+v\frac{\partial T}{\partial y}=\frac{\upsilon}{\rho Cp}\left[\frac{\partial u}{\partial y}\right]^2-\frac{1}{\rho Cp}\frac{\partial q_r}{\partial y}+\frac{k}{\rho Cp}\frac{\partial^2 T}{\partial y^2} \qquad \text{eq(4.3)}$$

Where k= thermal conductivity, ρ=density, Cp=specific heat capacity

Equation 4.1 is the continuity equation, equation 4.2 is the Momentum equation and eq 4.3. is the energy equation.

The boundary conditions are given as

Y=0, U=0 and V=0

$Y\to\infty$, $U\to U_\infty$ eq(4.4)

$Y\to 0$, $\frac{dT}{dy}=0$

$Y\to\infty$, T=0 eq(4.5)

From Rosseland approximation, the radiation flux is given as

$$q_r = \frac{-4\sigma}{3k_1}\frac{\partial T^4}{\partial y}$$ eq (4.6)

Where σ is the Steffan-Boltzman Constant and k1 is the absorption coefficient.

For simplification, since T is small, we can approximate T^4 to linear approximation using taylor's series approximation about free stream temperature T_∞.

$$T^4 = 4T_\infty^{\,3}T - 3T_\infty^{\,4}$$ eq(4.7)

From equations 4.6 and 4.7, we obtain

$$\frac{\partial q_r}{\partial y} = \frac{-16\sigma T_\infty^{\,3}}{3k_1}\frac{\partial^2 T}{\partial y^2}$$ eq (4.8)

Therefore, inserting equation 4.8 into equation 4.3, we obtain

$$u\frac{\partial T}{\partial x} + v\frac{\partial T}{\partial y} = \frac{\upsilon}{\rho C_p}\left[\frac{\partial u}{\partial y}\right]^2 + \left[\alpha + \frac{16\sigma T_\infty^{\,3}}{3\rho C_p k_1}\right]\frac{\partial^2 T}{\partial y^2}$$ eq (4.9)

Where α is the thermal diffusivity

The blasius flow equation is given in equation 1.92 in chapter one as

$$f''' + 0.5ff'' = 0$$ eq (4.9.B)

With dimensionless boundary conditions

η=0, f=0 and f'=0

η →∞, f'=1. And for temperature eq(4.10)

For temperature dimensionless temperature is given as

$$\theta(\eta) = \frac{T - T_\infty}{T_w - T_\infty}$$ eq(4.11)

Where Tw is the wall temperature and T∞ is the ambient fluid temperature.

From equation 4.9 and BCs of equation 4.5, we obtain

$$\theta'' + \frac{1}{2}\Pr\left[\frac{3Nr}{3Nr+4}\right]f\theta' + \Pr Ec\left[\frac{3Nr}{3Nr+4}\right]f''2 = 0$$ eq (4.12)

Y→0, $\frac{dT}{dy} = 0$

Y→∞, T=0 eq (4.13)

Where $\Pr = \frac{\mu C_p}{k}$, $Ec = \frac{U_\infty}{C_p\left[T_w - T_\infty\right]}$ and $Nr = \frac{kk_1}{4\sigma T_\infty^{\ 3}}$

The radiation parameter is the contribution of conduction to thermal radiation transfer.

For the case of Entropy Generation, Volumetric Entropy generation given in equation 1.3. Can be extended as

$$S_G = \frac{k}{T_\infty^{\ 2}}\left[\left[\frac{\partial T}{\partial y}\right]^2 + \frac{16\sigma T_\infty^{\ 3}}{3k_1}\left[\frac{\partial T}{\partial y}\right]^2\right] + \frac{\mu}{T_\infty}\left[\left[\frac{\partial T}{\partial y}\right]^2\right] \qquad \text{eq (4.14)}$$

In equation 4.14, the first term describes the entropy due to thermal dissipation (one due to thermal radiation and the other for the conduction and the second term for the dissipation caused by flow.

The dimensionless entropy generation Ns can be defined as

$$Ns = \frac{S_G}{S_0} = \frac{1}{\mathrm{Re}\, x}\left[\left(1 + \frac{4}{3Nr}\right)\theta'^2 + \frac{\Pr Ec}{\Omega} f''^2\right] \qquad \text{eq (4.15)}$$

Where $S_0 = \frac{k(T_w - T_\infty)U_\infty^{\ 2}}{T_\infty^{\ 2}\upsilon^2}$, $\Omega = \frac{T_\infty}{T_w - T_\infty}$ and $\mathrm{Re}_x = \frac{U_\infty x}{\upsilon}$

S_0 is the characteristic entropy generation, Ω is the dimensionless temperature difference and Rex is the local Reynolds Number.

The average entropy generation is found by

$$Nsavg = \frac{1}{N}\int_N Nsd\eta \qquad \text{eq (4.16)}$$

The Bejan Number is defined as the entropy generation due to heat to the overall entropy generation.

The Bejan number is given as

$$Be = \frac{\left(1 + \frac{4}{3Nr}\right)\theta'^2}{\left[\left(1 + \frac{4}{3Nr}\right)\theta'^2 + \frac{\Pr Ec}{\Omega} f''^2\right]} \qquad \text{eq (4.17)}$$

4.3. Results and discussions

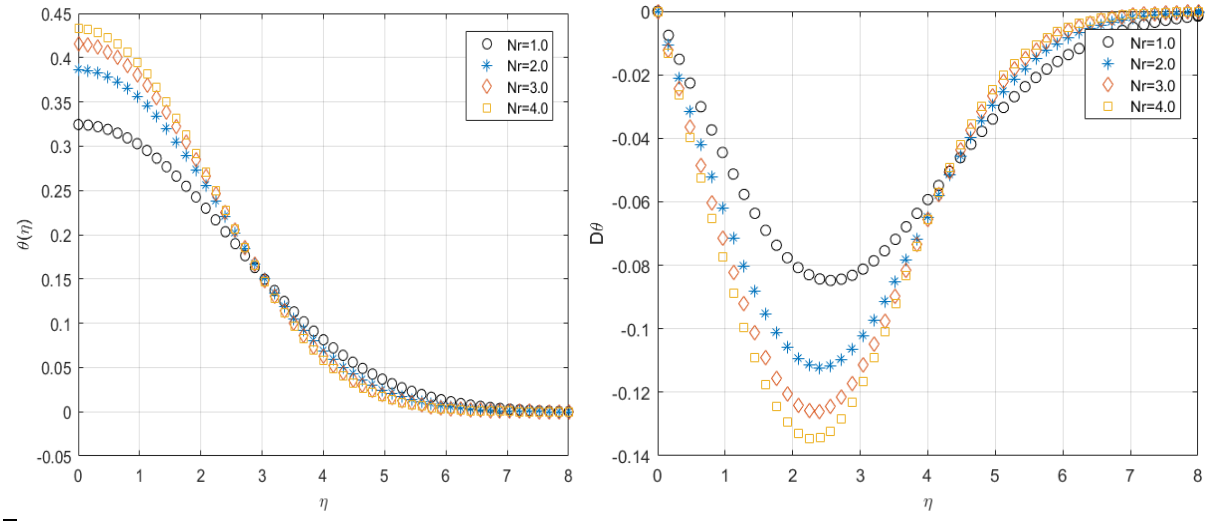

(A) (B)

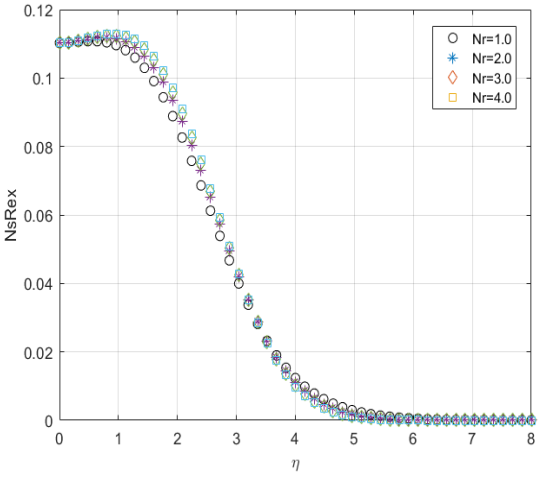

©

Fig 4.1. A. Temperature profile for varying radiation parameter (Nr)

Fig 4.1. B. Temperature Gradient profile for varying radiation parameter (Nr)

Fig 4.1. C. Entropy profile for varying radiation parameter (Nr)

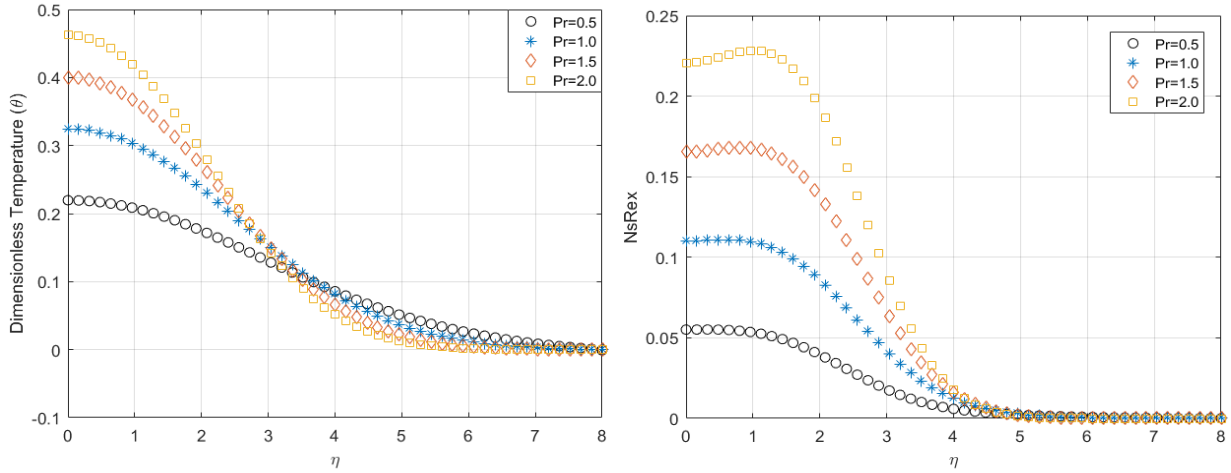

(A) (B)

Fig 4.2. A. Temperature profile for varying Prandtl Number (Pr)

Fig 4.2. B. Entropy profile for varying Prandtl Number (Pr)

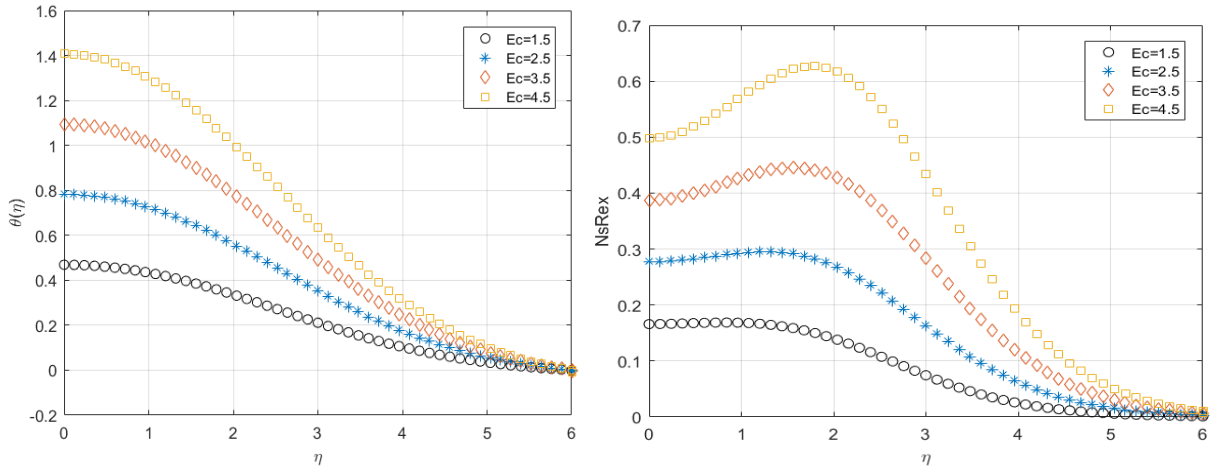

Fig 4.3. A. Temperature profile for varying Eckert Number (ec)

Fig 4.3. B. Entropy profile for varying Eckert Number (ec)

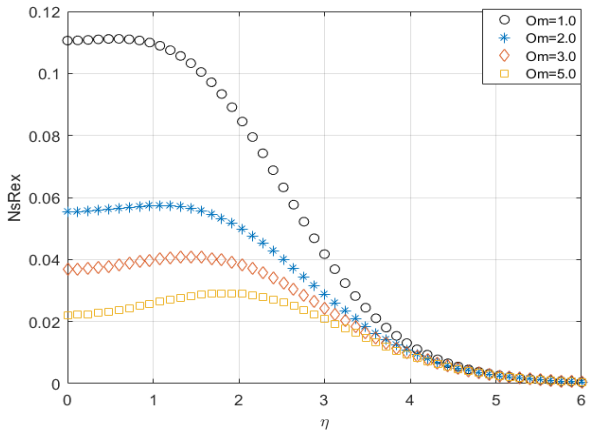

Fig 4.4 Plots to demonstrate the impact of dimensionless temperature difference (Omega) on Entropy generation

Figure 4.1. Shows the relation between the Radiation Parameter (Nr) and temperature, temperature gradient and radiation parameter (Nr), and Radiation Parameter (Nr) and volumetric entropy generation S_G . From figure 4.1A, we can observe that the dimensionless temperature at the plate is maximum due to the skin friction from the plate.

From figure 4.1.B, we can see that the gradient of the temperature is falling up to point close to where η=3, and so does the temperature. In this region, we can deduce that the thermal radiation governs the conduction because Nr is the ratio of Conduction to radiation.That describes the direct relation of the thermal radiation parameter to the entropy.

But after point where η>3, we can see that radiative heat is absorbed rather than dissipated, and hence, the entropy has an inverse relationship with the Radiation parameter. And finally at η=8, dimensionless temperature is zero, and so are the temperature gradient and Entropy generation, since there is no heat transfer at the surface.

Figure 4.2. Shows the effect of Prandtl's number on the temperature profile and the Entropy generation. From the governing equation of dimensionless entropy, we can see that the prandtl number has a direct relationship with the entropy generation. This makes sense since the prandtl number is the measure of dimensionless dissipation,i.e. ratio of flow to heat dissipation, and not absorption, the prandtl number has a direct relation with the entropy generation. For prandtl number less than one (heat dissipation governing) also, the NsRex vs η has the same relation and the plots are similar to that of 4.2.B.

From fig 4.2.B, we can see that starting from η=4, the entropy for all Pr values become zero. This is because as stated earlier, the region where η>=3,the second region, conduction is the governing heat transfer and as conductivity increases, the Pr tends to zero.

Figure 4.3. Entails the impact of the Eckert Number on the temperature and entropy profile. From Figure 4.3.A, we can deduce that since the temperature is the average molecular kinetic energy, the kinetic energy and the Eckert number have a direct relation.

Figure 4.3.B shows the entropy profile. The entropy increases with an increase in Eckert Number. We have seen that the Eckert number is the ratio of kinetic Energy to Enthalpy, and since entropy and Enthalpy have inverse relation, increase in Eckert number results in reduced enthalpy and in reverse, results in increased entropy.

Figure 4.4. Shows the impact of the dimensionless temperature difference. As seen previously, the dimensionless temperature difference describes the difference in temperature between the wall and the ambient fluid. If the dimensionless temperature difference between the wall and the ambient is small, the heat transfer would be minimal and results in smaller entropy generation. And Ω is given as the ambient temperature to the difference in temperature between ambient and the wall. As the difference between the ambient and the wall temperatures decreases, Ω increases and hence results in the decrease of Entropy. This inverse relation is shown in the figure, figure 4.4.

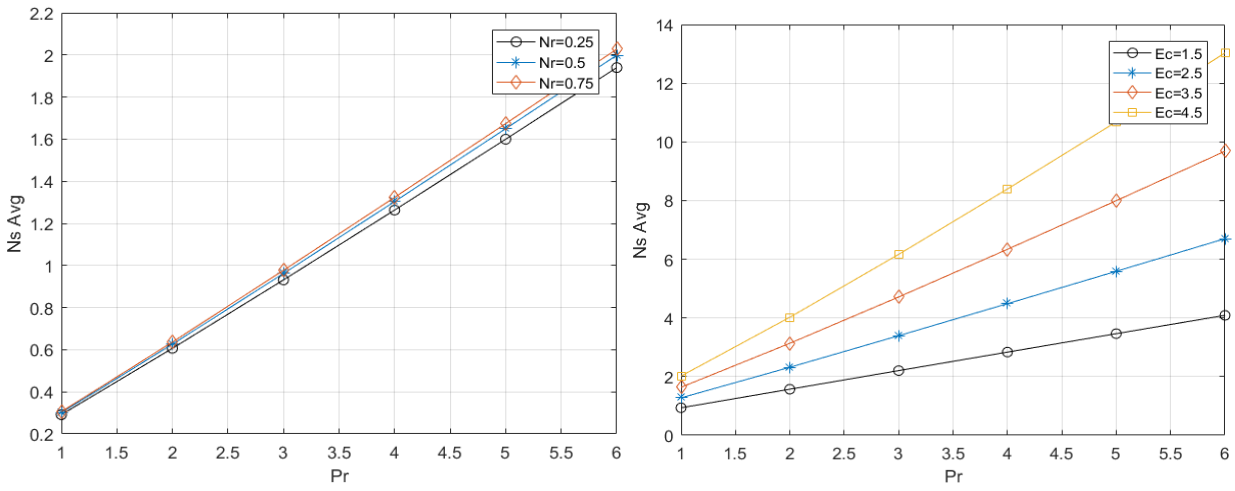

(A) (B)

Fig 4.5.A. Effect of (A) Radiation Parameter and (B) Eckert Number on the relation between average entropy and Prandtl Number

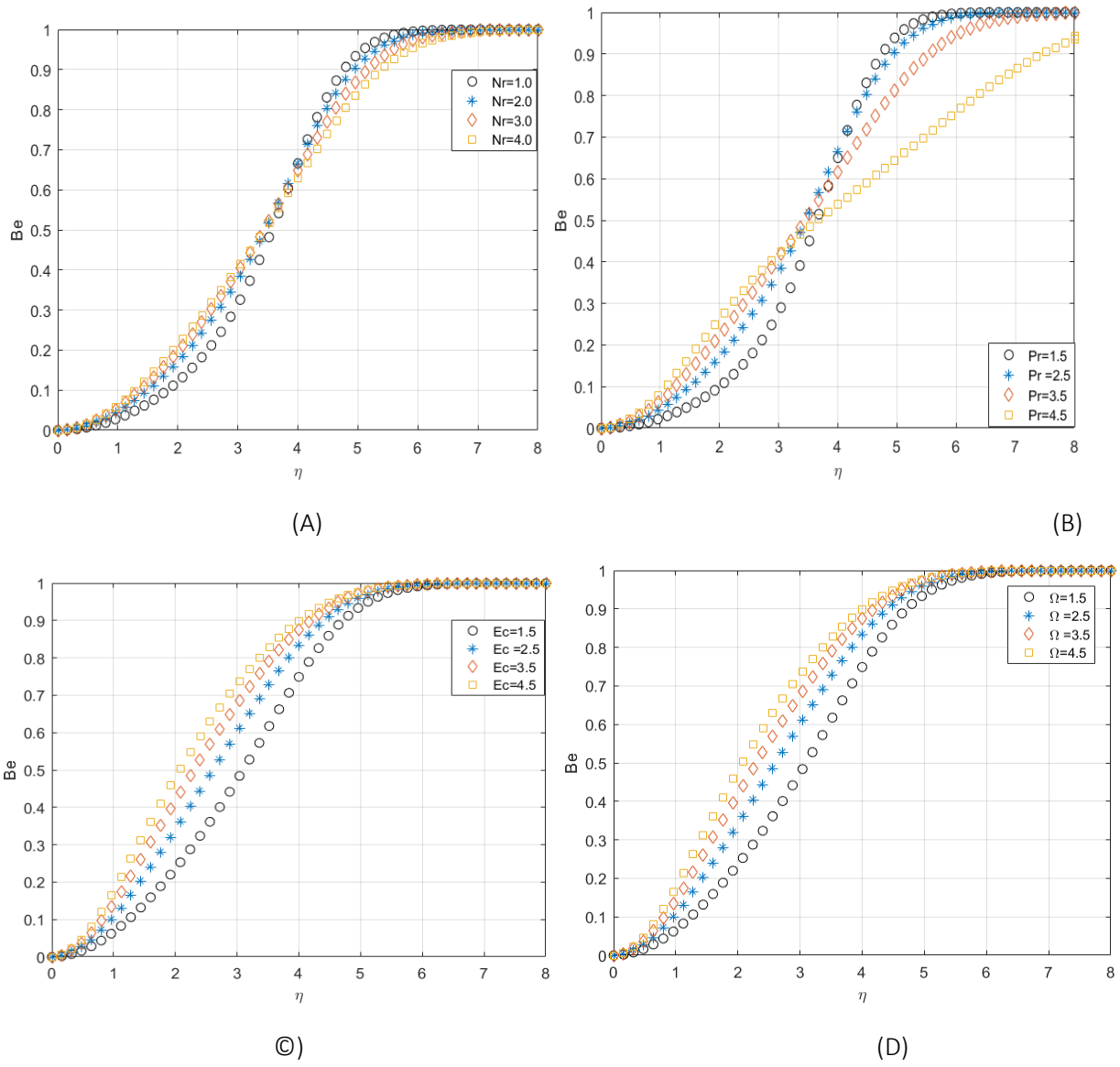

Fig 4.6.Relation between Bejan Number and dimensionless length with varying (A). Nr (B). Pr (C). Ec and (D). Ω

Figure 4.5.A shows the effect of Radiation Parameter on the relation between average entropy and prandtl number. We see that the average entropy increases with increase in Pr since dissipation increase. And the average entropy increases with an increase in radiation parameter. In Fig 4.5.B, we see the effect of Eckert Number on the average entropy vs Pr relation. Ns Average increases with an increase in Eckert number as the entropy and enthalpy in the Eckert number have an inverse relationship.

Figure 4.6 (A-D) shows the impact of Radiation parameter,Prandtl number, Eckert number and Temperature difference to the bejan number. For all four Bejan profiles, we can see that below the value of about η=3, entropy produced by viscosity governs. But after that, entropy due to heat governs since

Be>=0.5. Starting from η=5, to the surface, the Bejan number is almost one. This indicates that the viscosity effect almost vanishes and entropy due to heat transfer dominates.

4.4. Conclusion

The effect of entropy generation under thermal radiation for Blasius flat plate is analyzed. We have seen that for η<=3, the radiation parameter has direct relationship with the entropy showing there is an emission rather than absorption of heat. This effect is reversed for η>3, and thermal absorption takes place. This describes the inverse relationship between the Nr and entropy.

Both Prandtl number and Eckert number have a direct relation to the entropy generation. And the dimensionless temperature difference has an inverse relation to the entropy generation since minimal heat transfer ends up in lower entropy generation.

The average entropy is related to the Prandtl number with varying radiation parameter and is found out that they have direct relationship as can be seen in fig 4.5.A, and so does the Eckert Number in figure Fig 4.5.B.

Finally, the Bejan number which entails the contribution of entropy due to heat transfer to the overall entropy is discussed. It is shown that upto η<=3, the entropy due to the viscous dissipation governs and after η>4, the entropy due to heat transfer governs as Be>=0.5. But after η>5, the effect of entropy due to viscous dissipation vanishes so the entropy generation is almost entirely due to heat dissipation.

In an Engineering application, it is desirable to minimize the entropy generation by a system. To do so, in the case of this chapter, it is recommended to use a fluid with lower Pr. And also, since the Entropy generation is minimum for smaller Ec, it is recommended to reduce the friction between the fluid and the wall.

Chapter 5.

Numeric Solutions of Magneto-Hydrodynamic (MHD) Viscous Flow over a Shrinking Sheet and Extensions to Boundary Layer Flow Over a Porous Media

5.1. Numerical solutions of MHD viscous flow over a shrinking sheet

5.1.1. Background

The flow induced by a moving boundary is highly important in the extrusion processes in plastic and metal industries. MHD researches have importance in areas such as power generators, the cooling of reactors, polymer and metal industry, and spinning of filaments. In industrial applications, when sheets or filaments are made to cool, these get stretched. Cooling process is then controlled by applying the magnetic field to the filament; in order to get the final products with desired shapes.

In this paper, we try to see numerical solution for the resulting third order nonlinear ODEs and their comparison to analytic solutions given in [61].

This chapter contains two sections both of MHD applications to Boundary Layers in Cartesian Coordinates. The first section deals with Magneto-Hydrodynamic (MHD) Viscous Flow over a Shrinking Sheet while the second is Extensions to Boundary Layer Flow over a Porous Media.

Moving Boundary flow is a famous field of study and is important in metal and plastic industries as can be seen in [43-44]. Sakiadis [45] carried out a pioneering work in in boundary layer flow on a stretching surface with a constant speed. Tsou et al. [46] extended the work by experimentally verifying it. Several studies have been conducted using the boundary conditions [47-55]. Most solutions use boundary layer assumptions and are not exact solutions except for [47].

Miklavcic and Wang [56] investigated flow over a shrinking sheet. This solution is an exact solution of the Navier-Stokes equation.

The shrinking sheet problem was also extended to power-law shrinking velocity or other fluids [21–23].

Magneto-Hydrodynamic flow over a shrinking sheet was studied by Sajid [60]. Tiegang Fang * and Ji Zhang studied the closed form exact solution of Magneto hydrodynamics viscous flow over a shrinking sheet.

In this section, we shall try to verify the result using a shooting secant scheme [5] (Numerical Solution) and error analysis with [60] is conducted.

5.1.2. Mathematical Formulation

Consider a steady steady state 2-D flow over a stretching sheet. The shrinking velocity of the sheet is given as s $U_w = U_0X$, and the wall mass transfer is given by Vw(x).The x-axis is considered as a direction opposite to the shrinking sheet. The governing continuity and NS equations are given as follows

$$\frac{\partial u}{\partial x}+\frac{\partial v}{\partial y}=0 \qquad \text{eq(5.1)}$$

$$u\frac{\partial u}{\partial x}+v\frac{\partial v}{\partial y}=-\frac{1}{\rho}\frac{\partial P}{\partial x}+\upsilon\left[\frac{\partial^2 u}{\partial x^2}+\frac{\partial^2 u}{\partial y^2}\right]-\frac{\sigma B^2}{\rho}u \qquad \text{eq(5.2)}$$

$$u\frac{\partial v}{\partial x}+v\frac{\partial v}{\partial y}=-\frac{1}{\rho}\frac{\partial P}{\partial y}+\upsilon\left[\frac{\partial^2 v}{\partial x^2}+\frac{\partial^2 v}{\partial y^2}\right] \qquad \text{eq(5.3)}$$

Subject to Boundary Conditions

$U(x,0)=U_0X$, $V(x,0)=V_0X$ and $U(X,\infty)=0$ eq (5.4)

where u is the velocity in the X direction, v is the velocity in the y directions respectively, ϑ is the kinematic viscosity, p is the pressure, ρ is the density of the fluid, and σ is the electrical conductivity of the fluid.

The magnetic field B is applied in the vertical direction and the induced magnetic field is neglected. These equations are only valid for small magnetic Reynolds number.

Stream functions are given as

$$\psi(x,y)=f(\eta)x\sqrt{vU_0} \quad \text{and} \qquad \text{eq (5.5)}$$

$$\eta=y\sqrt{\frac{U_0}{v}} \qquad \text{eq (5.6)}$$

The resulting velocities can be expressed as

$$u=-\sqrt{U0}xf'(\eta) \quad \text{and} \qquad \text{eq(5.7)}$$

$$v=\sqrt{U_0V}xf(\eta) \qquad \text{eq(5.8)}$$

And mass transfer velocity is given by

$$u_w x = -\sqrt{U_0}\, x f'(0) \qquad \text{eq (5.9)}$$

The self-similar solution is given as

$$f''' + f f'' - f'^2 - M^2 f' = 0 \qquad \text{eq (5.10)}$$

Subject to dimensionless Boundary Conditions

$$f(0) = s,\ f'(0) = -1 \text{ and } f'(\infty) = 0 \qquad \text{eq (5.11)}$$

5.1.3. Methodology

From the continuity and the Navier Stokes equations which are two dimensional PDEs,self-similar solution is used to convert the PDE into a third order nonlinear ODE given in equation 5.10. Equation 5.10 is our governing equation subjected to dimensionless boundary conditions.

In this chapter, numerical solution of Shooting Secant method [5] is used. The third order nonlinear ODE is broken down into three first order nonlinear ODEs.

$$\frac{df}{d\eta} = p$$

$$\frac{dp}{d\eta} = q, \qquad \text{eq (5.12 A-C)}$$

$$\frac{dq}{d\eta} = (-f * q) + M^2 f'$$

5.1.4. Results and Discussions

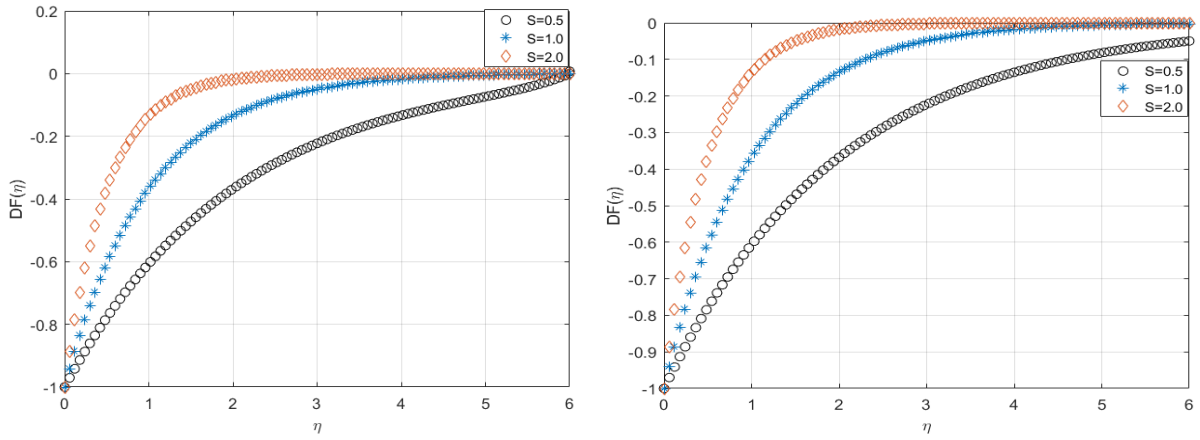

(A) (B)

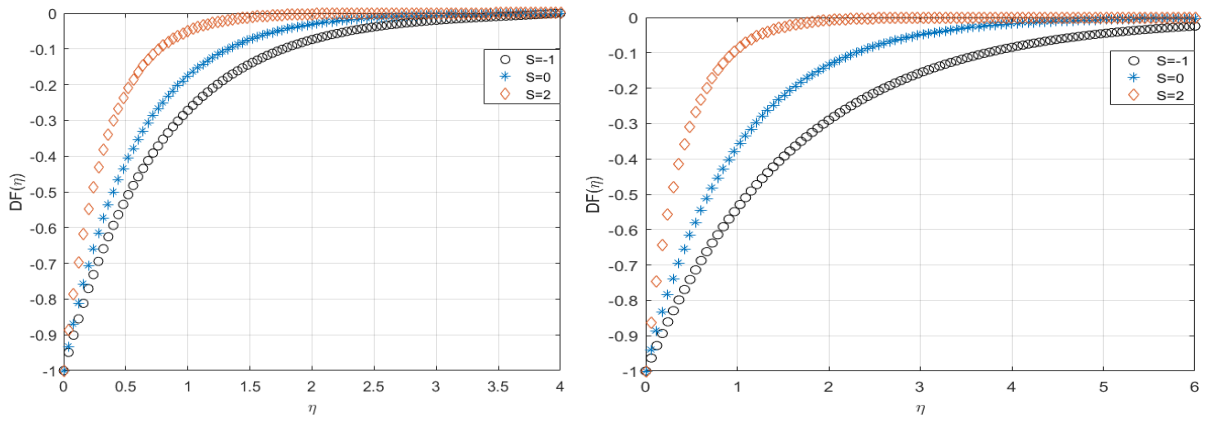

© (D)

Fig 5.1.4.(A-B) Velocity Profile for Magnetic parameter of 2.0 with varying Suction parameter (A) Numerical Solution and (B). Analytic Solution

Fig 5.1.4.(C-D) Velocity Profile for Magnetic parameter of 1.0 with varying Suction parameter (A) Numerical Solution and (B). Analytic Solution

Here, as can be seen from table 5.1 and figures 5.1.4(A-D), it can be seen that our numerical solutions for the velocity profile are in very good agreement with that of the analytic.

And also, Fig 5.1.4(A-D) show the velocity profile with varying suction parameter. It can be seen that as the suction increases, with positive S value, the velocity decreases and tends to zero, which can be taken as intuitively correct.

Here, from figure 5.1.4.A., it can be seen that for larger magnetic parameter M=2, the flow is blown away from the wall for small suction parameter.

For larger Suction parameter, the lower thickness of the flow takes the velocity of the wall. But in a close vicinity to the wall, the velocity profile gets drawn very close to the wall.

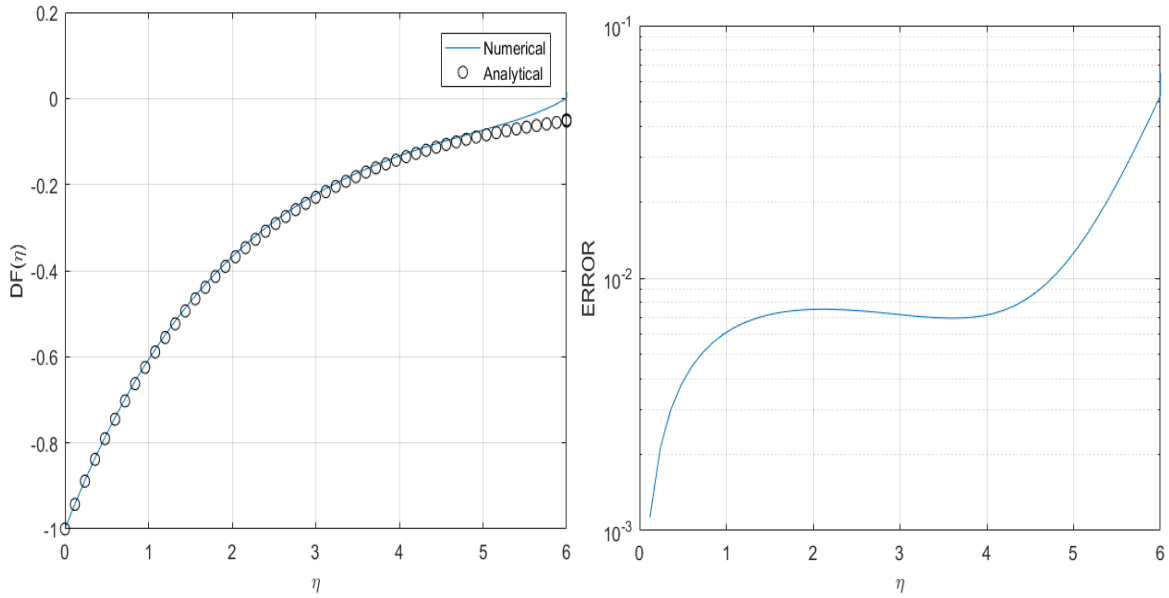

(A) (B)

Fig 5.1.5. A Comparison between analytic versus numeric solution for S=0.5 and Mp=1.0

Fig 5.1.5.B. Semilogy plot for S=0.5 and Mp=1.0

Table 5.1. Table for Analytic, Numerical and Absolute Error

ETA	Analytic Solution	Numerical Solution	Relative Error
0.00	-1	-1	0
0.60	-0.74	-0.75	4.40E-03
1.20	-0.55	-0.56	6.60E-03
1.80	-0.41	-0.41	7.40E-03
2.40	-0.3	-0.31	7.50E-03
2.80	-0.25	-0.26	7.30E-03
3.20	-0.2	-0.2	7.00E-03
3.60	-0.16	-0.17	6.90E-03
4.00	-0.14	-0.14	7.10E-03
4.40	-0.11	-0.11	8.20E-03
4.80	-0.085	-0.095	1.00E-02
5.20	-0.065	-0.08	1.50E-02
5.80	-0.034	-0.063	2.90E-02
6.00	-9.50E-05	-0.053	6.49E-02

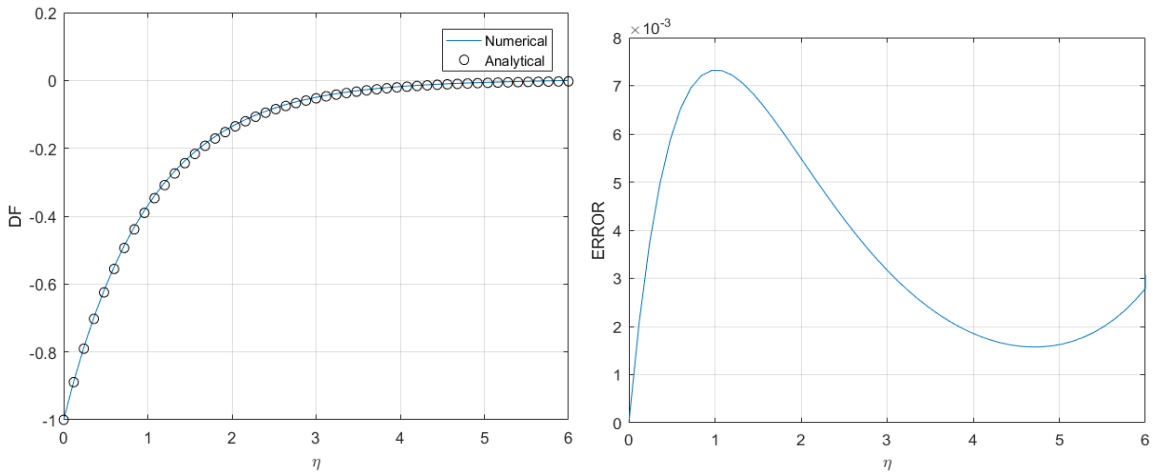

(A) (B)

Fig 5.1.5.C Comparison between analytic versus numeric solution for S=1.0 and Mp=1.0

Fig 5.1.5.D. Semilogy plot for S=1.0 and Mp=1.0

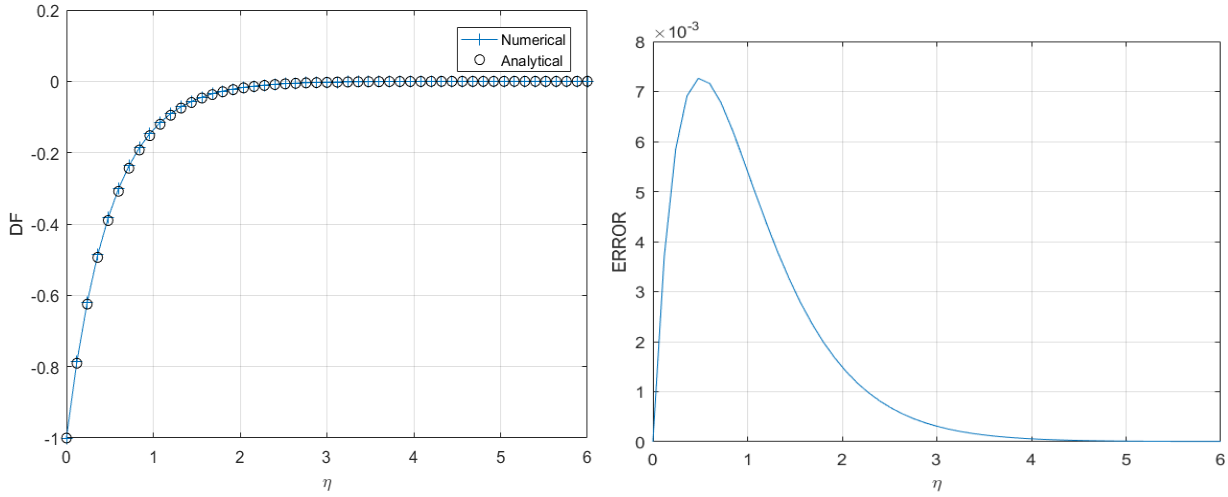

(A) (B)

Fig 5.1.6. A Comparison between analytic versus numeric solution for S=1.0 and Mp=1.0

Fig 5.1.6.B. Semilogy plot for S=1.0 and Mp=1.0

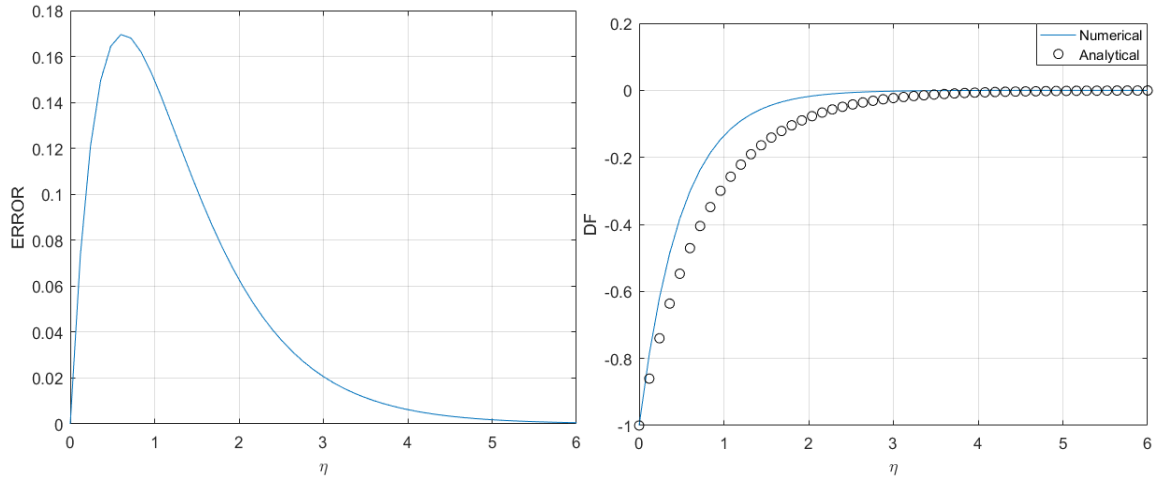

(A) (B)

Fig 5.1.7. A Comparison between analytic versus numeric solution for S=0.5 and Mp=2.0

Fig 5.1.7. B. Semilogy plot for S=0.5 and Mp=2.0

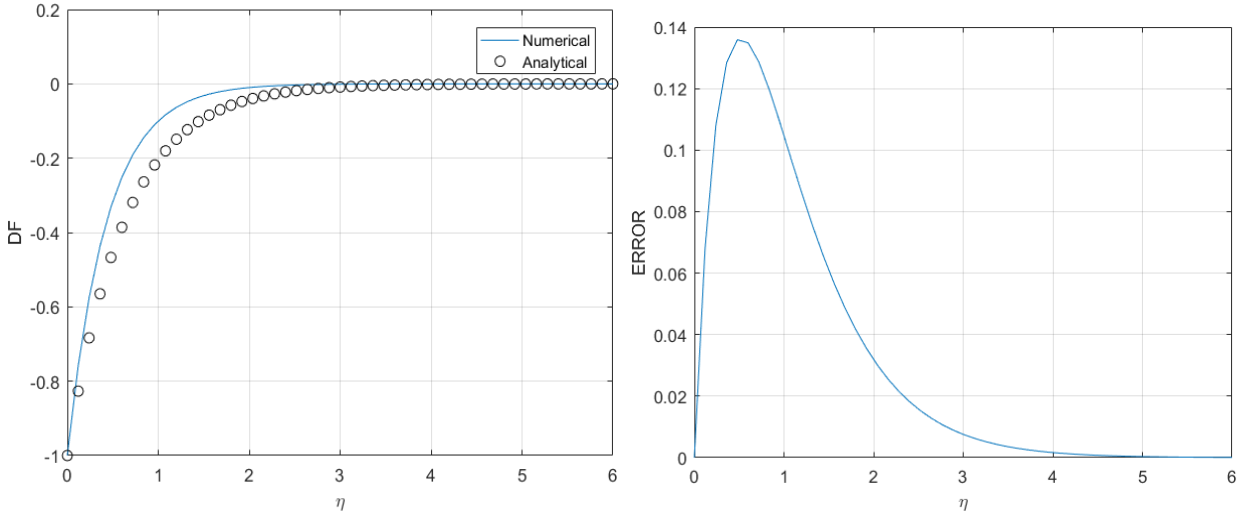

Fig 5.1.8. A Comparison between analytic versus numeric solution for S=1.0 and Mp=2.0

Fig 5.1.8. B. Semilogy plot for S=1.0 and Mp=2.0

Again, a comparison has been made for positive values of β, as can be seen from Figures (5.1.5-5.1.8), we can see that the numerical results are in a good agreement with that of the analytic results. By further minimizing the grid spacing and iterations, the error can further be reduced.

5.2. Numeric Solutions of Magneto-Hydrodynamic (MHD) Viscous Flow Extensions to Boundary Layer Flow Over a Porous Media

5.2.1. Background

The study of flow with mass transfer is widely applied in a variety of engineering sectors as in energy storage of Ground water. When porous materials such as material sheet with small holes is used at one edge and the other with free stream velocity is maintained, it creates injection/Suction through the boundary.

Porosity is represented by the normal relative velocity α (α>0 for suction and α<0 is assumed to be injection)

Numerous studies have been conducted in the area of MHD boundary layer flow of electrically conducting fluids.

Boundary layer flow of a conducting incompressible viscous fluid due to deformation of an elastic surface in uniformly applied magnetic field is studied by Pavlov [62]. Andersson [63] studied MHD viscous flow over a stretching plate and demonstrated the effect of magnetic field having the same effect as of viscoelasticity. Heat and mass transfer of viscous fluid in an electrically conducting fluid demonstrating that MHD decreases the boundary layer thickness has been show in studies. [64-67].

Hayata et al.[68] studied two dimensional magneto hydrodynamic boundary layer flow in a porous media using Homotopy Analysis Method (H.A.M.) to solve the governing ODEs.

Xu et al. [69] employed Homotopy Analysis Method to study the Boundary Layer Flow and Heat transfer of viscous flow of an electrically conductive flow. The paper demonstrated appliacation of magnetic field reduces the Boundary layer thickness but reduces the Thermal Boundary layer.

The study of fluid flows and mass transfer problems has significant applications in a wide variety of geophysical and engineering application such as flow of ground water energy storage and chemical reactors (Nield and Bejan [70])

Ramesh B. Kudenatti,1 Shreenivas R. Kirsur,2 Achala L. Nargund,3 and N. M. Bujurke4 [71] studied

Similarity Solutions of the MHD Boundary Layer Flow Past a Constant Wedge within Porous Media.

In this chapter, Numerical method of a shooting scheme [5] is employed to verify results from the analytic method. It is proven that the application of magnetic field reduces the flow of velocity and also reduces the boundary layer thickness. Error Analysis w.r.t [71] is demonstrated.

5.2.2. Mathematical Model

The Lorentz force is a body force that couples Fluid flow with magnetic field, neglecting the force due to electric field, it can be given as

$$J \times B = -\sigma B^2 q$$ eq(5.2.1.A)

Where J is the current density, B is the magnetic field strength, q is the velocity vector in X and Y directions and σ is the electrical conductivity

It is assumed that the magnetic Reynolds Number is small.

The governing differential equation for two dimensional flow is given as

$$\frac{\partial u}{\partial x} + \frac{\partial v}{\partial y} = 0$$ eq(5.2.1)

$$\frac{1}{\varepsilon^2}\left[u\frac{\partial u}{\partial x} + v\frac{\partial u}{\partial y}\right] = -\frac{1}{\rho}\frac{\partial P}{\partial x} + \upsilon\frac{\partial^2 U}{\partial y^2} - \frac{\upsilon}{K}u - \frac{\sigma B^2}{\rho\varepsilon}u$$ eq(5.2..2)

$$\frac{\partial P}{\partial y} = 0$$ eq(5.2..3)

Equation 5.2.1. is the continuity equation, equation 5.2.2 is the Navier stokes equation in the X direction which includes the drag term introduced by the application of the Magnetic field. And the third equation is the Navier stokes equation in the Y direction.

In equation 5.2.1, ε is the porosity is the thermal conductivity, K is the permeability of the porous medium, B is the magnetic field strength and the remaining terms are introduced earlier in the previous sections for boundary layer flow.

Again in Equation 5.2.2. the left hand side is the advection term with introduced porosity, and the right hand side is the forcing term which, from left to right, are given as force due to pressure term, force due to viscosity (shear stress), force due to porous medium and force due to coupling of the magnetic field.

The boundary layer equation for MHD flow for the mainstream velocity is given as

$$\frac{1}{\varepsilon^2}\left[u\frac{\partial u}{\partial x} + v\frac{\partial u}{\partial y}\right] = -\frac{1}{\varepsilon^2}U_{(X)}\frac{dU_{(x)}}{dx} + \upsilon\frac{\partial^2 U}{\partial y^2} - \frac{\upsilon}{K}(u - U_{(X)}) - \frac{\sigma B^2}{\rho\varepsilon}(u - U_{(X)})$$ eq (5.2.4)

The mainstream velocity (x) is related by the power-law relation (x) = $U_\infty x^m$, where U_∞ is mainstream velocity which is constant and m defines the strength of pressure gradient.

Boundary Conditions are given as

@Y=0, U=0 and V=Vω and eq (5.2.5)

@Y=∞, U=$U_{(X)}$.

Applying law of similarity, we obtain the stream function and the dimensionless length are given as

$$\psi = \sqrt{\frac{2\upsilon x U_{(x)}\varepsilon^2}{1+m}}\, f(\eta)$$ and eq(5.2.6)

$$\eta = \sqrt{\frac{U_{(x)}(1+m)}{2\varepsilon^2 \upsilon x}}\, y \qquad \text{eq(5.2.7)}$$

Finally, the governing dimensionless equation for the MHD Boundary layer is given as

$$f'''(\eta) + f(\eta) f''(\eta) + \beta(1 - f'^2(\eta)) - (\Omega + M^2)(f'(\eta) - 1) = 0 \qquad \text{eq(5.2.8)}$$

Subject to dimensionless Boundary Conditions

$$\begin{aligned} f(0) &= \alpha \\ f'(0) &= 0 \\ f'(\infty) &= 1 \end{aligned} \qquad \text{eq(5.2.9)}$$

Equation 5.2.8 is the modified falkner skan equation which accounts for the effect of MHD on a porous surface,

α is the suction/Injection parameter, whereby positive values indicate suction whereas negative values indicate injection, and a zero value indicates impermeable (i.e. No suction or injection). The dimensionless equation is given as $\alpha = -(1/\epsilon)\sqrt{2x/(m+1)]U(x)Vw)}$. β is a parameter for pressure gradient given by $2m/(1+m)$. Positive β value is favorable pressure gradient and negative one is adverse pressure gradient.

M is the magnetic parameter (Hartmann's Number) given by $M = B_0^{\,2}\sqrt{2\sigma\varepsilon / \rho U_\infty (\mathrm{m}+1)}$, which relates the electromagnetic force to the viscous force. And Ω is given as the dimensionless permeability, given as $2\epsilon 2\ (U\infty/])\ (m-2)/(m+1)\mathrm{Re}(m-1)$.

5.2.3. Results and Discussions

TABLE FOR COMPARISON OF [71] FOR CONFORMATION

As the table on the described reference paper has numerical and analytical results, I have selected few and ultimate parameters for conformation purposes on the table listed below.

Table 2. Selected parameters for Comparison for alpha value of -2.5

MP	alpha	Beta	Om	L	Exact Solution on [71]	Numerical on Kudenatti's Paper [71]	Numerical
1	-2.5	0.5	0.1	4	0.55406	0.55406	0.55406
1	-2.5	1.5	0.1	4	0.86272	0.86328	0.86327
1	-2.5	2.5	0.1	4	1.13996	1.139960	1.139975
1	-2.5	0.5	0.5	4	0.66494	0.66503	0.665026772
1	-2.5	1.5	0.5	4	0.9616	0.95955	0.95956568
1	-2.5	2.5	0.5	4	1.22414	1.22549	1.2255
1	-2.5	0.5	1	4	0.79464	0.79464	0.7946369
1	-2.5	1.5	1	4	1.07365	1.07367	1.073699251
1	-2.5	2.5	1	4	1.3274	1.32796	1.327990346

Selected parameters for Comparison from Table 2 for alpha value of 1

MP	alpha	Beta	Om	L	Exact Solution on Kudenatti's paper [71]	Numerical on Kudenatti's Paper [71]	Numerical
2	1	1	0.3	4	3.17575	2.98078	2.980794476
2	1	2.5	0.3	4	3.68438	3.36234	3.362396
2	1	3	0.3	4	3.83702	3.478420	3.4785
2	1	1	1.5	4	3.24889	3.05951	3.2102647
2	1	2.5	1.5	4	3.74628	3.43084	3.48657
2	1	3	1.5	4	3.89618	3.54436	3.672163
2	1	1	100	1	10.8331	10.78467	10.78468
2	1	2.5	100	1	10.9767	10.88218	10.8822096
2	1	3	100	1	11.0258	10.91448	10.9145127

As can be seen from the table above, the numerical from the Kudenatti's paper [71] is close to a four decimal points with that of my result.

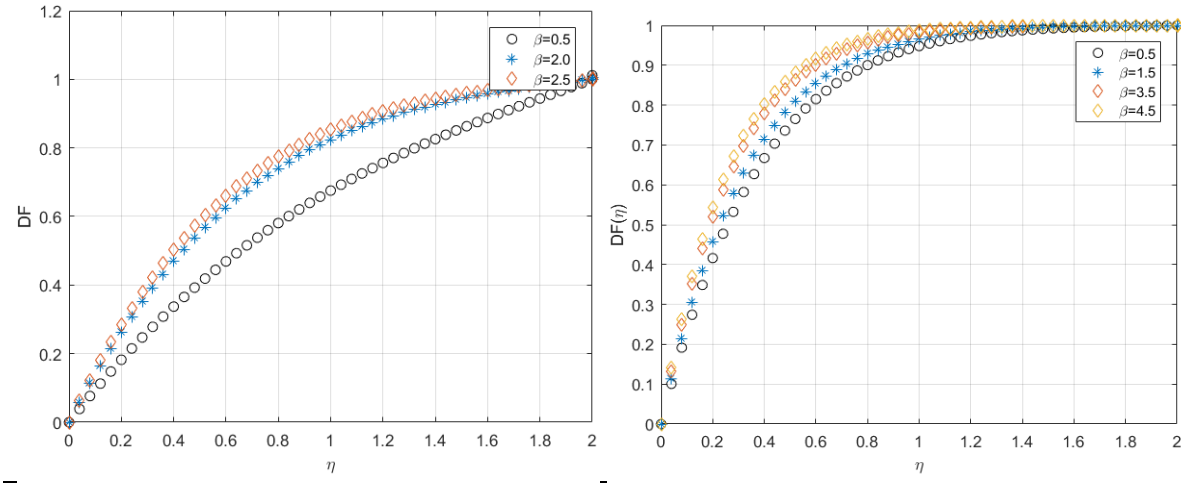

(A) (B)

Fig 5.2.3.1.A. Velocity profile for parameters Ω = 1.4, M = 0.5, α = -1.5

Fig 5.2.3.1.B. Velocity profile for parameters Ω = 0.95, M = 1.0, α = 1.5

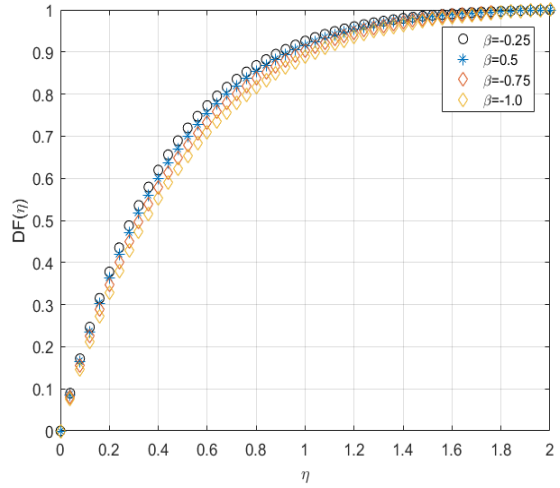

Fig 5.2.3.1.C. Velocity profile for parameters Ω = 1.0, M = 1.0, α = 1.4

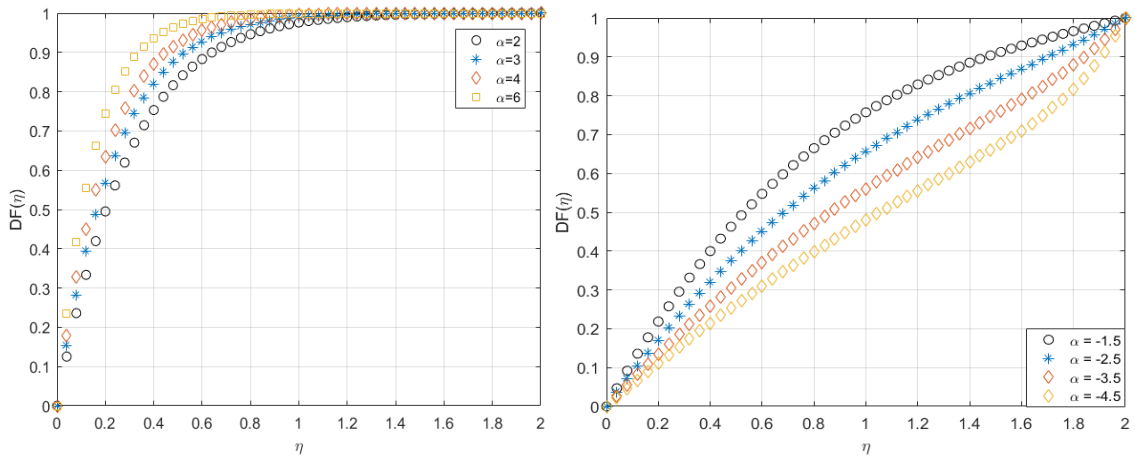

(A) (B)

Fig 5.2.3.2.A. Velocity profile for parameters Ω = 2.0, M = 0, β = 1.3

Fig 5.2.3.2.B. Velocity profile for parameters Ω = 2.0, M = 0.5 β = 1.4

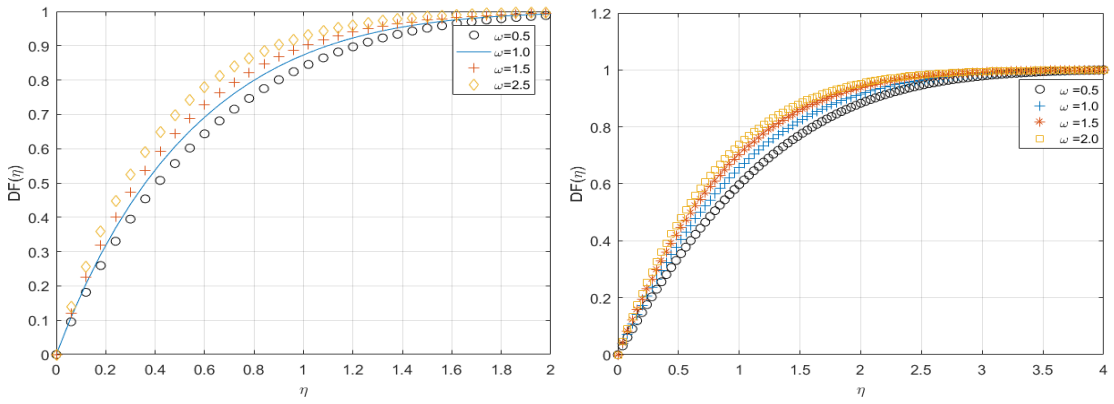

(A) (B)

Fig 5.2.3.3.A. Velocity profile for parameters α = 1.5, M = 1.0, β = −1.5

Fig 5.2.3.3.B. Velocity profile for parameters α = −1.6, M = 0.5, β = 1.0

From Table 1, we can see that there is a fairly good agreement of the numerical result to that of the analytic one from [71] . This validates the result of this paper.

Figures 5.2.3.1.(A-C) shows the velocity profile for varying β values with adverse and favorable pressure term. We can see that as the positive value of β increases, the velocity reduces through the boundary layer and tends to zero. This tells us that for positive β values, the pressure gradient is towards the wall and as it increases, the velocity decreases.

But for negative values of β, as the value of β gets away from zero, the velocity increases. This tells us that the pressure gradient is reversed and is away from the wall. And as it gets away from zero, the velocity increases through the boundary layer.

Figure 5.2.3.2.(A-B) shows for positive value of α, which indicates suction, it can be seen that the velocity tends to one (increases) with an increase in the suction parameter α. But for the negative values of α indicating injection, as the α value tends away from zero, the velocity reduces and when it tends towards zero, the velocity increases. We can also see from figure 5.2.3.2.(A-B) that, the velocity profile is blown away from the wall for injection, where α<0.

From Figure 5.2.3.2.(A-B), we can see that as the porosity parameter increases, for both suction and injection cases, the velocity also increases.

5.2.4. Far Field Behavior

The impact of Magnetic parameter (MP) or the Hartmann Number, the pressure term (β) and the Suction parameter (α) is shown in Fig 5.2.3.4.(A –C). The boundary layer thickness is found by the equation given as

$$\sigma = \int_0^\infty [1 + f'(\eta)] d\eta \qquad 5.2.10.$$

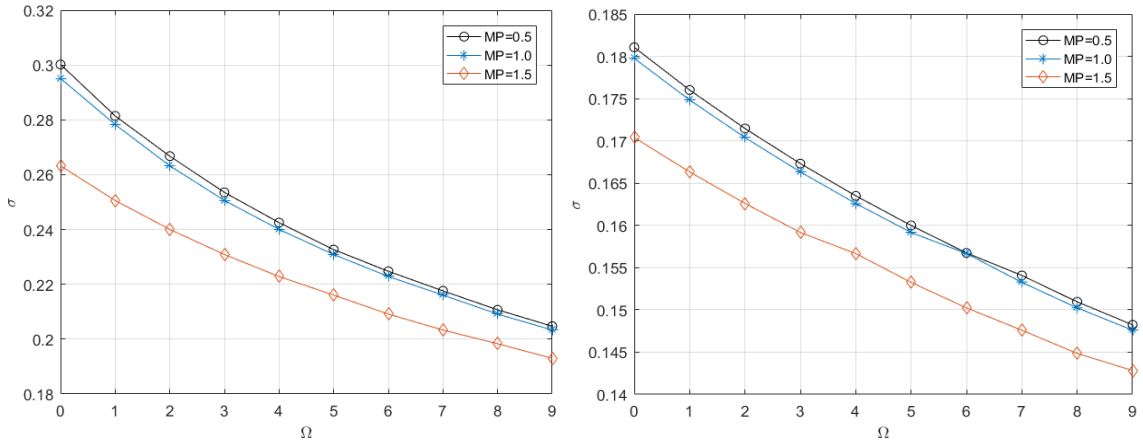

Fig 5.2.3.4.A. Velocity profile for parameters α = 2.5, β = 1.0

Fig 5.2.3.4.B. Velocity profile for parameters α = 5.0, β = 1.0

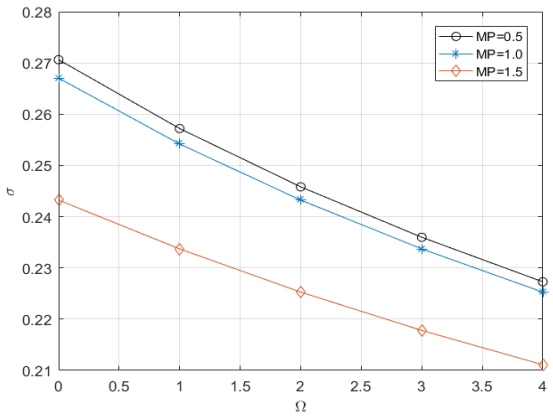

Fig 5.2.3.4.C. Velocity profile for parameters α = 2.5, β = 2.0

As can be seen from Fig 5.2.3.4.A, it can be seen that the application of Magnetic field reduces the boundary layer thickness, thus reducing the flow velocity.

We can also see from Fig 5.2.3.4.B that as the suction parameter α increases, the boundary layer is further reduced, and so does the flow velocity.

Finally, Fig 5.2.3.4.C shows that as the pressure term β is increased, the boundary layer thickness decreases and so does flow velocity.

Chapter 6

Temperature and Flow Profiles for A Stagnation-Point flow over a stationary Sheet in a Nano-fluid

6.1. Background

Nano fluids are engineered fluids, amalgamated with nanoparticles to enhance the thermal properties of base fluids. It is an emerging and highly applicable area used in many industries like coolants in automobiles, advanced heat sinks and nuclear coolants.

Numerous studies have been conducted in the area of stagnation point flow and Nano fluids.

Hiemenz [72] is considered the first to study the two dimensional stagnation point flow over a stationary plate. He use the Similarity method to reduce the Navier Stokes into nonlinear ODEs. Homann [73] extended the problem to axisymmetric stagnation point flow. Mahapatra and Gupta [74] studied stagnation point flow past a stretching sheet.

Wang [76] investigated two-dimensional axisymmetric stagnation flow towards a shrinking sheet in a viscous fluid. This research became an eye opening to the area of stagnation point flow towards stretching/shrining sheet and many researches were produced afterwards, [77, 80] to mention a few.

All of the above fluids mentioned above are Newtonian and viscous. Most fluids like water, ethylene glycol, and engine oil have limited heat transfer properties. Therefore, in order to enhance the thermal conductivity, studies have been conducted to introduce nanoparticles. Solids, such as metals, on the other hand have higher thermal conductivity to that of liquids. Therefore, it was obvious to introduce solid nanoparticles at create suspension Nano fluids which have superior to the base fluids alone.

Background of Nano fluids has many industrial application in the areas of engine cooling systems, electronics, nuclear cooling systems and biomedical applications.

Nano fluids are widely studied in various literatures [77-91]. . The paper by Khan and Pop [79] was the first which considered the problem on stretching sheet in Nano fluids.

Another model have been used in the study conducted by in several papers [92-100]. Norfifah Bachok1, Anuar Ishak2* and Ioan Pop [101] used this model to study stagnation point flow of Cu, Al_2O_3 and TiO_2 over a stretching/shrinking sheet

Norfifah Bachok1, Anuar Ishak2* and Ioan Pop [102] studied Stagnation-point flow over a stretching/shrinking sheet in a Nano fluid with Pr=6.2. In this chapter, a stagnation point flow over a stationary plate is conducted for nanoparticles of Cu, Al_2O_3 and TiO_2 and water as a base fluid.

In this paper, a stagnation point flow of Nano fluids over a stationary plate is studied. Three nanoparticles are considered namely Alumina (Al2O3), Copper (Cu) and Titania (TiO2) with a base fluid of water is considered in this paper.

6.2. Mathematical Formulation

$$\frac{\partial u}{\partial x}+\frac{\partial v}{\partial y}=0 \qquad \text{eq(6.1)}$$

$$u\frac{\partial u}{\partial x}+v\frac{\partial u}{\partial y}=U_{\infty}\frac{dU_{\infty}}{dx}+\frac{\mu_{nf}}{\rho_{nf}}\frac{\partial^2 U}{\partial y^2} \qquad \text{eq(6.2)}$$

$$u\frac{\partial T}{\partial x}+v\frac{\partial T}{\partial y}=\alpha_{nf}\frac{\partial^2 U}{\partial y^2} \qquad \text{eq(6.3)}$$

Subject to Boundary Conditions

u = 0 v = 0, T = Tw at y = 0 and $\qquad$ eq(6.4)

u → U∞ (x), T → T∞ as y → ∞,

Where μ_{nf} is the viscosity of the Nano fluid and α_{nf} is the thermal diffusivity of the Nano fluid and ρ_{nf} is the density of the Nano fluid.

$$\alpha nf = \frac{knf}{\rho Cp\ nf},\ \rho nf = (1-\phi)\rho f+\phi\rho s,\ \mu nf = \frac{\mu f}{(1-\phi)^{2.5}},$$
$$\rho Cp\ nf = (1-\phi)(\rho Cp)_f + \phi(\rho Cp)s, \qquad \text{eq(6.5)}$$
$$\frac{knf}{kf} = \frac{(ks+2kf)-2\phi(kf-ks)}{(ks+2kf)+\phi(kf-ks)}$$

Here, Φ is the volume fraction of the nanoparticle, (rCp)nf is the Nano fluid's heat capacity, knf is the thermal conductivity of the Nano fluid, kf is the thermal conductivities of the fluid and ks is the thermal conductivities of the solid fractions, and ρf and ρs are the densities of the fluid and of the solid fractions, respectively. It should be mentioned that the use of the above expression for knf is only used for spherical nanoparticles and no other shapes of nanoparticles. Also, the viscosity of the Nano fluid μnf has been approximated by Brinkman [40] as viscosity of a base fluid μ_f containing dilute suspension of fine spherical particles.

Introducing dimensionless variables, we obtain the following dimensionless numbers.

$$\theta(\eta) = \frac{[T - T\infty]}{[Tw - T\infty]}$$

$$\eta = \left[\frac{b}{\nu f}\right]^{1/2} \gamma, \quad \text{and} \qquad \text{eq (6.5-6.7)}$$

$$\psi = f(\eta) * (\nu fb)^{1/2} x,$$

The governing differential equations can be reduced and given as

$$\frac{1}{(1-\phi)^{2.5}(1-\phi+\phi\rho s/\rho f)} f''' + ff'' - f'^2 + 1 = 0$$

$$\frac{1}{Pr} * \frac{knf/kf}{-\phi + 1 + \phi(\rho Cp)s/(\rho Cp)} \theta'' + f\theta' = 0 \qquad \text{eq (6.8-6.9)}$$

Subject to Boundary Conditions

$$f(0) = 0,\ f'(0) = 0,\ \theta(0) = 1$$
$$f'(\eta) \to 1,\ \theta(\eta) \to 0 \qquad \text{eq (6.10)}$$

The Skin friction Coefficient (Cf) and the Nusselt Number (Nu) are given as

$$Cf = \frac{\tau w}{\rho_f U_\infty^{\ 2}} \text{ and } Nu = \frac{xqw}{kf(Tw - T\infty)} \qquad \text{eq (6.11)}$$

$$\tau w = \mu_{nf} * \frac{\partial u}{\partial y} \ @\ y = 0,\ qw = -knf * \frac{\partial T}{\partial y} \ @\ y = 0, \qquad \text{eq (6.12)}$$

with μnf is the the dynamic viscosity and knf is thermal conductivity of the Nano fluids.

$$C_f Re_x^{1/2} = \frac{1}{(1-\phi)^{2.5}} f''(0) \text{ and} \qquad \text{eq (6.13)}$$

$$Nu/Re_x^{1/2} = -\frac{k_{nf}}{k_f} \theta'(0) \qquad \text{eq (6.14)}$$

6.3. Results and Discussions

Table 6.1: f''(0) values for varying ε and Φ values

LEGEND	
	Present Results
[102]	Norfifah Results

ε	Φ[102] = 0.0	Φ = 0.0	Φ[102] = 0.1	Φ = 0.1	Φ[102] = 0.2	Φ= 0.2
2	-1.8873	-1.8873065	-2.21711	-2.2171106	-2.29882	-2.2988218
1	0	0	0	0	0	0
0.5	0.7133	0.7132949	0.8379	0.83794	0.868824	0.8688244
0	1.23259	1.2325876	1.447977	1.4479774	1.501346	1.5013457
-1.15	1.08223	1.0822315	1.271347	1.2713471	1.318205	1.3182054
-1.2	0.9324	0.9324741	1.095419	1.0954199	1.135794	1.1357964
-1.2465	0.5543	0.5542057	0.686379	0.686393	0.711678	0.7116917

Table 6.2: CfRex 1/2 values for varying ε and Φ values

LEGEND	
	Present Results
[102]	Norfifah Results

Epsilon	Phi	Cu-water[102]	Cu-water	Al203-water[102]	Al203-water	TiO2-water[102]	TiO2-water
-0.5	0.1	2.2865	2.8866	1.9440	1.9441	1.9649	1.9651
	0.2	3.1826	3.1825	2.4976	2.498	2.5413	2.5415
0	0.1	1.8843	1.8843	1.6019	1.602	1.6192	1.6193
	0.2	2.6226	2.6227	2.0584	2.0584	2.0942	2.0942
0.5	0.1	1.0904	1.0905	0.9271	0.9271	0.9371	0.9371
	0.2	1.5177	1.1578	1.1912	1.1912	1.2118	1.2119

Table 6.3: NuxRex $^{1/2}$ values for varying ε and Φ values

LEGEND	
	Present Results
[102]	Norfifah Results

Epsilon	Phi	Cu-water[102]	Cu-water	Al203-water[102]	Al203-water	TiO2-water[102]	TiO2-water
-0.5	0.1	0.8385	0.8385	0.7272	0.7272	0.7082	0.7082
	0.2	1.0802	1.0803	0.8878	0.8879	0.8423	0.8423
0	0.1	1.4043	1.4043	1.3305	1.33052	1.301	1.3012
	0.2	1.6692	1.6693	1.5352	1.5352	1.4691	1.4691
0.5	0.1	1.8724	1.8724	1.8278	1.8279	1.7898	1.7897
	0.2	2.1577	2.1577	2.07	2.0699	1.9867	1.9867

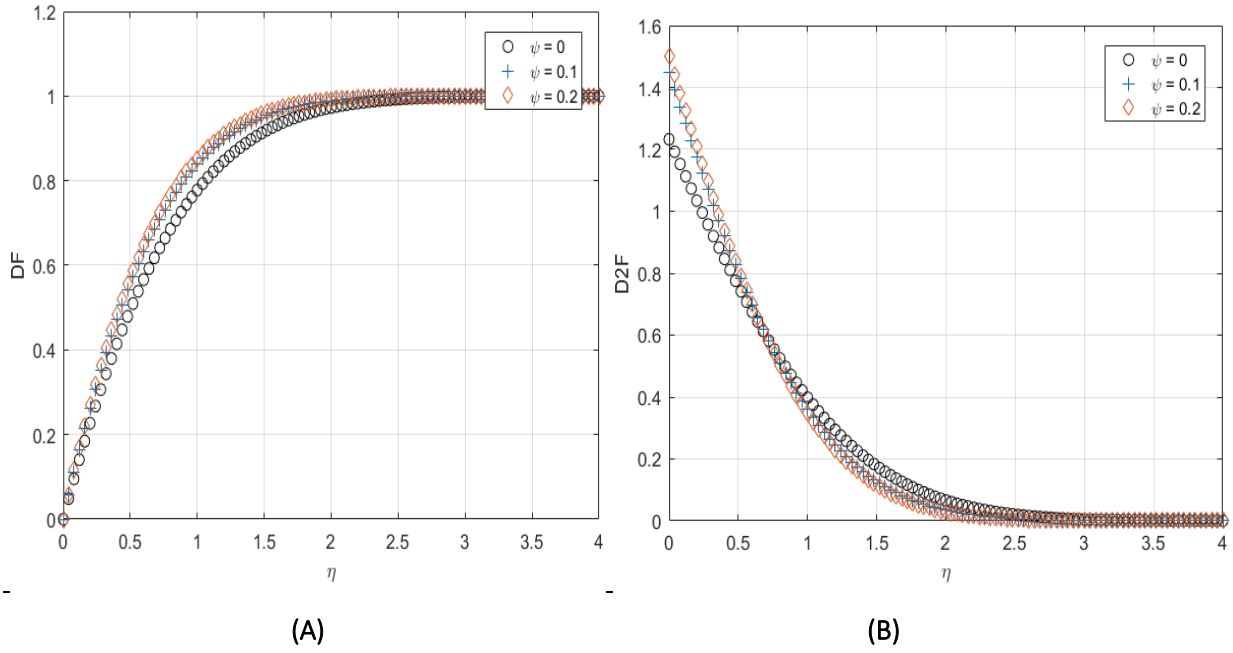

(A) (B)

Figure 6.1.A-B. f' and f'' profile for varying volume fraction

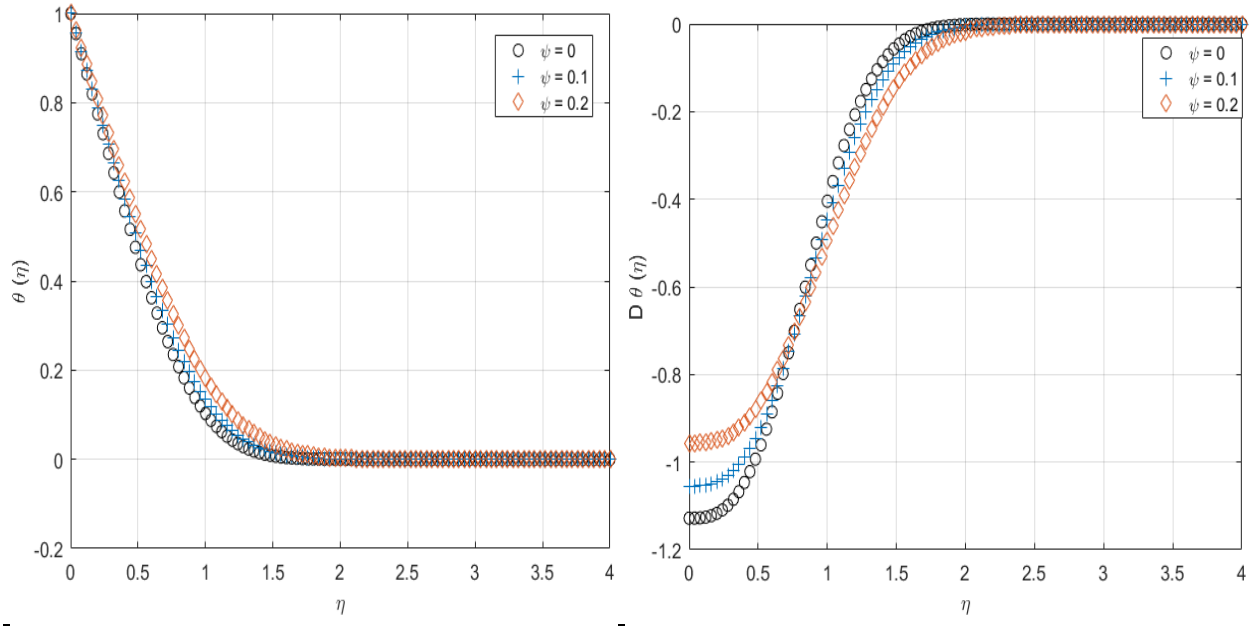

(C) (D)

Figure 6.2.A-B. θ and θ' (Temperature and Temperature flux) profile for varying volume fraction

We assume a stagnation point flow, the velocity at the wall is zero.

As can be seen from Fig 6.1 and 6.2., the flow velocity of the flow increases as the volume fraction increases within a close vicinity to the wall. Going further away from the wall, the flow velocity maintains the free stream velocity.

It can also be seen from 6.1.B that as the volume fraction increase, the drag induced on the wall increases, since the drag force is proportional to the second derivative of the stream function f.

With regards to temperature, it can be seen that from Figure 6.2.A that the temperature at the vicinity of the wall is higher for higher volume fraction. Further away, it can be seen that the temperature for all volume fraction fluids maintain tends to zero. From Fig 6.2.D, we can see that the temperature gradient at the base with higher volume fraction is higher. Going further, we can see that the effect is reversed and the gradient is lower for higher volume fraction up to a certain distance. Starting from the mid height of the boundary layer up to the free stream surface, the gradient becomes zero.

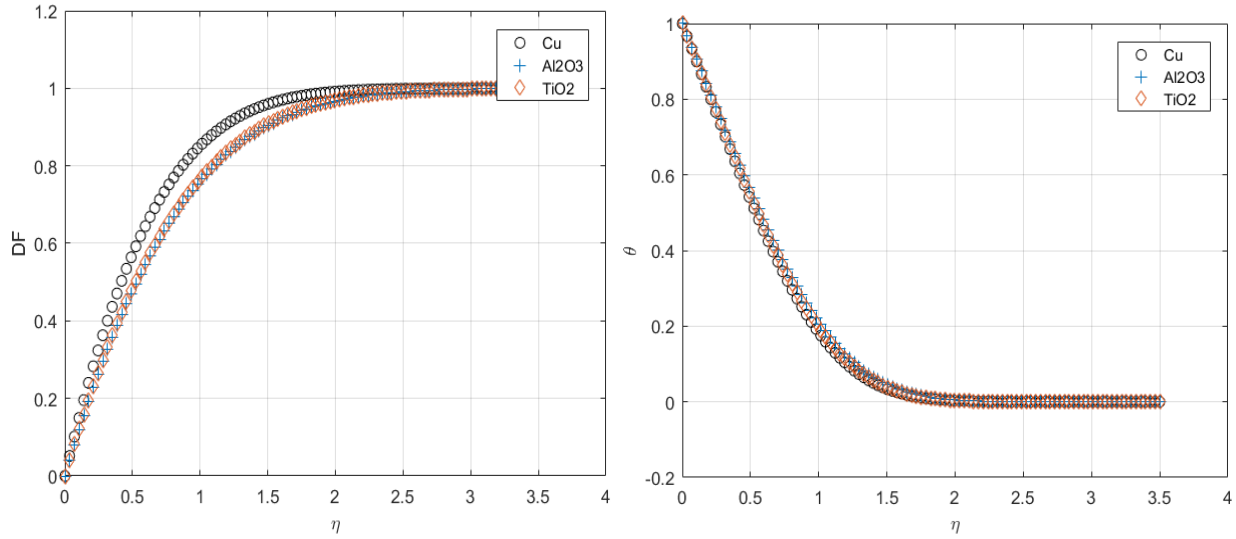

(A) (B)

Figure 6.3 A-B. f' and f'' profile for varying nanoparticles for volume fraction of 0.1

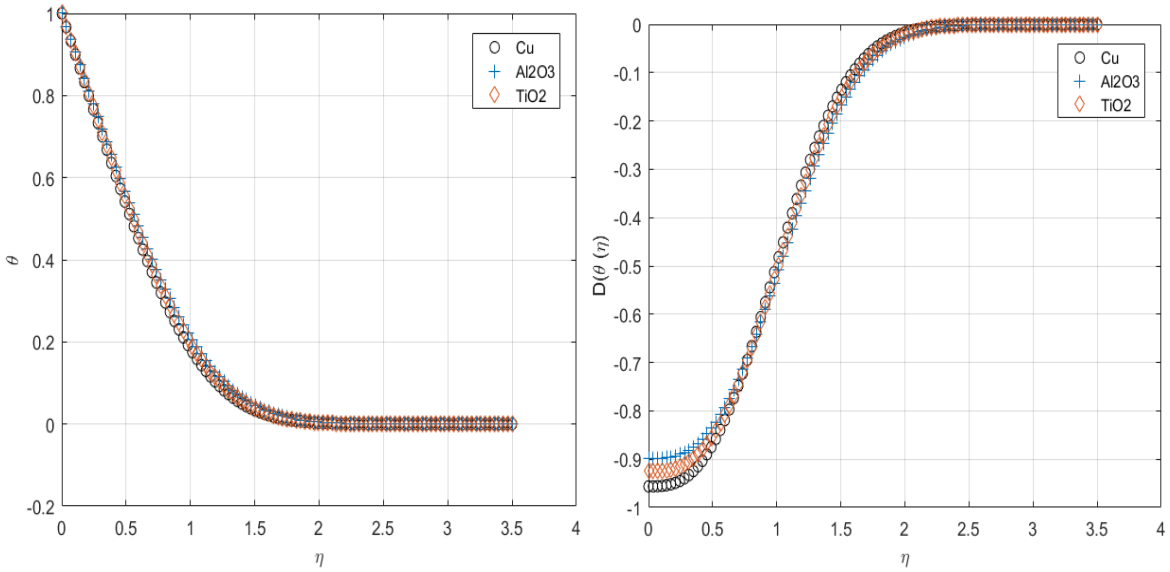

(C) (D)

Figure 6.3.C-D. θ and θ' profile for varying Nano particles for volume fraction of 0.1

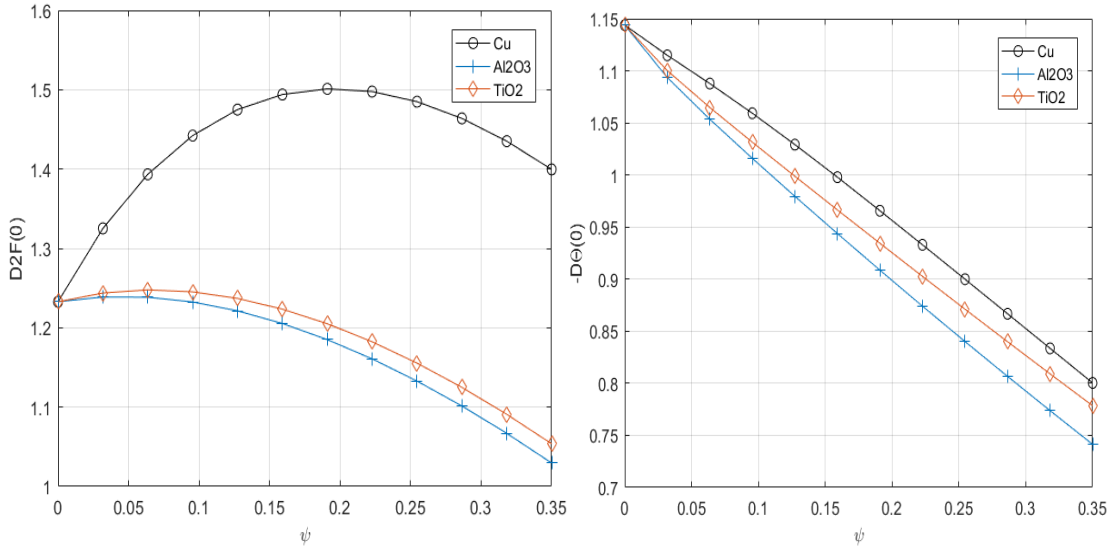

Figure 6.4.A-B. f'' and θ' profile for varying increasing volume fraction and different Nano particles

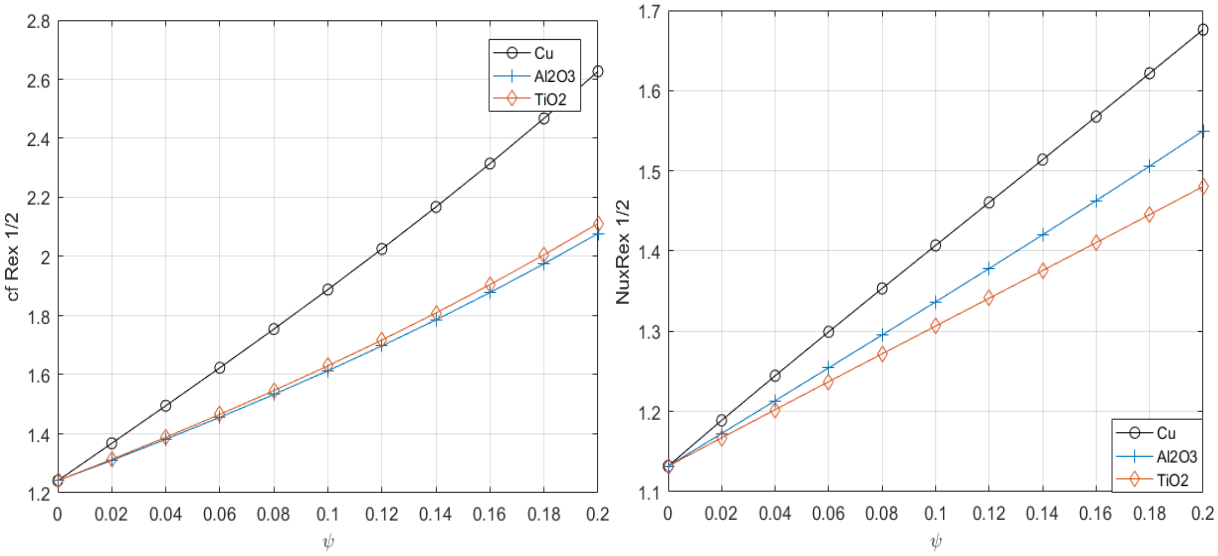

Figure 6.5.A-B. f'' and θ' profile for varying increasing volume fraction and different Nano particles

From Figure 6.3., we can see that the flow velocity for Cu is higher at the vicinity of the wall and further away, all Nano fluids maintain the free stream velocity.

It can also be seen that the temperature profile is similar for all Nano fluids.

Figure 6.4 (A-D) shows that the drag force (Skin friction) on the wall is higher for Cu nanoparticles, followed by Al_2O_3 and TiO_2.

The Nusselt number of Cu is higher which gives higher performance rank, followed by TiO_2 and Al_2O_3.

In conclusion, further researches can be conducted in this area by finding suitable base fluids to enhamce their thermal performance.

Chapter 7

A Comprehensive Numerical Approach to a Thermal Explosion Problem.

7.1. Analysis of Homogeneous Material

7.1.1. Background

A thermal explosion is one where the primary cause is the auto-catalysis produced by the self-heating effect of the reaction mixtures. For an exothermic reaction the heat evolved during the course of the reaction raises the temperature of the reacting mixtures, thereby accelerating the reaction rates, leading to further heating and further reaction, until an explosion occurs. Such a thermal reaction stabilizes when the rate of generation of heat is compensated by thermal dissipation through thermal convection and conductivity or by radiation.

Some studies have been conducted in the area of thermal explosion. Evaluation of criticality of explosiveness of chemical reactions mathematically has been conducted in [103] and [104].

Formulation of the problem was first introduced by Frank-Kamenetskii ([104]).Reactant consumption is neglected in the formulation. Analytical methods of solving thermal explosion problem are indicated in previous studies [105-107].

O.D. Makinde [108] employed Analytical and Dynamical Analysis of thermal explosion to solve for the criticality of thermal explosion.

In this chapter, it has been tried to employ numerical (Shooting Secant method) and further dynamical analysis for the thermal explosion. In addition, study of heterogeneity of materials is considered as a second part of this chapter.

Thermal stability for explosion find its way in different applications like incinerators, jet and rocket propulsion, fire prevention and safety, material processing industries and the like.

In thermal stability problem, finding the critical points and parameters whereby explosion occurs are of primary concern. In this section, we shall see the thermal explosion property of homogeneous and heterogeneous materials as well.

7.1.2. Mathematical Formulation

For economic and efficiency reasons, heterogeneity is adopted to effectively control thermal explosion.

The classical formulation of this problem is first introduced by Frank-Kamenetskii ([104]). By Neglecting the reactant consumption, the governing differential equation is given as

$$k\frac{d^2T}{\partial y^2}+QC_0A\left[\frac{KT}{\upsilon h}\right]^m e^{\frac{E}{RT}}=0 \quad \text{Eq (7.1.2.1)}$$

Subject to Boundary conditions

$$\frac{dT}{dx}(0)=0, T(\infty)=0 \quad \text{Eq (7.1.2.2)}$$

Where Q is heat due to reaction, T is the absolute temperature, C0 the initial concentration of the reactant species, T0 is the wall temperature, E is the activation Energy, R is the universal gas constant, a the slab half width, , h the Planck's number constant, K the Boltzmann's constant, μ frequency of the vibration, y is distance measured in the normal direction to the plane and m is the exponent corresponding to a manner such that m={-2, 0, ½} represent numerical exponent for the three types of reactions namely Sensitized, Arrhenius and Bimolecular kinetics respectively.

Using similarity theory to non dimensionalize the parameters, we use

$$y=\frac{y'}{L}, \theta=\frac{E(T-T_0)}{RT_0^{\,2}}, \varepsilon=\frac{RT_0}{E}, \lambda=\frac{QAEa^2e^{\frac{E}{RT_0}}C_0K^mT_0^{\,m-2}}{\upsilon^m h^m RK} \quad \text{Eq (7.1.2.3)}$$

Using the above transformation, we obtain a governing dimensionless equation as

$$\frac{d^2\theta}{\partial y^2}+\lambda\left[1+\varepsilon\theta\right]^m e^{\left[\frac{\theta}{1+\varepsilon\theta}\right]}=0 \quad \text{Eq (7.1.2.4)}$$

Subject to dimensionless boundary conditions as

$$\frac{d\theta}{dy}(0)=0, \theta(1)=0 \quad \text{Eq (7.1.2.5)}$$

7.1.3. Results and Discussion

Table 7.1.1. Table for critical (Frank Kasenatti's Parameter) λ values for all types of reactions

m	ε	$\theta_{max}[1]$	θ_{max}	$\lambda_c[1]$	λ_c
-2	0.1	2.222394	2.201409	1.31388753	1.31385000
0	0.1	1.524356	1.517492	0.988207804	0.98820000
0.5	0.1	1.420244	1.410923	0.932216072	0.93220000

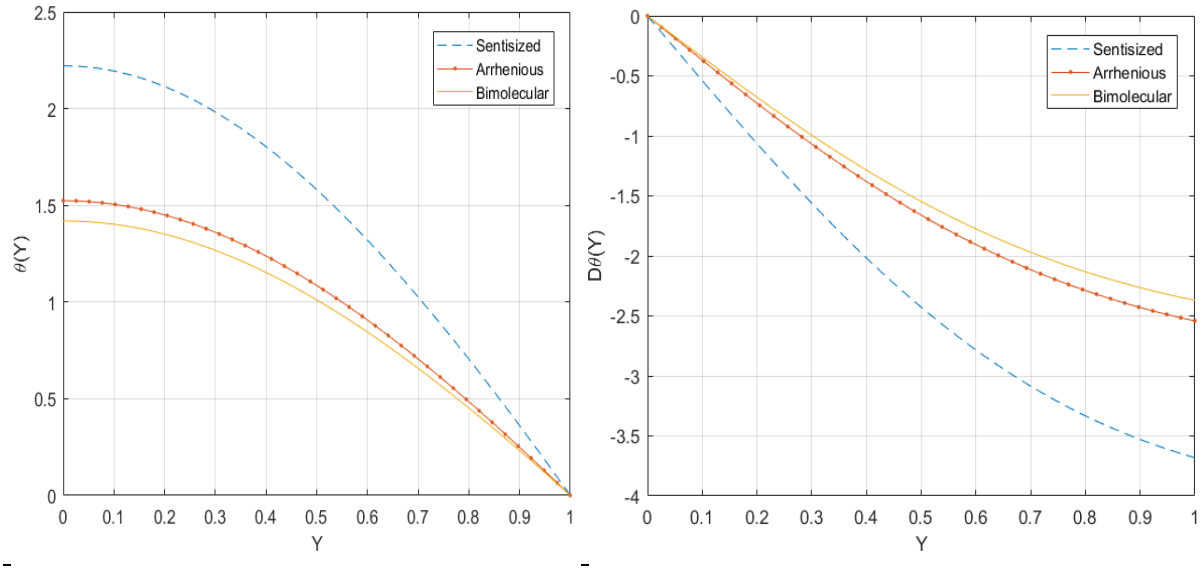

(A) (B)

Figure 7.1.4.1 (A-B) Temperature and Temperature flux profile for all reaction types with 0.1 activation energy

Figure 7.1.4. (A-B) shows the temperature and the temperature flux for the three types of reactions (Sensitized, Arrhenius and Bimolecular) with activation energy parameter of one. The Maximum temperature is found to be different for three different reaction types. Sensitized reactions have higher temperature threshold, significant to the Arrhenius and Bimolecular, followed by Arrhenius and finally the bimolecular reaction. This means that thermal explosion in Bimolecular reaction occurs faster than to that of the Arrhenius and Sensitized reactions.

The temperature profile shows that the flux at the wall is highest for Sensitized, significant to the Arrhenius and Bimolecular, followed by Arrhenius and finally the bimolecular reaction.

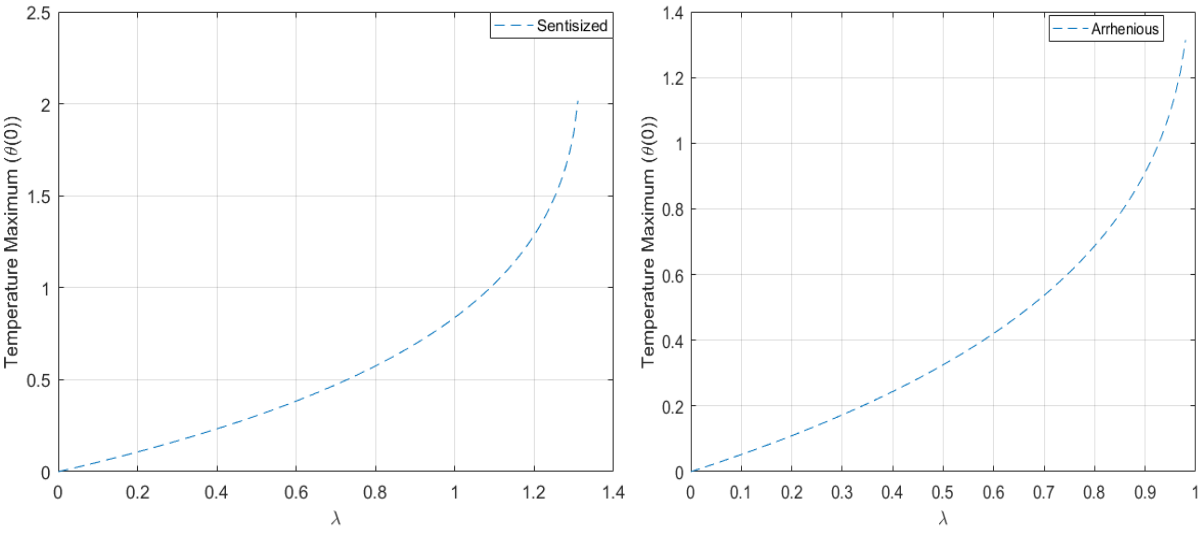

(A) (B)

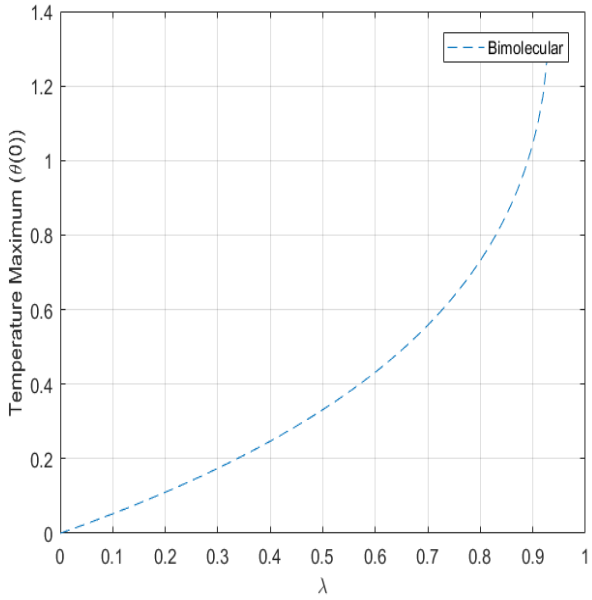

(C)

Figure 7.1.4.2. (A-C) Temperature and Temperature flux profile for all reaction types with 0.1 activation energy

Figure 7.1.4.2. (A-C) shows the criticality of temperature and Frank-Kamenetskii parameter (λ critical) above which, thermal explosion takes place. It can be noticed here that for Sensitized reaction, the critical temperature and the critical Frank- Kamenetskii is higher as compared to that of the Arrhenius and Bimolecular.

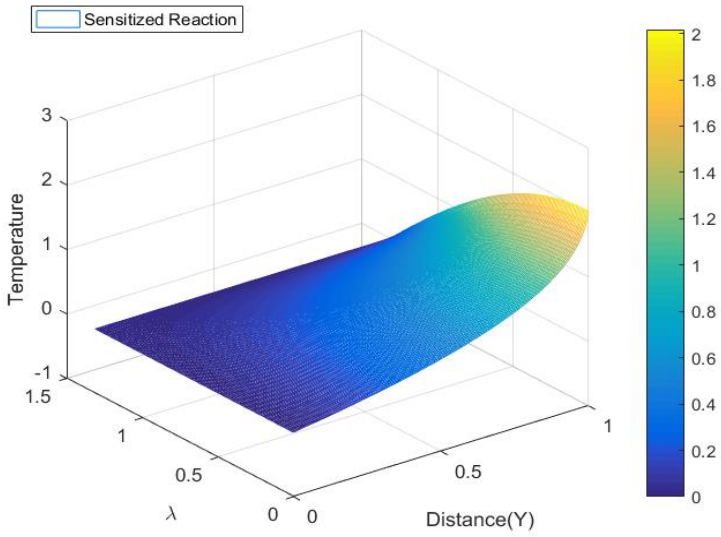

(A)

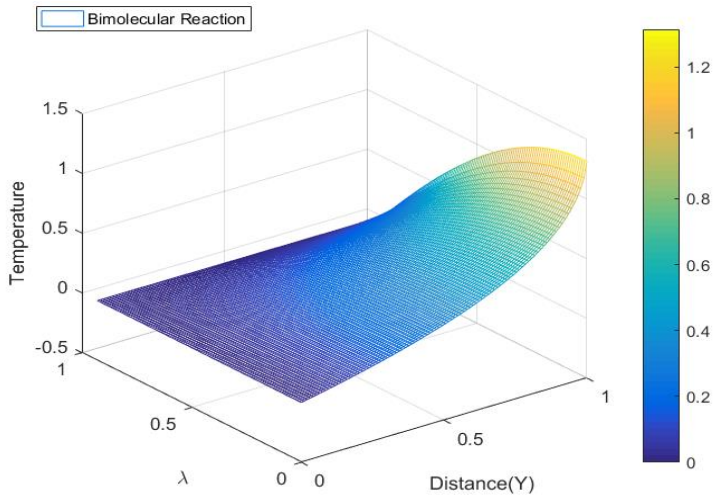

(B)

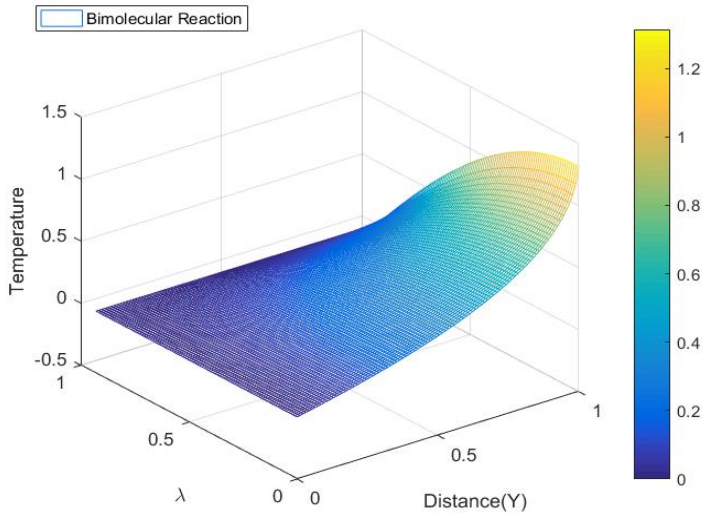

(C)

Fig 7.1.4.3.(A-C) Three dimensional Plot relating distance, λ_C and Temperature for Sensitized, Arrhenius and Bimolecular Reactions respectively

TABLE 7.1.2: CRITICALITY FOR VARYING BETA (HETEROGENIOUS CASE)

M	BETA	CRITICAL LAMBDA	MAXIMUM TEMPERATURE
Sensitized Reaction			
-2	-1	0.5612	2.2390
-2	-0.5	0.9072	2.1748
-2	0	1.28135	2.1976
-2	0.5	1.7276	2.2611
-2	1	2.2608	2.3035
Arrhenius Reaction			
0	-1	0.4215	1.5235
0	-0.5	0.6825	1.4933
0	0	0.9638	1.5109
0	0.5	1.2988	1.5458
0	1	1.6985	1.5768
Bimolecular Reaction			
0.5	-1	0.4241	1.3591
0.5	-0.5	0.6949	1.2977
0.5	0	0.9301	1.3872
0.5	0.5	1.3214	1.3365
0.5	1	1.7144	1.3803

7.1.4. Dynamical Analysis

Considering the Second Order BVP

$$\frac{d^2\theta}{dy^2} + \lambda\left[1+\varepsilon\theta\right]^m e^{\left[\frac{\theta}{\theta+1}\right]} = 0 \qquad \text{Eq (7.1.5.1)}$$

A) Break in to system of first order nonlinear ODEs

B) Try different scenarios to determine the bifurcation parameter and find the equilibrium points.

C) Find the Jacobean Matrix of each system

D) Find the Linearization at each equilibrium points and determine the eigenvalue and corresponding stability.

E) Determine the bifurcation point and bifurcation type if any

F) Do a Phase Plane analysis on the system and do a numerical experiment on a parameter(s). A routine (Program) called PPlane9 is used to obtain phase diagrams for this paper.

7.1.4.1. Steps for Qualitative Analysis First-Order System of ODEs

After breaking of a second order nonlinear ODE in to system of system of first order nonlinear ODEs we follow the following steps to find the stability information of the system.

STEP 1: Find all the equilibrium points. The equilibrium points are obtained by setting the derivatives of the dependent variables to zero.

STEP 2: Find the Jacobian matrix of the system

STEP 3: Compute the Jacobian matrix at each equilibrium points

STEP 4: Find the eigenvalue of the Jacobian matrix at each equilibrium points to check stability of the System.

STEP 5: Give information about stability based on the eigenvalue and plot the phase portrait

STEP 6: Do a phase plane analysis on the system

STEP 7: Do a numerical experiment on a parameters

7.1.4.2. Hand Computation of Eigenvalues and Stability of First Order ODEs

Based on the above steps we will show how compute and determine using a hand computation and then we will confirm and experiment on MATLAB using PPlane9 and in-built functions.

2.1.2.1. Solution to Fin Problem

Before doing stability analysis we have to be breaking the second order ODE in to first order system of ODE, we do this through the following steps:

Step 1: Rewrite the original equation in to the following form

$$\frac{d^2\theta}{dy^2} + \lambda\left[1+\varepsilon\theta\right]^m e^{\left[\frac{\theta}{\theta+1}\right]} = 0 \qquad \text{Eq (7.1.5.2)}$$

Step 2: Introduce new variables T and S.

We denote T = θ, and S = θ'.

Derivation of both T and S yields

T' = S Eq (7.1.5.3)

S' = $-\lambda\left[1+\varepsilon\theta\right]^m e^{\left[\frac{\theta}{\theta+1}\right]}$

Step 3: Determine the equilibrium points by setting

T' = 0 and Eq (7.1.5.4)

S' = 0

$-\lambda\left[1+\varepsilon\theta\right]^m e^{\left[\frac{\theta}{\theta+1}\right]}$ =0 Eq (7.1.5.5)

Hence,

$$T = \frac{-1}{\varepsilon}$$

Therefore, we have an Equilibrium point ($\frac{-1}{\varepsilon}$,0) Eq (7.1.5.6)

Step 4: Determine the Jacobian of the system.

$$J(T,S)=\begin{bmatrix} 0 & 1 \\ \dfrac{\Gamma^2}{1+\beta\xi} & \dfrac{-\beta}{1+\beta\xi} \end{bmatrix}$$

Step 5: Calculate the jacobian at each equilibrium point to compute the Eigenvalues and Eigenvectors.

Here below, pplane9 is used to undertake the phase plane analysis. Two cases are shown in the Phase Plane analysis since we have two main parameters. First, we will see a case for varying Inhomogeneity index (β). Then, we shall vary and see how the system behaves for varying Thermo geometric parameter (r). Properties including the Jacobean and the Eigenvalues as well as the Eigenvectors are presented.

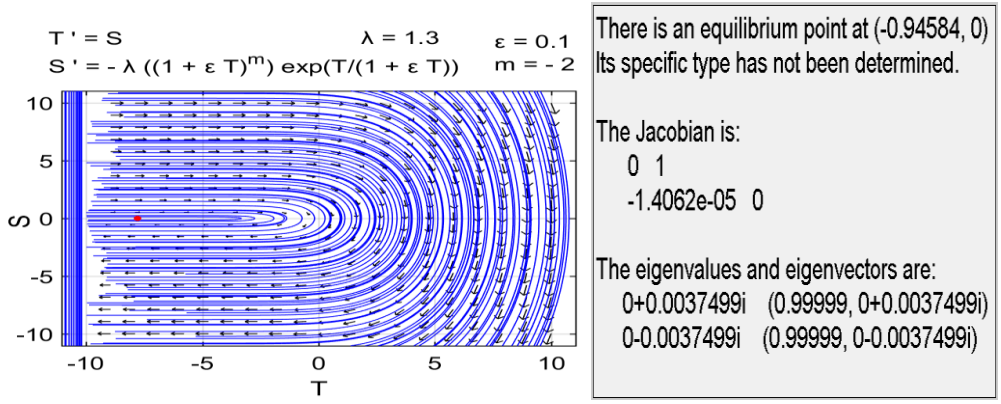

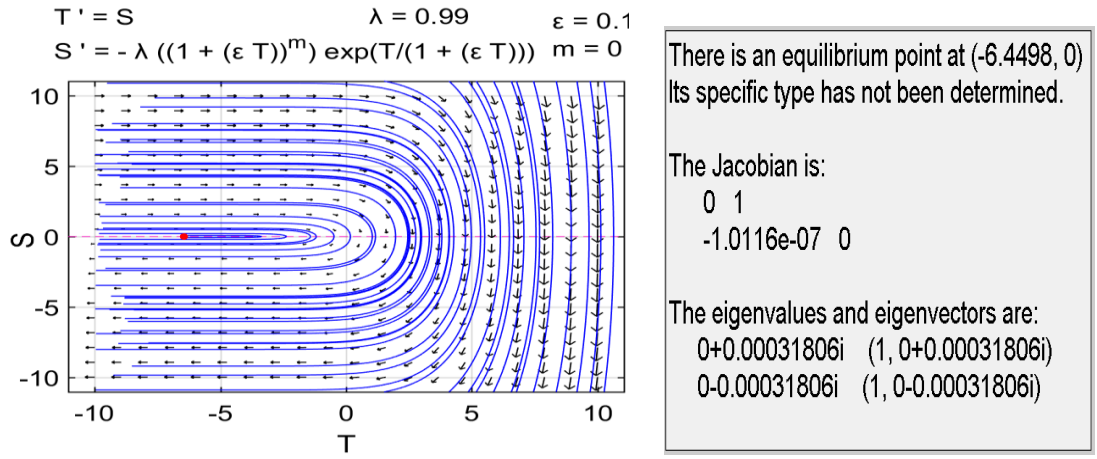

Fig 7.1.4.3.(A-B) Phase plane diagrams for the Two types of reactions.

As can be seen from fig 7.1.4.3.(A-B),we can see that there is one equilibrium point which is neutral. This can be seen since the eigenvalues are zero, there is no exaggeration and diminishing of the system and remains the same.

Dynamical analysis has been also conducted for points above and below the critical points. It is noticed that the system remains the same with neutral nodal point and no bifurcation takes place for varying λ parameter.

Further studies need to be conducted to illustrate the dynamics of the system.

7.2. Heterogeneous conductivity case for Thermal Explosion

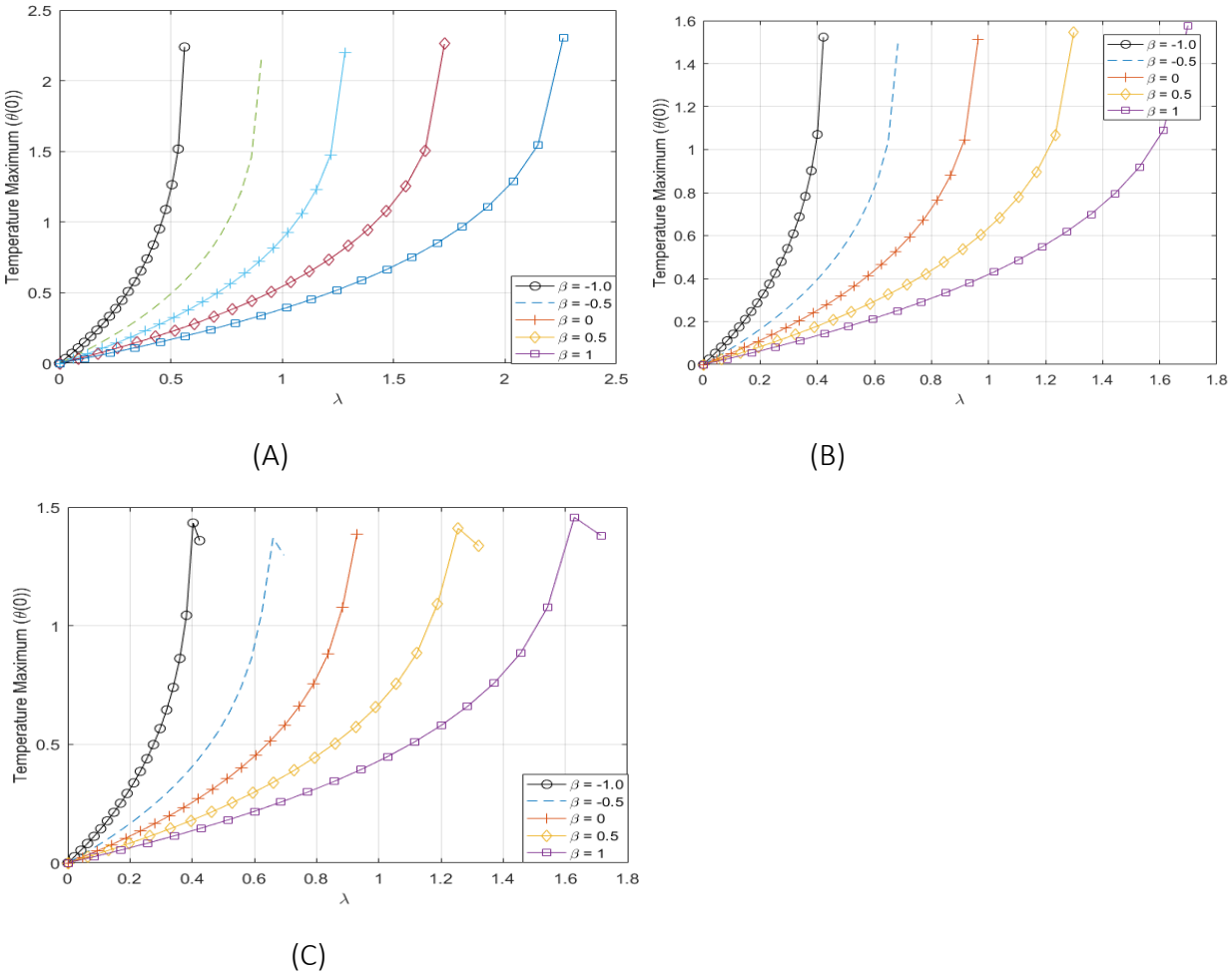

Fig 7.2.1.(A-C) Critical Temperature and Critical λ values for varying thermal conductivity for Sensitized, Arrhenius and Bimolecular Reaction cases.

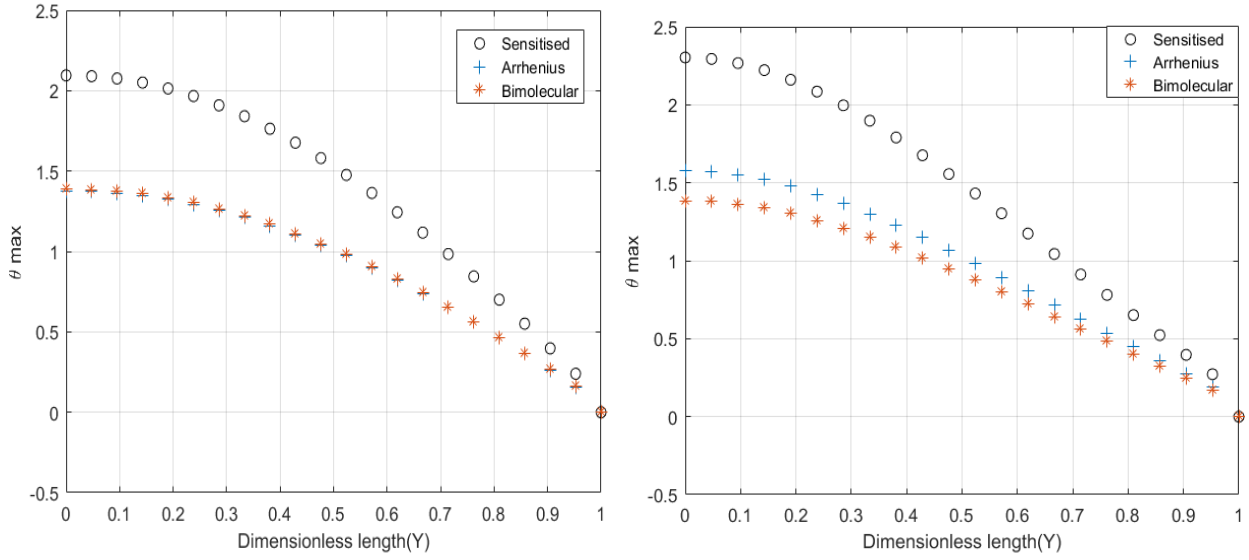

(A) (B)

7.2.2.(A-B) Temperature profile for thermal conductivity parameter (β) values of 0 and 1 for Sensitized, Arrhenius and Bimolecular Reactions.

Fig 7.2.1.(A-C) Critical Temperature and Critical λ values for varying thermal conductivity for Sensitized, Arrhenius and Bimolecular Reaction cases.

In Figures 7.2.1. (A-C), we can see that as the thermal conductivity (β) increases, the critical Frank-Kamenetskii parameter increases and the maximum temperature (θmax) slightly increases for increase in β.This can be clearly seen in Figures 7.2.2. for β =0 and β = 1.

APPENDIX

Previous work has been conducted by the Okey Oseloka Onyejekwe (Prof.), Yohannes Demiss Belete and the author Nahom Alemseged Worku, refered as **"Numerical Calculations for a Boundary Layer Flow past a Moving Vertical Porous Plate with Suction/Injection and Thermal Radiation"**,initial page found below,which can be used in reference for chapter four of this thesis "Blasius Flow and Entropy Generation under Thermal Radiation".

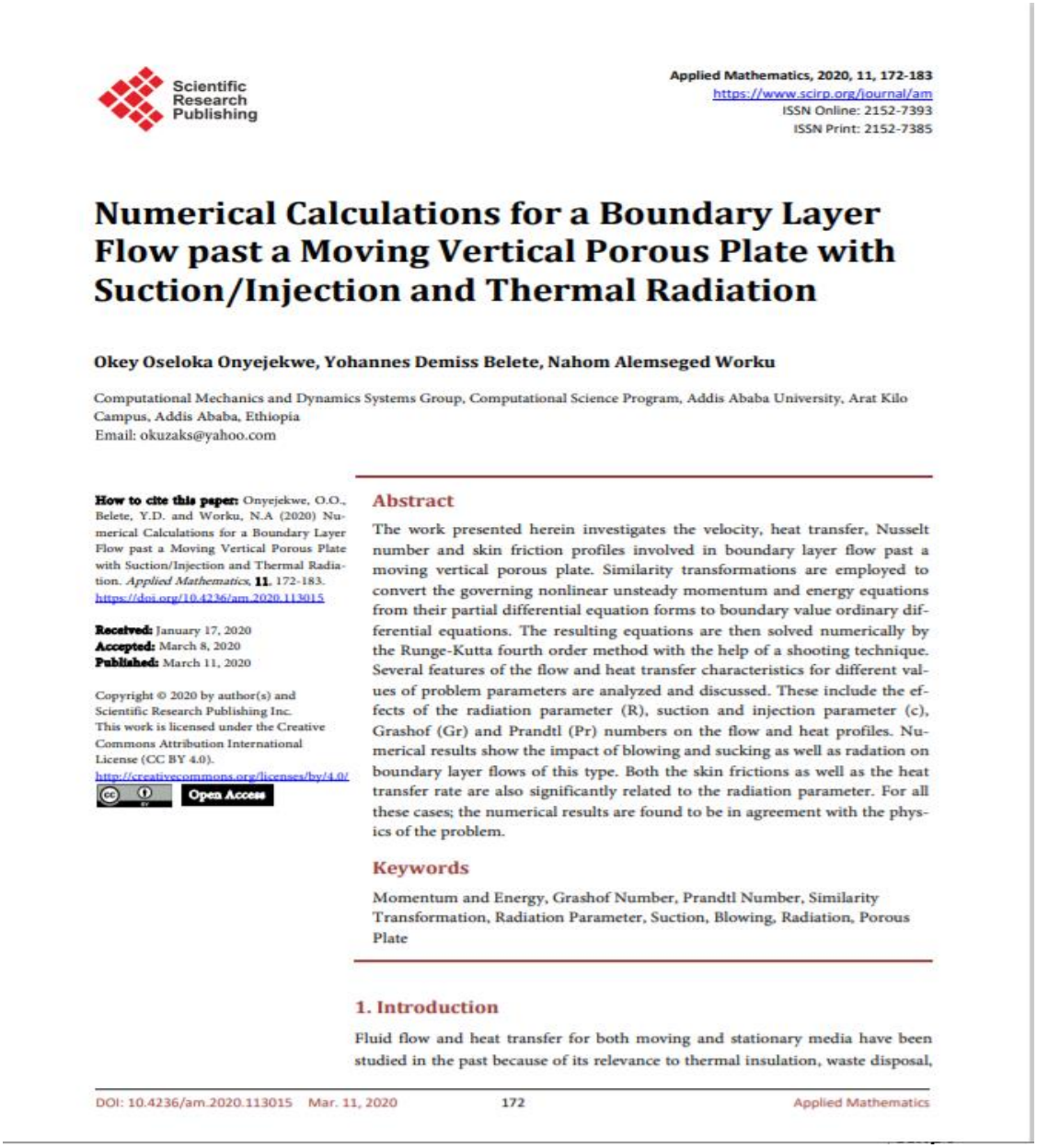

Scientific Research Publishing

Applied Mathematics, 2020, 11, 172-183
https://www.scirp.org/journal/am
ISSN Online: 2152-7393
ISSN Print: 2152-7385

Numerical Calculations for a Boundary Layer Flow past a Moving Vertical Porous Plate with Suction/Injection and Thermal Radiation

Okey Oseloka Onyejekwe, Yohannes Demiss Belete, Nahom Alemseged Worku

Computational Mechanics and Dynamics Systems Group, Computational Science Program, Addis Ababa University, Arat Kilo Campus, Addis Ababa, Ethiopia
Email: okuzaks@yahoo.com

How to cite this paper: Onyejekwe, O.O., Belete, Y.D. and Worku, N.A (2020) Numerical Calculations for a Boundary Layer Flow past a Moving Vertical Porous Plate with Suction/Injection and Thermal Radiation. *Applied Mathematics*, **11**, 172-183.
https://doi.org/10.4236/am.2020.113015

Received: January 17, 2020
Accepted: March 8, 2020
Published: March 11, 2020

Abstract

The work presented herein investigates the velocity, heat transfer, Nusselt number and skin friction profiles involved in boundary layer flow past a moving vertical porous plate. Similarity transformations are employed to convert the governing nonlinear unsteady momentum and energy equations from their partial differential equation forms to boundary value ordinary differential equations. The resulting equations are then solved numerically by the Runge-Kutta fourth order method with the help of a shooting technique. Several features of the flow and heat transfer characteristics for different values of problem parameters are analyzed and discussed. These include the effects of the radiation parameter (R), suction and injection parameter (c), Grashof (Gr) and Prandtl (Pr) numbers on the flow and heat profiles. Numerical results show the impact of blowing and sucking as well as radation on boundary layer flows of this type. Both the skin frictions as well as the heat transfer rate are also significantly related to the radiation parameter. For all these cases; the numerical results are found to be in agreement with the physics of the problem.

Keywords

Momentum and Energy, Grashof Number, Prandtl Number, Similarity Transformation, Radiation Parameter, Suction, Blowing, Radiation, Porous Plate

1. Introduction

Fluid flow and heat transfer for both moving and stationary media have been studied in the past because of its relevance to thermal insulation, waste disposal,

For chapter two, an addition has been made in this thesis and a compilation of a small MATLAB app (GUI) has been built and some illustration has been made.

COPPER

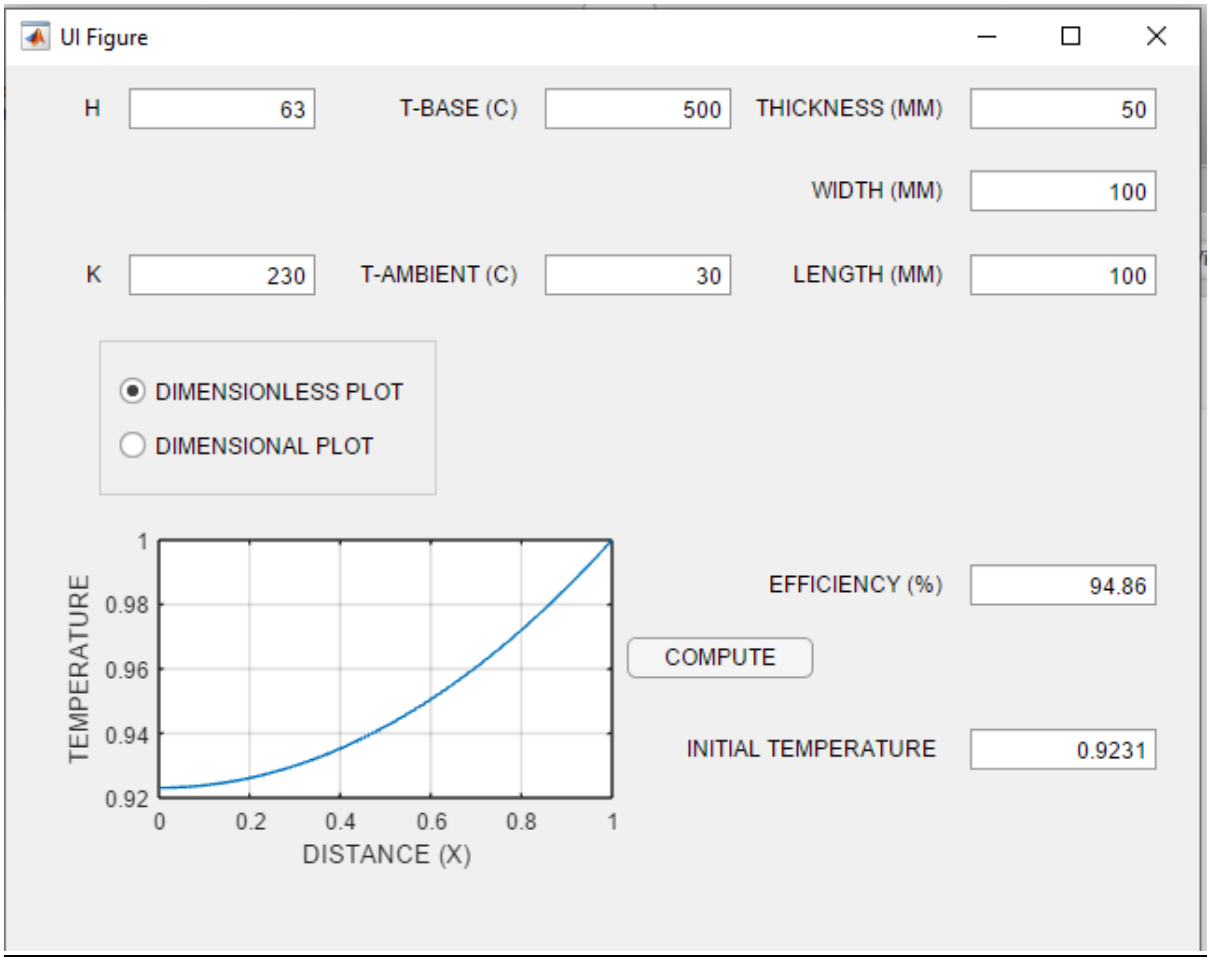

Fig A.1. Performance of heat transfer of fins made of Copper

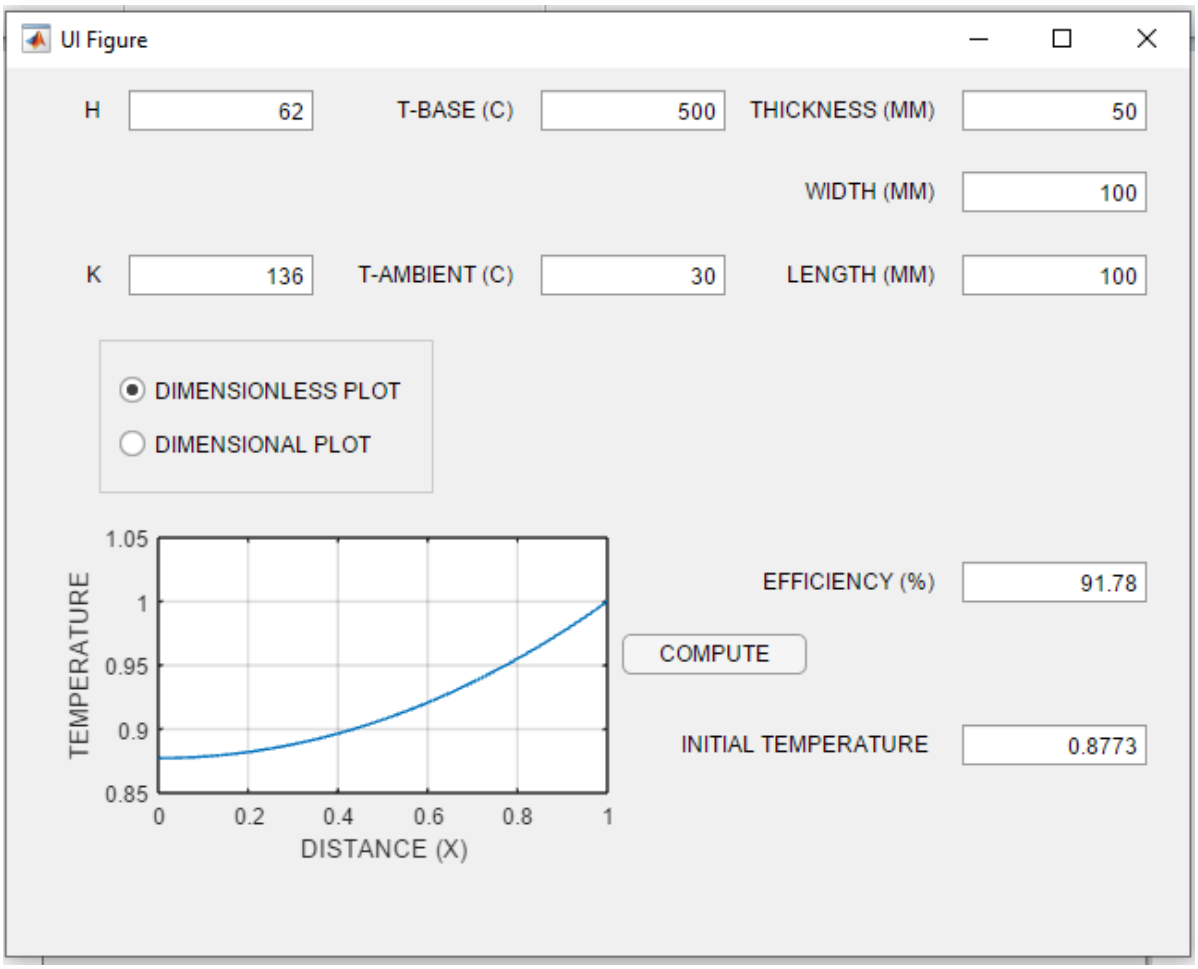

Fig A.2. Performance of heat transfer of fins made of Aluminum

This MATLAB App (GUI) is made by the author (Nahom A. Worku) of "Appdesigner" tool in MATLAB software using simple relation to the thermo geometric parameter. It accepts values of Thermal Conductivity (K) and heat transfer Coefficient (H) and dimensions to plot dimensionless and dimensional temperature profile and Efficiency.

This section is intended to show the practical experience for analysis of fins. It is intended to verify what was explained in Chapter 2.Figure A.1. And A.2. Are used to compare Aluminum and Copper fins and their performance.

As can be seen, copper is slightly more efficient than Aluminum for the same geometric properties. But Aluminum has a very good efficiency too. But due to reasons of cost and Weight, and their close efficiency, Aluminum is favored over Copper.

Gauss's Divergence Theorem

Assume U be a vector field. The Gauss divergence theorem approximates the volume integral, which is the Div (U) with the surface integral for flux terms. This is useful because it is intuitive to study as surface parameters rather than volumetric parameters. The relation can be given as

$$\iiint_v \nabla \cdot U dV = \iint_s U \cdot n ds$$

Where n is the outward unit normal to the surface

We use the Outward Unit normal as fluxes are assumed to enter or leave the control volume perpendicular to the surface.

Maxwell's Laws

The core idea of electromagnetism is that the movement of electric charges induces magnetism. Maxwell clearly put the relations between the electrostatic, current movement and induction of magnetism due to the charge movements. The two concepts, electricity and Magnetism occur in pairs and are physically inseparable in most physical phenomenon.

Maxwell's laws are composed of four basic equations.

Gauss's Law of Electrostatics

This law explains how electric charges create electric field, and is mathematically denoted as

$$\nabla . E = \frac{\rho_c}{\varepsilon_0}$$

Where ρ_c is the current density and

ε_0 is the permittivity of the medium

This means that the net inflow and outflow of electric field over a control volume is directly proportional to the density of charges in that area.

Gauss's Law of Magnetism

This law states that the net inflow and outflow of magnetic field over a control volume is zero, which is mathematically be written as

$$\nabla . B = 0$$

Faraday's Law

The faraday's law relates the Electric and magnetic field.

Faraday's law states that the curl of the Electric field is equal to the rate of change of Magnetic field in the negative direction.

$$\nabla \times E = -\frac{\partial B}{\partial t}$$

Ampere's Maxwell's Equation

The Ampere-Maxwell's law states that magnetic field can be induced due to electric fields from stationary charges and electric current from moving charges. This can mathematically be written as

$$\nabla \times B = \mu_0 J + \frac{1}{C^2}\frac{\partial E}{\partial t}$$

Where μ_0 is the permeability of free space (Constant)

J is the Current Density and

C is the speed of light

From the Ampere Maxwell's law, we can see that light is an electromagnetic waves.

Lorentz Force

The Lorentz force is a force due to the effect of Electric and magnetic field in a charged medium.

The Lorentz force is made of two components, electric and magnetic force. This can mathematically be given as

$$F = q*E + qv*B$$

Where q is charge, E is the electric field and B is the magnetic field.

The first term from the equation is from the idea of electrostatic which states that force due to electric field is equal to the product of Electric field and charge. The second term is the contribution of the force due to the effect of the magnetic field created by the movement of charge with a velocity v.

Now, dividing the force with an infinitesimal volume V_0, we obtain the relation

$\frac{F}{V_0} = \frac{q*E}{V_0} + \frac{(q*v)\times B}{V_0}$, which is equivalent to

$$f = \rho_c * E + \rho_c * \mathrm{B} * v$$

But the current density J = $\rho_c * v$, hence

$$f = \rho_c * E + J \times B$$

But the impact of Electric field can be ignored as for the case in chapter 5 for MHD flow, when coupled with the Navier Stokes equation. The force term that shall be introduced in Navier Stokes equation as can be seen feom chapter 5 is

$$f = J \times B$$

In MHD flow, the fluid flow velocity and the electric charge velocity is assumed to be equal.

References

[1]. Aziz, A and Enamul-Huq, S. M. Perturbation solution for convecting fin with temperature dependent thermal conductivity, J Heat Transfer 1973; 97:300–1.

[2]. Aziz, A. Perturbation solution for convecting fin with internal heat generation and temperature dependent thermal conductivity, Int. J Heat Mass Transfer 1977; 20: 1253-5.

[3]. Chowdhury M. S. H., Hashim I., Abdulaziz O .Comparison of homotopy analysis method and homotopypermutation method for purely nonlinear fin-type problems, Communications in Nonlinear Science and Numerical Simulation 2009; 14: 371-78.

[4]. Khani F., AhmadzadehRaji M., HamediNejad H. Analytical solutions and efficiency of the nonlinear fin problem with temperature-dependent thermal conductivity and heat transfer coefficient, Commun Nonlinear SciNumerSimulat 2009:14: 3327-3338. Page 29 of 40 30

[5]. Class notes from Professor Okey Oseloka Onyejekwe

[6]. Hosseini, K., Daneshian, B. Amanifard, N. And Ansari. R. Homotopy Analysis Method for a Fin with Temperature Dependent Internal Heat Generation and Thermal Conductivity. International Journal of Nonlinear Science. 2012; 14(2):201-10.

[7]. Moitheki, R.J. Hayat, T. and Malik, M.Y. Some exact solutions of the fin problem with a power law temperature dependent thermal conductivity .Nonlinear Analysis Real world Application 2010; 11; 3287 – 3294.

[8]. R. J. Moitsheki and C. Harley, "Transient heat transfer in longitudinal fin of various profiles with temperature-dependent thermal conductivity and heat transfer coefficient," Pramana: Journal of Physics, vol. 77, no. 3, pp. 519–532, 2011.

[9] C. Harley and R. J. Moitsheki, "Numerical investigation of the temperature profile in a rectangular longitudinal fin," Nonlinear Analysis: Real World Applications, vol. 13, no. 5, pp. 2343–2351, 2012.

[10（1）]. Thermal analysis of longitudinal fin with temperature-dependent properties 2 and internal heat generation using Galerkin's method of weighted residual," Applied Thermal Engineering Volume 99, 25 April 2016, Pages 1316-1330

[10.（2）]. Asymptotic and Dynamical Analyses of Heat Transfer through a Rectangular Longitudinal "Journal of Applied Mathematics 2013(7)DOI: 10.1155/2013/987327"

[11] S. A. Fazeli, S. M. H. Hashemi, H. Zirakzadeh, M. Ashjaee, Experimental and numerical investigation of heat transfer in a miniature heat sink utilizing silica nanofluid, Superlattices and Microstructures, 51 (2012) 247-264. http://dx.doi.org/10.1016/j.spmi.2011.11.017

[12] T. C. Hung, W. M. Yan, X. D. Wang, C. Y. Chang, Heat transfer enhancement in microchannel heat sinks using nanofluids, International Journal of Heat and Mass Transfer, 55 (2012) 2559-2570. http://dx.doi.org/10.1016/j.ijheatmasstransfer.2012.01.004

[13] S. M. H. Hashemi, S. A. Fazeli, H. Zirakzadeh, M. Ashjaee, Study of heat transfer enhancement in a nanofluid-cooled miniature heat sink, International Communications in Heat and Mass Transfer, 39 (2012) 877-884. http://dx.doi.org/10.1016/j.icheatmasstransfer.2012.04.005

[14] S. M. Kim, I. Mudawar, Analytical heat diffusion models for different micro-channel heat sink crosssectional geometries, International Journal of Heat and Mass Transfer, 53 (2010) 4002-4016. http://dx.doi.org/10.1016/j.ijheatmasstransfer.2010.05.019

[15] P. Naphon, O. Khonseur, Study on the convective heat transfer and pressure drop in the micro-channel heat sink, International Communications in Heat and Mass Transfer, 36 (2009) 39-44. http://dx.doi.org/10.1016/j.icheatmasstransfer.2008.09.001

[16] D. Lelea, Effects of inlet geometry on heat transfer and fluid flow of tangential micro-heat sink, International Journal of Heat and Mass Transfer, 53 (2010) 3562-3569. http://dx.doi.org/10.1016/j.ijheatmasstransfer.2010.04.018

[17] T. C. Hung, W. M. Yan, W. P. Li, Analysis of heat transfer characteristics of double-layered microchannel heat sink, International Journal of Heat and Mass Transfer, 55 (2012) 3090-3099. http://dx.doi.org/10.1016/j.ijheatmasstransfer.2012.02.038 Communications on Advanced Computational Science with Applications 12 of 13 http://www.ispacs.com/journals/cacsa/2014/cacsa-00018/ International Scientific Publications and Consulting Services

[18] L. Chai, G. Xia, M. Zhou, J. Li, Numerical simulation of fluid flow and heat transfer in a micro channel heat sink with offset fan-shaped reentrant cavities in sidewall, International Communications in Heat and Mass Transfer, 38 (2011) 577-584. http://dx.doi.org/10.1016/j.icheatmasstransfer.2010.12.037

[19] Z. M. Wan, G. Q. Guo, K. L. Su, Z. K. Tu, W. Liu, Experimental analysis of flow and heat transfer in a miniature porous heat sink for high heat flux application, International Journal of Heat and Mass Transfer, 55 (2012) 4437-4441. http://dx.doi.org/10.1016/j.ijheatmasstransfer.2012.04.013

[20] M. H. Babaei, Z. Chen, Transient hyperbolic heat conduction in a functionally graded hollow cylinder, Journal of Thermophysics and Heat Transfer, 24 (2010) 325-330. http://dx.doi.org/10.2514/1.41368

[21] M. Jabbari, S. Sohrabpour, M. R. Eslami, Mechanical and thermal stresses in a functionally graded hollow cylinder due to radially symmetric loads, International Journal of Pressure Vessels and Piping, 79 (2002) 493-497. http://dx.doi.org/10.1016/S0308-0161(02)00043-1

[22] Y. Tanigawa, Some basic thermo elastic problems for nonhomogeneous structural materials, Applied Mechanics Reviews, 148 (1995) 287-300. http://dx.doi.org/10.1115/1.3005103 [25] L. H. You, J. J. Zhang, X. Y. You, Elastic analysis of internally pressurized thick-walled spherical pressure vessels of functionally graded materials, International Journal of Pressure Vessels and Piping, 82 (2005) 347-354. http://dx.doi.org/10.1016/j.ijpvp.2004.11.001

[23] Z. S. Shao, K. K. Ang, J. N. Reddy, T. J. Wang, Nonaxisymmetric thermomechanical analysis of functionally graded hollow cylinders, Journal of Thermal Stresses, 31 (2008) 515-536. http://dx.doi.org/10.1080/01495730801977879

[24] S. M. Hosseini, M. Akhlaghi, M. Shakeri, Transient heat conduction in functionally graded thick hollow cylinders by analytical method, Heat and Mass Transfer, 43 (2007) 669-675. http://dx.doi.org/10.1007/s00231-006-0158-y

[25] A. Acosta-Iborra, A. Campo, Approximate analytic temperature distribution and efficiency for annular fins of uniform thickness, International Journal of Thermal Science, 48 (2009) 773-780. http://dx.doi.org/10.1016/j.ijthermalsci.2008.05.012

[26] M. Asgari, M. Akhlaghi, Transient thermal stresses in two-dimensional functionally graded thick hollow cylinder with finite length, Archive of Applied Mechanics, 80 (2010) 353-376. http://dx.doi.org/10.1007/s00419-009-0321-2 Communications on Advanced Computational Science with Applications 13 of 13 http://www.ispacs.com/journals/cacsa/2014/cacsa-00018/ International Scientific Publications and Consulting Services

[27] Improvement of thermal efficiency in computer heat sink using functionally graded materials Rahim Hassanzadeh1* , Mehmet Bilgili2

[28] Blasius H 1908 Grenzschichten in flussigkeiten mit kleiner ¨ reibung Z. Math. Phys. 56 1–37

[29] Howarth L 1938 On the solution of the laminar boundary layer equations Proc. London Math. Soc. A 164 547–79

[30] Abussita A M M 1994 A note on a certain boundary layer equation Appl. Math. Comput. 64 73–7

[31] Wang L 2004 A new algorithm for solving classical Blasius equation Appl. Math. Comput. 157 1–9

[32] Hossain M A, Alim M A and Rees A D 1999 The effect of radiation on free convection from a porous vertical plate Int. J. Heat Mass Trans. 42 181–91

[33] Hossain M A, Khanafer K and Vafai K 2001 The effect of radiation on free convection flow of fluid with variable viscosity from a porous vertical plate Int. J. Therm. Sci. 40 115–24

[34] Raptis A, Perdikis C and Takhar H S 2004 Effect of thermal radiation on MHD flow Appl. Math. Comput. 153 645–9

[35] Cortell R 2008 Radiation effects in the Blasius flow Appl. Math. Comput. 198 333–8

[36] Bejan A 1982 Second-law analysis in heat transfer and thermal design Adv. Heat Transfer 15 1–58 5 Phys. Scr. 85 (2012) 035008 A S Butt et al

[37] Yilbas B S, Shuja S Z and Budair M O 1999 Second law analysis of swirling flow in a circular duct with restriction Int. J. Heat Mass Transfer 42 4027

[38] Arpaci V S 1987 Radiative entropy production—lost heat into entropy Int. J. Heat Mass Transfer 30 2115–23

[39] Abu-Hijleh A K, Jadallah I N and Nada E A 1998 Entropy generation due to natural convection from a horizontal isothermal cylinder in oil Int. Commun. Heat Mass Transfer 25 1135

[40] Mahmud S and Fraser R A 2003 The second law analysis in fundamental convective heat transfer problems Int. J. Therm. Sci. 42 177–86

[41] Mahmud S and Fraser R A 2002 Thermodynamic analysis of flow and heat transfer inside channel with two parallel plates Exergy 2 140–6

[42] Adnan Saeed Butt1 , Sufian Munawar1 , Asif Ali1 and Ahmer Mehmood2: Entropy generation in the Blasius flow under thermal radiation.

[43] Altan T, Oh S, Gegel H. Metal forming fundamentals and applications. Metals Park, OH: American Society of Metals; 1979.

[44] Tadmor Z, Klein I. Engineering principles of plasticating extrusion. Polymer science and engineering series. New York: Van Nostrand Reinhold; 1970.

[45.A] Sakiadis BC. Boundary-layer behavior on continuous solid surface: I. Boundary-layer equations for two-dimensional and axisymmetric flow. J AIChe 1961;7:26–8.

[45.B] Sakiadis BC. Boundary-layer behavior on continuous solid surface: II. Boundary-layer equations for two-dimensional and axisymmetric flow. J AIChe 1961;7:221–5.

[46] Tsou FK, Sparrow EM, Goldstain RJ. Flow and heat transfer in the boundary-layer on a continuous moving surface. Int J Heat Mass Transfer 1967;10:219–35.

[47] Crane LJ. Flow past a stretching plate. Z Angew Math Phys 1970;21(4):645.

[48] Banks WHH. Similarity solutions of the boundary-layer equations for a stretching wall. J Mech Theor Appl 1983;2:375–92.

[49] Elbashbeshy EMA. Heat transfer over a stretching surface with variable surface heat flux. J Phys D: Appl Phys 1998;31:1951–4.

[50] Liao SJ. A new branch of solution of boundary-layer flows over a permeable stretching plate. Int J Non-linear Mech 2007;42:819–30.

[51] Ali ME. On thermal boundary-layer on a power-law stretched surface with suction or injection. Int J Heat Fluid Flow 1995;16:280–90.

[52] Liao SJ. A new branch of solutions of boundary-layer flows over a stretching flat plate. Int J Heat Mass Transfer 2005;49(12):2529–39.

[53] Magyari E, Keller B. Heat and mass transfer in the boundary-layers on an exponentially stretching continuous surface. J Phys D: Appl Phys 1999;32(5):577–85.

[54] Magyari E, Keller B. Exact solutions for self-similar boundary-layer flows induced by permeable stretching walls. Euro J Mech B: Fluid 2000;19(1):109–22.

[55] Magyari E, Ali ME, Keller B. Heat and mass transfer characteristics of the self-similar boundary-layer flows induced by continuous surfaces stretched with rapidly decreasing velocities. Heat Mass Transfer 2001;38(1–2):65–74.

[56] Wang CY. Exact solutions of the steady state Navier–Stokes equations. Ann Rev Fluid Mech 1991;23:159–77.

[57] Miklavcic M, Wang CY. Viscous flow due to a shrinking sheet. Quart Appl Math 2006;64(2):283–90.
[21] Fang T. Boundary layer flow over a shrinking sheet with power-law velocity. Int J Heat Mass Transfer 2008;51(25–26):5838–43.

[58] Hayat T, Abbas Z, Sajid M. On the analytic solution of magnetohydrodynamic flow of a second grade fluid over a shrinking sheet. J Appl Mech: Trans ASME 2007;74(6):1165–71.

[59] Sajid M, Hayat T, Javed T. MHD rotating flow of a viscous fluid over a shrinking surface. Non-linear Dyn 2008;51(1–2):259–65.

[60] Sajid M, Hayat T. The application of homotopy analysis method for MHD viscous flow due to a shrinking sheet. Chaos, Soliton Fractals 2007. doi:10.1016/j.chaos.2007.06.019.

[61] Tiegang Fang *, Ji Zhang , Closed-form exact solutions of MHD viscous flow over a shrinking sheet "Commun Nonlinear Sci Numer Simulat 14 (2009) 2853–2857"

[62] K. B. Pavlov, "Magnetohydrodynamic flow of an incompressible viscous fluid caused by deformation of a surface," Magnitnaya Gidrodinamika, vol. 4, pp. 146–147, 1974.

[63] H. I. Andersson, "MHD flow of a viscoelastic fluid past a stretching surface," Acta Mechanica, vol. 95, no. 1, pp. 227–230, 1992.

[64] T. Watanabe and I. Pop, "Hall effects on magnetohydrodynamic boundary layer flow over a continuous moving flat plate," Acta Mechanica, vol. 108, no. 1–4, pp. 35–47, 1995.

[65] K. A. Yih, "The effect of uniform suction/blowing on heat transfer of magnetohydrodynamic Hiemenz flow through porous media," Acta Mechanica, vol. 130, no. 3-4, pp. 147–158, 1998.

[66] V. Sobha and K. Ramakrishna, "Convective heat transfer past a vertical plate embedded in porous medium with an applied magnetic field," Journal of the Institution of Engineers: Mechanical Engineering Division, vol. 84, no. 3, pp. 130–134, 2003.

[67] E. H. Aly, M. Benlahsen, and M. Guedda, "Similarity solutions of a MHD boundary-layer flow past a continuous moving surface," International Journal of Engineering Science, vol. 45, no. 2–8, pp. 486–503, 2007.

[68] T. Hayata, R. Sajjada, Z. Abbasc, M. Sajidd, and A. A. Hendie, "Radiation effects on MHD flow of Maxwell fluid in a channel with porous medium," International Journal of Heat & Mass Transfer, vol. 54, pp. 854–862, 2011.

[69] H. Xu, S.-J. Liao, and I. Pop, "Series solutions of unsteady three-dimensional MHD flow and heat transfer in the boundary layer over an impulsively stretching plate," European Journal of Mechanics. B. Fluids, vol. 26, no. 1, pp. 15–27, 2007.

[70] D. A. Nield and A. Bejan, Convection in Porous Media, Springer, 2nd edition, 1999.

[71] Ramesh B. Kudenatti,1 Shreenivas R. Kirsur,2 Achala L. Nargund,3 and N. M. Bujurke4

Similarity Solutions of the MHD Boundary Layer Flow Past a Constant Wedge within Porous Media

[72]. Hiemenz K: Die Grenzschicht an einem in den gleichförmigen Flüssigkeitsstrom eingetauchten geraden Kreiszylinder. Dingler's Polytech J 1911, 326:321-324.

[73]. Homann F: Der Einfluss grosser Zahigkeit bei der Stromung um den Zylinder und um die Kugel. Z Angew Math Mech 1936, 16:153-164.

[74]. Mahapatra TR, Gupta AS: Heat transfer in stagnation-point flow towards a stretching sheet. Heat Mass Tran 2002, 38:517-521.

[75]. Miklavčič M, Wang CY: Viscous flow due to a shrinking sheet. Quart Appl Math 2006, 64:283-290.

[76]. Wang CY: Stagnation flow towards a shrinking sheet. Int J Non Lin Mech 2008, 43:377-382.

[77]. Lok YY, Ishak A, Pop I: MHD stagnation-point flow towards a shrinking sheet. Int J Numer Meth Heat Fluid Flow 2011, 21:61-72.

[78]. Bachok N, Ishak A, Pop I: Melting heat transfer in boundary layer stagnation-point flow towards a stretching/shrinking sheet. Phys Lett A 2010, 374:4075-4079.

[79]. Bachok N, Ishak A, Pop I: On the stagnation-point flow towards a stretching sheet with homogeneous-heterogeneous reactions effects. Comm Nonlinear Sci Numer Simulat 2011, 16:4296-4302.

[80]. Ishak A, Lok YY, Pop I: Stagnation-point flow over a shrinking sheet in a micropolar fluid. Chem Eng Comm 2010, 197:1417-1427.

[81]. Trisaksri V, Wongwises S: Critical review of heat transfer characteristics of nanofluids. Renew Sustain Energ Rev 2007, 11:512-523.

[82]. Wang X-Q, Mujumdar AS: A review on nanofluids - part I: theoretical and numerical investigations. Brazilian J Chem Eng 2008, 25:613-630.

[83]. Ding Y, Chen H, Wang L, Yang C-Y, He Y, Yang W, Lee WP, Zhang L, Huo R: Heat transfer intensification using nanofluids. KONA 2007, 25:23-38.

[84]. Wang X-Q, Mujumdar AS: Heat transfer characteristics of nanofluids: a review. Int J Thermal Sci 2007, 46:1-19.

[85]. Wang X-Q, Mujumdar AS: A review on nanofluids - part II: experiments and applications. Brazilian J Chem Eng 2008, 25:631-648.

[86]. Nield DA, Kuznetsov AV: The Cheng-Minkowycz problem for natural convective boundary layer flow in a porous medium saturated by a nanofluid. Int J Heat Mass Tran 2009, 52:3187-3196.

[87]. Kakaç S, Pramuanjaroenkij A: Review of convective heat transfer enhancement with nanofluids. Int J Heat Mass Tran 2009, 52:3187-3196.

[88]. Nield DA, Kuznetsov AV: The Cheng-Minkowycz problem for the double diffusive natural convective boundary layer flow in a porous medium saturated by a nanofluid. Int J Heat Mass Tran 2011, 54:374-378.

[89]. Murshed SMS, Leong KC, Yang C: Thermophysical and electrokinetic properties of nanofluids - a critical review. Appl Therm Eng 2008, 28:2109-2125.

[90]. Kuznetsov AV, Nield DA: Natural convective boundary layer flow of a nanofluid past a vertical plate. Int J Thermal Sci 2010, 49:243-247. 27. Kuznetsov AV, Nield DA: Double-diffusive natural convective boundarylayer flow of a nanofluid past a vertical plate. Int J Thermal Sci 2011, 50:712-717. 28. Khan AV,

Pop I: Boundary-layer flow of a nanofluid past a stretching sheet. Int J Heat Mass Tran 2010, 53:2477-2483.

[91]. Bachok N, Ishak A, Pop I: Boundary layer flow of nanofluids over a moving surface in a flowing fluid. Int J Thermal Sci 2010, 49:1663-1668.

[92]. Tiwari RK, Das MK: Heat transfer augmentation in a two-sided lid-driven differentially heated square cavity utilizing nanofluids. Int J Heat Mass Tran 2007, 50:2002-2018.

[93].. Abu-Nada E: Application of nanofluids for heat transfer enhancement of separated flow encountered in a backward facing step. Int J Heat Fluid Flow 2008, 29:242-249.

[94].. Muthtamilselvan M, Kandaswamy P, Lee J: Heat transfer enhancement of Copper-water nanofluids in a lid-driven enclosure. Comm Nonlinear Sci Numer Simulat 2010, 15:1501-1510.

[95].. Abu-Nada E, Oztop HF: Effect of inclination angle on natural convection in enclosures filled with Cu-water nanofluid. Int J Heat Fluid Flow 2009, 30:669-678.

[96].. Talebi F, Houshang A, Shahi M: Numerical study of mixed convection flows in a squre lid-driven cavity utilizing nanofluid. Int Comm Heat Mass Tran 2010, 37:79-90.

[97].. Ahmad S, Rohni AM, Pop I: Blasius and Sakiadis problems in nanofluids. Acta Mech 2011, 218:195-204.

[98].. Bachok N, Ishak A, Nazar R, Pop I: Flow and heat transfer at a general three-dimensional stagnation point flow in a nanofluid. Physica B 2010, 405:4914-4918.

[99].. Bachok N, Ishak A, Pop I: Flow and heat transfer over a rotating porous disk in a nanofluid. Physica B 2011, 406:1767-1772.

[100]. Yacob NA, Ishak A, Pop I, Vajravelu K: Boundary layer flow past a stretching/shrinking surface beneath an external uniform shear flow with a convective surface boundary condition in a nanofluid. Nanoscale Research Letters 2011, 6:314.

[101]. Oztop HF, Abu-Nada E: Numerical study of natural convection in partially heated rectangular enclosures filled with nanofluids. Int J Heat Fluid Flow 2008, 29:1326-1336.

[102]. Oztop HF, Abu-Nada E: Numerical study of natural convection in partially heated rectangular enclosures filled with nanofluids. Int J Heat Fluid Flow 2008, 29:1326-1336.

[103] Bebernes J., Eberly D.: Mathematical problems from combustion theory. Springer-Verlag, New York, 1989.

[104] Frank Kamenetskii D. A.: Diffusion and Heat Transfer in chemical kinetics. Plenum Press, New York, 1969.

[105] Makinde O. D.: Heat and mass transfer in a pipe with moving surface-effect of viscosity variation and energy dissipation. Quaestiones Mathematicae 24, 93-104, 2001.

[106] Sergeyev A. V., Goodson D. Z.: Summation of asymptotic expansions of multiple valued functions using algebraic approximations-application to anharmonic oscillators. J. Phys. A31, 4301-4317, 1998.

[107] Tourigny Y., Drazin P. G.: The asymptotic behaviour of algebraic approximants. Proc. Roy. Soc. London A456, 1117-1137, 2000.

[108] O. D. Makinde: Exothermic explosion in a slab: A case study of Series of Summation Technique

[109] H K Versteeg and W Malalasekera: An Background to Computational Fluid Dynamics: The Finite Volume Method:Pearson: Seventh Edition

[110] Dr. Hermann Schlichting: Boundary Layer Theory : McGRAW-HILL BOOK COMPANY : Seventh Edition

[111] D. A. Kaminski and M.K.Jensen : An Background to Fluids and Thermal Engineering: John Wiley & Sons, Inc (2005).

[112] L. C. Woods: Thermodynamics of fluid systems: Oxford University Press, Oxford, (1975).

[113] Steven H. Strogatz: Nonlinear Dynamics and Chaos: PERSEUS BOOKS Reading, Massachusetts

[114] https://www.usgs.gov/special-topic/water-science-school/science/how-much-water-there-earth?qt-science_center_objects=0#qt-science_center_objects